Surfactants, Interfaces and Pores

a theoretical study

Promotor: dr. J. Lyklema, emeritus hoogleraar in de fysische chemie, met bijzondere aandacht voor de grensvlak- en kolloïdchemie

Co-promotoren:

dr. A. de Keizer,

dr. ir. F.A.M. Leermakers, beiden universitair docent bij het departement Biomoleculaire Wetenschappen

Surfactants, Interfaces and Pores

a theoretical study

Proefschrift
ter verkrijging van de graad van doctor
op gezag van de rector magnificus
van de Landbouwuniversiteit Wageningen,
dr. C.M. Karssen,
in het openbaar te verdedigen
op woensdag 14 januari 1998
des namiddags te vier uur in de Aula

CIP-DATA KONINKLIJKE BIBLIOTHEEK, DEN HAAG

Huinink, H.P.

Surfactants, Interfaces and Pores: a theoretical study/H.P. Huinink
[S.l.: s.n.].-Ill.
Thesis Wageningen. - With ref. - With summary in Dutch
ISBN 90-5485-792-7
subject headings: lattice theory/surfactant adsorption/pores

Cover photography: G.J. Huinink (contains a fragment of Job 28:11 v.v.)

NWO

These investigations were supported by the Netherlands Foundation for Chemical Research (SON) with financial aid from the Netherlands Organisation for Scientific Research (NWO).

Voorwoord

De wetenschap heeft het tot haar deugd gemaakt om haar kinderen zo streng mogelijk in het pad van de objectiviteit te onderwijzen. In dit voor u liggende boekje beschrijf ik de resultaten van mijn betrokkenheid bij de groei van één van haar spruiten. Ik kan me zo voorstellen dat een intensieve wandeling door dit met formules gelardeerde bos u, ongeacht uw wandelroute, een diep gevoel van eenzaamheid kan geven. Of u begrijpt er niets van en hebt het gevoel dat zelfs de mossprietjes te hoog zijn om aan te raken, of u begrijpt er alles van en vraagt zich vertwijfeld af waarom de bomen nog langer bomen worden genoemd. Nu moet u niet denken dat ik de kinderen van de wetenschap als ongewenst beschouw. Ik wil u er alleen maar op wijzen dat de invloed van hun moeder niet onderschat moet worden. Ze voedt hen met de melk van de algemeen geldigheid en verschoont hen met luiers van het determinisme. Denk niet dat ik verlang dat zij het anders doet. Zeker niet! Ik wil alleen maar zeggen dat haar kinderen noch wereldverbeteraars noch criminelen zijn. Ze zijn domweg haar kinderen.
U moet beseffen dat u bij het lezen van de bladzijden volgend op dit voorwoord een bril opzet die een zeker beeld van de werkelijkheid oplevert. En zoals veel brildragers weleens overkomt, kan het zijn dat ik of u op een zeker moment het besef van het montuur verliezen, zodat we gaan denken dat we onze bril kwijt zijn. Dit nu is buitengewoon hinderlijk, want de supermontuurlijke realiteit kan zo warm en vriendelijk zijn. Want daar zijn de mensen. In de brilleglazen zie je slechts een agglomeraat van cellen, een complex reactievat, samengebalde sexuele driften, overlevingsstrategieën en gedragspatronen. In het supermontuurlijke is daar Hans Lyklema, die ik een klein beetje heb leren kennen in de afgelopen tijd, Trudy van wie ik zo ben gaan houden dat ik mijn leven met haar wil gaan delen, Frans Leermakers met wie ik tot mijn groot genoegen ettelijke witte en zwarte borden heb vol gekladderd, Arnout Bosse en al de andere filosoofjes met wie ik de bomen tot in de hemel heb doen laten groeien, Arie de Keizer die ijverig mijn theoretische excessen heeft gevolgd, Bert Torn met wie ik vele uren heb volgepraat en nog vele anderen.
Namen, namen en nogeens namen en waag het eens om één van deze namen te verwisselen. Daar in het buitenbrillige zijn ook liefde en haat, mildheid en bitterheid, betrokkenheid en jaloezie, vreugde en pijn en leven en dood. Ik bewijs niets en vind dat ook niet nodig. De analyse is als het mes van een

anatoom, het confronteert de toeschouwer met de structuur van een dode en niet van een levende. De echte levende vindt men slechts wanneer men vrijwillig kiest om zichzelf kinderlijk afhankelijk te maken van de ander, wat zeker niet eenvoudig en allerminst risicoloos is.

Denk nu niet dat de onderneming van dit boekje ongewenst en minderwaardig is. Uiteindelijk zijn de inhoud van dit boekje en de fenomenen van het buitenmontuurlijke op één en dezelfde realiteit betrokken: de schepping van God, die heeft laten zien Wie Hij is in Jezus. Ik weet het, het is een dwaas verhaal en het is de ultiemste vorm van dwaasheid om hieraan te refereren in het boekje zoals dat voor u ligt. Het is zelfs voor een diep-religieus mens te dwaas om los te lopen dat God mens wordt en vervolgens Zich laat kruisigen. Maar het is wel diepste verklaring van liefde die de schepping op zich afgevuurd kan krijgen. Het is deze schepping waarbinnen de liefde een plek heeft naast het molecuul, waar het onnavolgbare complex Henk wetenschap bedrijft en ook gelooft. De schepping die zoveel waard is dat elke poging om haar te quantificeren in geld waanzin is en elk detail het waard is om naar te kijken.

Wellicht heeft u het benauwd gekregen van dit spervuur van irrationele gedachtengangen. Het lijkt me daarom goed dit voorwoord te beëindigen. Ik wens u een goede reis door de vijf hoofdstukken. En of u er doorheen komt of niet en of u het zinnig vindt of niet, er rest een feestje voor mij en voor u.

Chapter 2: published in the Journal of Physical Chemistry, 100, 9948 (1996)
Chapter 3: published in Langmuir, 13, 6452 (1997)
Chapter 4: published in Langmuir, 13, 6618 (1997)
Chapter 5: submitted to Langmuir

Contents

Chapter 1

Introduction

1.1 Surfactants, detergents or amphiphiles

How do you manage to keep so much water in your body? What is the magic of the white powder, you add to ordinary water, that your shirt becomes clean? Why is it possible that we can discuss about the need to cover the golden liquid with a layer of bubbles? The number of answers will be much more than three and each answer will generate new questions, which have to be answered. Therefore, it will not be tried to answer any of these questions between the page you are reading and the last one. However, you have to become aware of the fact that a type of molecules exists, which plays a crucial role in all three questions.

"Detergent", "surfactant" or "amphiphile" are a few names, used to refer to this type. The word "detergent" is often used because the molecules can be used for cleaning. With the words "surfactant" and "amphiphile" the macro-world is left behind and the micro-world is entered. The label "surfactant" refers to the tendency of the molecules to accumulate in large amounts at solid-liquid, liquid-liquid and liquid-gas interfaces. It describes one aspect of its behavior. On the other hand, with the word "amphiphile" we are on the way to discover the roots of this behavior. Due to its anisotropic chemical structure, the different sides of a surfactant prefer ("phile") to stick in or on different phases ("amphi").

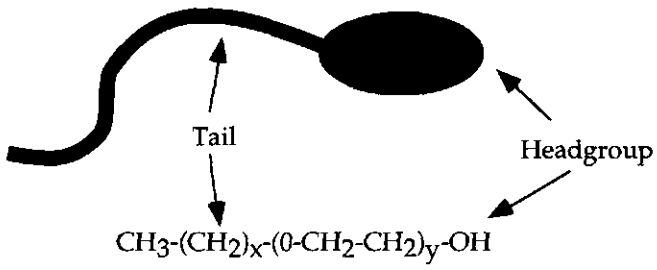

Figure 1 Above: schematical picture of a surfactant molecule. Below: the chemical formula of a well know class of nonionic surfactants.

The chemical structure of a surfactant can be divided into two parts: the headgroup and the tail(s)[1], see figure 1. The most common type of tails, both in synthetic and natural surfactants, is the aliphatic one. Although the chemical structure of the headgroup varies considerably, surfactants can be divided into three classes: anionic, nonionic and cationic surfactants, of which the headgroups carry a negative, zero and positive charge, respectively.

1.2 Surfactants in water

If surfactants are dissolved in water, the molecules form aggregates above a certain concentration, in which the headgroups (hydrophilic parts) are in contact with water and the tails (hydrophobic parts) stick together. The driving force for aggregation is the repulsion between the hydrophobic tails and water. To be more precise, water is a liquid with a strong coherence due to the presence of a network of hydrogen-bonds. The hydrophobic part of a surfactant molecule locally destroys the favorable coherence of the water[2].
The first aggregates are small, have a more or less spherical shape and are called micelles. The concentration at which these micelles appear is known as the "critical micelle concentration" (CMC). This concentration can be determined rather easily with various techniques[1,3], like osmotic pressure measurements, light scattering, conductivity measurements in the case of charged surfactants and surface tension measurements, because the behavior of these physical properties change abruptly at this point.
The shape and the number of the aggregates are very sensitive to the surfactant concentration, the temperature, the ionic strength and the molecular architecture[4-6]. Besides spherical micelles, there may occur linear micelles, bilayers (plate-like structures) and sponge phases[7], figure 2. With advanced techniques, it has become possible to identify the various morphologies, which can exist in concentrated surfactant solutions[6,8,9].
Phospholipids, surfactant-like molecules, which are present in every living creature, form large plate-like structures, called membranes. These membranes serve as boundaries between the complex and fragile inner world of an organism and its rough and hostile environment. Due to the presence of these boundaries, we are also able to retain so much water in our bodies.

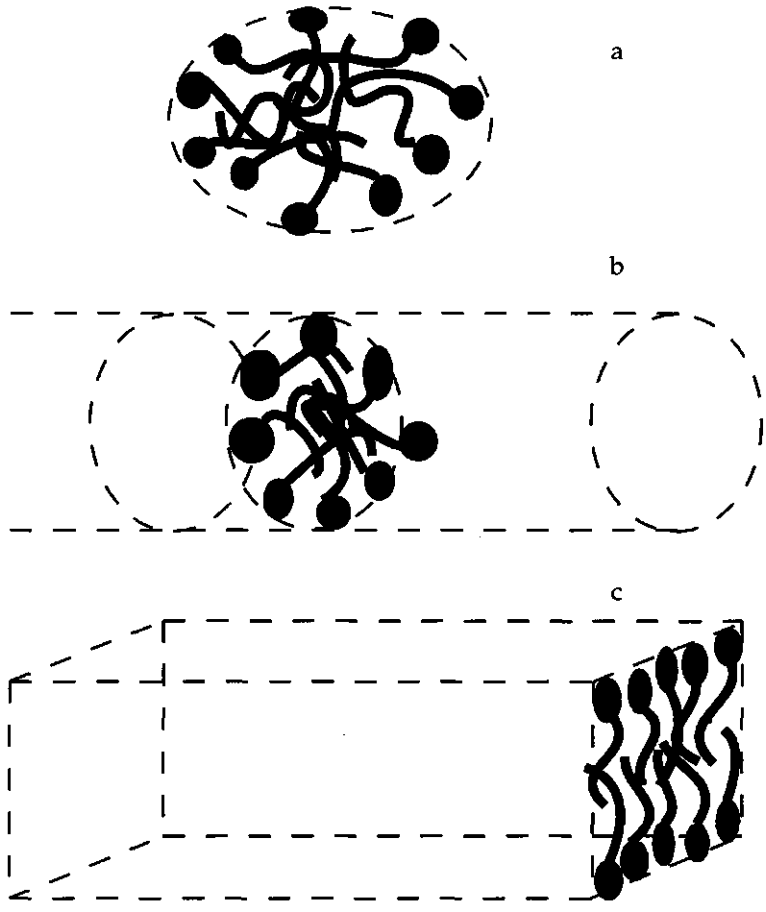

Figure 2 Three different types of structures of surfactant aggregates in solution: (a) the spherical micelle, (b) the cylindrical micelle and (c) the bilayer.

1.3 Surfactants at interfaces

As already mentioned, surfactants can accumulate in high amounts at interfaces between two different phases due to their amphiphilic character. Clothes can be cleaned because surfactants adsorb at the surfaces of the textile or the soil particle[10,11] and keeps dirt particles and textile apart.

This study is focused on the adsorption behavior of surfactants at solid-water interfaces. Irrespective what type of surface or surfactant, the driving force for adsorption is the surface-surfactant interaction. The high adsorbed amounts are a consequence of the repulsion between the hydrophobic tails and water. As in solution, this interaction stimulates the formation of aggregates. The morphology of a surface associate can not be studied with the techniques,

used for aggregates in solution, and has been a topic of discussion for years. Atomic force microscopy (AFM) has been used to obtain unambiguous information about the structure of surfactant layers. As in solution, spherical, linear and bilayer structures are formed[12,13]. The surface-surfactant interaction has a strong influence on the resulting morphology[14].

The area of surfactant adsorption can be divided into four sub-areas, figure 3. The driving force for adsorption at a hydrophilic surface is an attractive interaction between the headgroup of the surfactant and the surface. Therefore, the adsorbed layer consists of aggregates, in which the hydrophobic tails are screened from the solution and the headgroups have contact with both the surface and the solution. Adsorption on a hydrophobic surface is driven by the poor wetting behavior of the solid, the adsorbed molecules screen the unfavorable surface-solution interaction. The surfactant molecules arrange themselves in layers or aggregates, such that the headgroups and tails are in contact with the solution and the surface, respectively.

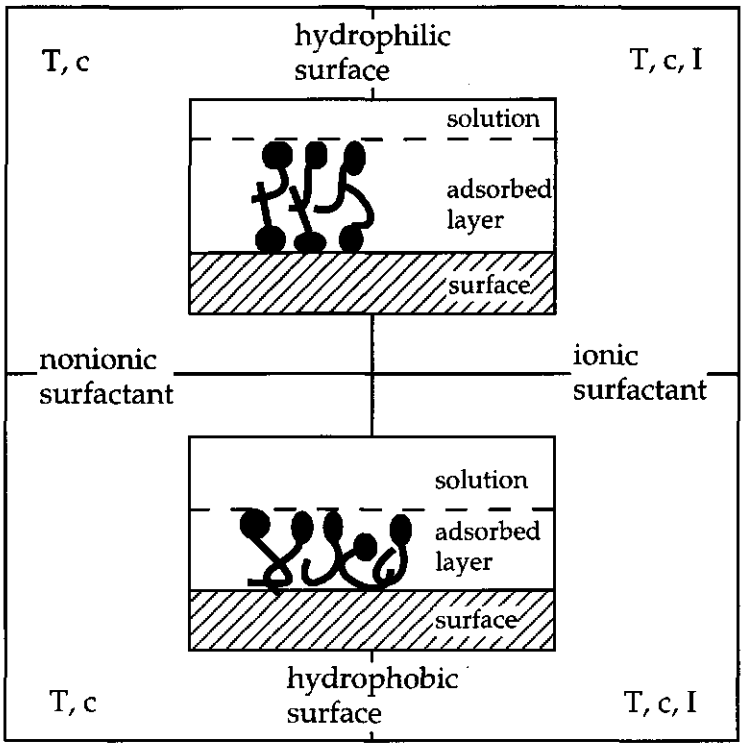

Figure 3 The four different sub-areas of surfactant adsorption. The important variables are written in the corners: T (temperature), c (surfactant concentration) and I (ionic strength).

The main difference between the areas of the ionic and nonionic surfactants is the influence of the ionic strength. Although even the behavior of the nonionic surfactants can be influenced by the salinity of the solution through subtle mechanisms[15-17], the influence on the behavior of ionic surfactants is much more pronounced[18].

1.4 Surfactants and pores

Although a lot of solid substances seem to be macroscopically inert, they often are porous on molecular length scales. The specific surface area of substances, like carbon, certain types of silica and cellulose fibers, is very high due to the presence of small pores. If surfactants adsorb from an aqueous solution onto a porous medium, most of the adsorption may take place at the solid surfaces inside the pores. This may alter the adsorption behavior. The physical properties of a liquid inside a pore can differ from the properties of the same liquid outside the pore.

If a gas is confined in one or more dimensions, abrupt changes, like condensation, can be promoted[19]. Energetic or entropic interactions of the gas with the solid surface can alter the stability of both the liquid and the gas phase. The energetic interaction is related to the balance between the adhesion and cohesion of the liquid. The entropic interaction originates from the fact that the liquid structure is perturbed by the solid surface. This entropic interaction becomes important when the perturbation is not yet quenched at a distance of the order of the pore size. The correlation length ξ of a liquid is a measure of the decay length of a perturbation in the liquid. Under normal conditions ξ is of the same order as the molecular diameter. Only in the neighborhood of so-called critical points ξ diverges[19]. An example is shown in figure 4. In this figure, density profiles of a liquid are drawn for different correlation lengths. Due to the fact that the liquid molecules have no interaction with the surface, depletion layers develop.

Roughly speaking, the correlation length is a measure of the thickness of an adsorption or a depletion layer. To observe significant influences of a pore on the adsorbed amount, the pore size has to be of the order of the layer thickness. Away from any critical point, this layer thickness is of the order of one or two molecular diameters. Influences on polymer adsorption or depletion will be observed when the pore diameter and the radius of gyration have the same order of magnitude[20,21]. If the pore diameter is of the same order as a micelle size, surfactant adsorption behavior will also change.

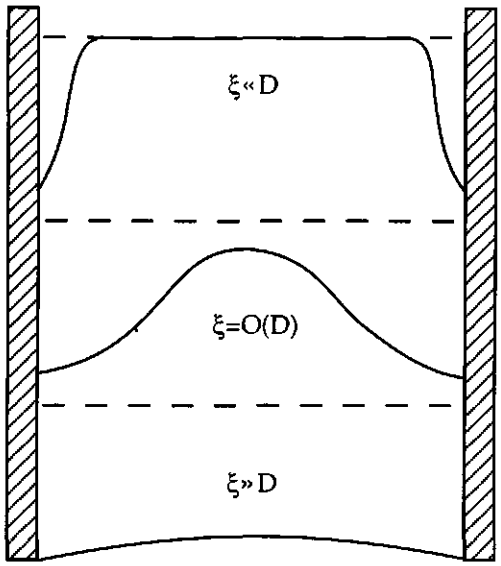

Figure 4 Density profiles of a liquid inside a pore for different correlation lengths ξ. In this example, the liquid-surface interaction is repulsive The dashed lines are the corresponding densities of the liquid outside the pore and D is the diameter of the pore.

1.5 Theory of surfactant adsorption

Experiments do not present us facts. The output results from experiments are like shadows on a wall, both the position of the light source, the posture of the illuminated object and the structure of the wall determine the shape of the resulting shadow. Even if we know these three variables, our knowledge will be restricted by the fact that a shadow only contains information about the shape of the object. It is theory, which tries to reconstruct from the shadow, with the help of the available knowledge about the light source and the structure of the wall, the shape of the original object.

For the understanding of adsorption, adsorption isotherms have always been the most important pieces of experimental information. Various models have been developed to explain these isotherms[22-27]. However, it is difficult to evaluate the performances of these models, because the shapes of adsorption isotherms are not unique. However, new criteria and demands can be formulated with the help of the recent advances with modern techniques like AFM. The ultimate goal is a model which combines molecular detail with a realistic description of the morphology of and interactions between the aggregates.

In this study two types of lattice theories will be used to study surfactant adsorption: the Scheutjens-Fleer theory[28], applied to surfactant adsorption by Böhmer et al.[26], and the Herzfeld model[29] for polydisperse particles. The first one, which will be refered to with the abbrevation MFL (Mean Field Lattice), predicts the structure of an adsorbed layer or a surface aggregate with the help of a detailed molecular model. However, the price of this molecular detail is high, the MFL theory is not able to treat the interactions between the surface aggregates. On the other hand, the Herzfeld model can be used to study the influence of these interactions on the adsorption. But, now every molecular detail is lacking.

1.6 Outline of this study

This thesis contains three chapters on surfactant adsorption and one dealing with the structure of the water phase and its dielectric permittivity. All four chapters have in common that the described studies should lead to a better understanding of the behavior of adsorbed surfactant layers in porous media.
In the second chapter we present calculations on the dielectric permittivity of water. The lattice model, which is used, has proven to be adequate for the description of bulk water[30]. The study on the dielectrics of bulk water was planned to be a first step towards a better description of water in charged pores and adsorption of ionic surfactants from aqueous media. However, unexpected results for inhomogeneous systems induced us not to pursue further investigations with this model.
The third and fourth chapter deal with the influence of confinement on nonionic surfactant adsorption at a hydrophilic surface. An analytical and a MFL theory have been used to investigate the relation between the curvature and the stability of the adsorbed layer in a cylindrical pore.
The theories, used in the third and fourth chapter, contain a mean-field approximation. Homogeneity parallel to the solid surface is assumed. Density gradients are only allowed in the direction perpendicular to the surface. However, surfactants often adsorb in discrete aggregates. This means that the adsorbed layer is not homogeneous. Therefore, in chapter five the Herzfeld model is applied to the case of surfactant adsorption. This model takes the discrete nature of the adsorption layer into account.

References

1 Ottewill, R. H., in *Surfactants*, edited by Tadros, T. F. (Academic Press, London, 1983).

2 Lyklema, J., *Fundamentals of Inteface and Colloid Science* vol 1(Academic Press, London, 1991).

3 Mukerjee, P. and Mysels, K. J., *Critical Micelle Concentrations of Aqueous Surfactant Systems* (NSRDA, Washington, 1970).

4 Mitchell, D. J., Tiddy, G. J. T., Waring, L., Bostock, T. and McDonald, M. P., *J. Chem. Soc., Faraday Trans. I* **79,** 975 (1983).

5 Israelachvili, J. N., in *Physics of Amphiphiles: Micelles, Vesicles and Microemulsions*, edited by Degiorgio, V. and Corti, M. (Elsevier, Amsterdam, 1985).

6 Laughlin, R. G., *The Aqueous Phase Behavior of Surfactants* (Academic Press, London, 1994).

7 Wennerström, H. and Evans, D. F., *The Colloidal Domain* (VCH publishers, New York, 1994).

8 Porte, G., in *Micelles, Membranes, Microemulsions and Monolayers*, edited by Gelbart, W. M., Ben-Shaul, A. and Roux, D. (Springer-Verlag, Berlin, 1994).

9 Boden, N., in *Micelles, Membranes, Microemulsions and Monolayers*, edited by Gelbart, W. M., Ben-Shaul, A. and Roux, D. (Springer-Verlag, Berlin, 1994).

10 Rosen, M. J., *Surfactants and Intefacial Phenomena* (John Wiley & Sons, New York, 1978).

11 Kissa, E., in *Detergency*, Vol. 20, edited by Cutler, W. G. and Kissa, E., (Marcel Dekker, New York, 1987).

12 Manne, S., Cleveland, J. P., Gaub, H. E., Stucky, G. D. and Hansma, P. K., *Langmuir* **10,** 4409 (1994).

13 Patrick, H. N., Warr, G. G., Manne, S. and Aksay, I. A., *Langmuir* **13,** 4349 (1997).

14 Grant, L. M. and Ducker, W. A., *J. Phys. Chem.* **101,** 5337 (1997).

15 Lange, H., in *Nonionic Surfactants*, Vol. 1, edited by Schick, M. J. (Marcel Dekker, New York, 1967).

16 Becher, P., in *Nonionic Surfactants*, Vol. 1, edited by Schick, M. J. (Marcel Dekker, New York, 1967).

17 Rupprecht, H., *Progr. Colloid Polym. Sci.* **65,** 29 (1978).

18 Koopal, L. K., in *Coagulation and Floculation*, edited by Dobias, B. (Marcel Dekker, New York, 1993).

19 Thommes, M., Findenegg, G. H. and Schoen, M., *Langmuir* **11,** 2137 (1995).
20 Gennes, P. G. de, *Scaling Concepts in Polymer Physics* (Cornell University Press, Ithaca, 1979).
21 Gorbunov, A. A. and Skvortsov, A. M., *Adv. Coll. Interface Sci.* **62,** 31 (1995).
22 Kronberg, B., *J. Coll. Interface Sci.* **96,** 55 (1983).
23 Koopal, L. K., Wilkinson, G. T. and Ralston, J., *J. Coll. Interface Sci.* **126,** 493 (1988).
24 Levitz, P., *Langmuir* **7,** 1595 (1991).
25 Zhu, B. and Gu, T., *Adv. Coll. Interface Sci.* **37,** 1 (1991).
26 Böhmer, M. R., Koopal, L. K., Janssen, R., Lee, E. M., Thomas, R. K. and Rennie, A. R., *Langmuir* **8,** 2228 (1992).
27 Lajtar, L., Narkiewicz-Michalek, J., Rudzinski, W. and Partyka, S., *Langmuir* **9,** 3174 (1993).
28 Scheutjens, J. M. H. M. and Fleer, G. J., *J. Phys. Chem.* **83,** 1619 (1979).
29 Herzfeld, J., *J. Chem. Phys.* **76,** 4185 (1982).
30 Besseling, N. A. M. and Lyklema, J., *J. Phys. Chem.* **98,** 11610 (1994).

Chapter 2

Lattice approach to the dielectric permittivity of water

Abstract A lattice theory, based on a quasi-chemical approach, has been combined with a semi-macroscopical theory to calculate the permittivity of water. At low field strength the magnitude and the temperature dependency of the calculated permittivity agree with experimental data. The high-field dielectric behavior of water has also been studied. If the field strength increases the permittivity goes through a maximum, which has not been found experimentally. This maximum is caused by the fact that orientation of dipoles in the field is strongly cooperative due to hydrogen-bonding.

2.1 Introduction

The dielectric constant of polar liquids is a classical subject in physical chemistry. This is not surprising because this property is very sensitive to the structure of a liquid[1]. The quality of many theories, including those dealing with electric double layer structure[2] and solvation forces[3], depends on the description of the polarization. In an electric double layer the electric field is inhomogeneous and near the charged wall its strength may increase as high as values of 10^8-10^9 Vm^{-1}. In such a high field the dielectric behavior may no longer be linear. Therefore, the quality of a description of a double layer depends on the level of the treatment of the dielectric behavior in high and low fields.

One of the first attempts to calculate the permittivity of a polar liquid has been made by Onsager[4]. Due to his neglecting of dipole-dipole interactions the calculated values turned out to be too low. A more refined treatment of the local order, by Kirkwood[5] and later by Fröhlich[6], resulted in theories which could satisfactorily predict the permittivity of water in the absence of an applied field. All these theories consider water as consisting of spherical molecules with ideal dipoles, treating the surrounding medium as a continuum with a certain dielectric constant. Phenomena like electrostriction and saturation are beyond the scope of these semi-macroscopic theories. However, extending these theories a few semi-macroscopic theories to

calculate dielectric saturation have been developed[7] by Booth[8,9], Buckingham[10] and Schellman[11].

Over the last two decades much progress in the calculation of dielectric constants of multipole liquids has been made using integral theories[12]. Some attempts have been made to perform calculations on electrostriction and dielectric saturation phenomena[13-15].

Although the progress made with integral theories in the domain of permittivity calculations and the structure of the electric double layer seems to leave little room for further use of semi-macroscopic theories, there is at least one reason to reconsider the latter type of approaches. Lattice theories are namely much easier to use for complex fluids like water and for the properties of such liquids adjacent to surfaces. A prerequisite is of course that the local order can be satisfactorily described. In fact, the combination of lattice calculations and a semi-macroscopic approach could also give additional insight into the structure of liquids near charged interfaces and into the phenomena of electrosorption.

In the present study a First Order Self-Consistent Field theory (FOSCF), developed by Besseling and Scheutjens[16], is combined with the reaction field approach of Onsager[4]. The FOSCF theory has been developed to study systems of molecules with orientation-dependent interactions. For water the model has shown to work very satisfactorily in explaining hydrogen bonding ratios, the density maximum, the surface tension and several other properties[17]. In the present paper dielectric properties of bulk water are calculated for low and high static fields. The local order is treated in the quasi-chemical approximation, non-local interactions are treated with an Onsager reaction-field[18]. This separate treatment of short-range and long-range interactions seems a bit artificial, but for water, where strong hydrogen bonds dominate all other interactions, it seems to be a fruitful approach[19]. Whether or not the separate treatment of short-range and long-range interactions, as done in our theory, is realistic in all situations, will be studied in section 2.8.

With the use of a propagator formalism, originally developed for polymer adsorption[20,21] and later applied to surfactant systems[22], a number of phenomena can be addressed, for instance electrosorption. However, in the present paper we shall restrict ourselves to the dielectric permittivity in high and low fields and its temperature dependence.

2.2 The water model

In the Besseling-Scheutjens model, adopted in this study, the liquid molecules are placed on a body-centred cubic(bcc)-lattice. In this model a molecule has eight nearest neighbors. In figure 1 a diagram of the water molecule has been drawn. In two directions the molecule has proton-donor faces (D), in two others proton-acceptor faces (A) and all other faces are indifferent (I). A and D faces have a tetrahedral arrangement. A vacancy is considered as an isotropic molecule of the same size with identical faces in each direction (V). In table 1 contact energies $\{u_{\alpha\beta}\}$ of different combinations of faces are listed. These values are identical to those used in earlier studies with the FOSCF-theory; they have been obtained by fitting the experimental pressure and density of water in coexistence with vapor at 273.16 K[17]

To the water molecule an ideal dipole has been assigned of moment 1.84 D[23]. The water molecule has an isotropic polarizability of $1.65 \cdot 10^{-40}$ Cm^2V^{-1} [24].

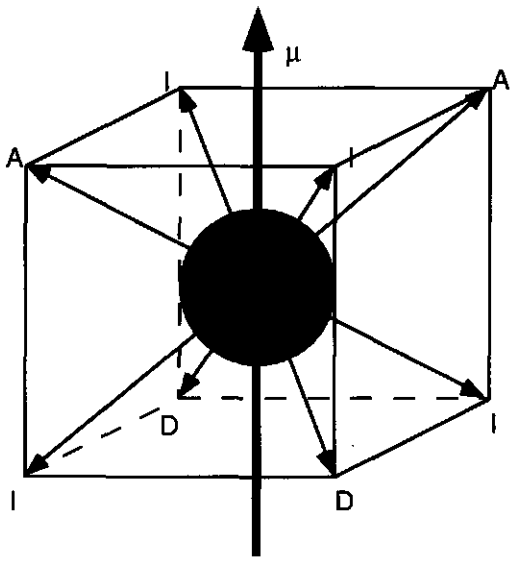

Figure 1 The water model. Arrows to the corners correspond with the directions of the nearest neighbor contacts in the b.c.c. lattice. A is an acceptor face, D is a donor face and I is an indifferent face. The bold vector marked with μ shows the direction of the permanent dipole moment.

contact type	contact energy (K)
D-A	-2414.23
D-D	210.2
D-I	210.2
A-A	210.2
A-I	210.2
I-I	210.2

Table 1 A listing of the different types of water-water interactions. Interactions with vacancy faces have not been listed because they are obviously equal to zero.

2.3 The lattice

As already mentioned, a bcc lattice has been used. It consists of two intertwined diamond lattices. The dimensions of the unit cells are chosen in such a way that the distance between two nearest neighbors is 0.276 nm. This value is equal to the O-O distance in ice at 273 K, measured with X-ray diffraction[25].

The lattice is divided in layers perpendicular to the electric field and chosen in such a way that the dipole of water can have three orientations: parallel, perpendicular or anti-parallel to the field. Within each lattice layer a molecule has no nearest neighbors, but both adjacent layers contain four nearest neighbors. Therefore, in this configuration a molecule has only two directions to form contacts, forward and backward, as counted in the direction of the electric field.

Only one layer, bound by two identical layers, has to be considered because in this paper we are only interested in the response of a liquid to a homogeneous electric field. The layer has a volume V and contains L lattice sites.

2.4 Configuration statistics in the quasi-chemical approximation

For a detailed description of the FOSCF model the literature must be consulted[16] In this section only a short flight over the theory will be made.

In the FOSCF model the quasi-chemical approximation is used. In this approximation pairs of molecules can have different probabilities. In the FOSCF extension of this approximation, probabilities are assigned, not to pairs of molecules, but to pairs of contact faces. The probability of finding a contact between certain faces is independent of the other contacts which can

be formed. As mentioned earlier, water is treated as a molecule with eight contact faces.

The grand partition function is maximized with respect to the distribution of the molecules $\{n_A^o\}$ and the contacts $\{n_{\alpha\beta}^d\}$, n_A^o is the number of molecules A with a certain orientation o and $n_{\alpha\beta}^d$ is the number of contacts in direction d between the faces α and β. We note that the set $\{n_A^o\}$ also includes vacancies. Therefore, each sum over A also contains these vacancies.

For the degeneracy Ω of a system the following formula was derived:

$$\ln\Omega(\{n_A^o\},\{n_{\alpha\beta}^d\}) = -\sum_{\alpha,\beta,d} n_{\alpha\beta}^d \ln g_{\alpha\beta}^d - \sum_{A,o} n_A^o \ln\phi_A^o \qquad (1)$$

where ϕ_A^o is defined as n_A^o/L, the volume fraction of molecules A with an orientation o. The quantity $g_{\alpha\beta}^d$ is the correlation function of the faces α and β in a direction d. This function is defined as follows.

$$g_{\alpha\beta}^d = \frac{\phi_{\alpha\beta}^d}{\phi_\alpha^d \phi_\beta^{-d}} \qquad (2)$$

In (2) $\phi_{\alpha\beta}^d \equiv n_{\alpha\beta}^d/L$, $\phi_\alpha^d \equiv n_\alpha^d/L$ and $\phi_\beta^{-d} \equiv n_\beta^{-d}/L$, where n_α^d is the number of faces α in direction d.

In equation (1) the second term on the right hand side corresponds with ideal mixing. After multiplication with k this leads to the mixing entropy of a system. With the first term local order, due to the contact interactions, is taken into account.

The potential energy is given by

$$U(\{n_A^o\},\{n_{\alpha\beta}^d\}) = \frac{1}{2}\sum_{\alpha,\beta,d} n_{\alpha\beta}^d \upsilon_{\alpha\beta} + \sum_{A,\,o} n_A^o \upsilon_A^o \qquad (3)$$

Where υ_A^o is the energy of the ideal dipole of a molecule A with orientation o in an electric field E. Given the choice of the lattice layers with respect to E, there are three of such orientations. The exchange energy of an $\alpha\beta$-contact, $\upsilon_{\alpha\beta}$, is related to the contact energy $u_{\alpha\beta}$ through:

$$\upsilon_{\alpha\beta} = u_{\alpha\beta} - (u_{\alpha\alpha} + u_{\beta\beta})/2 \qquad (4)$$

In earlier studies with the FOSCF model the potential energy of the system was independent of the distribution $\{n_A^o\}$. However, because now the interaction of a molecule with an electric field is studied this energy becomes dependent on the number of molecules and their orientations. This is covered by the last term on the right-hand side of (3). In the following section an expression for υ_A^o will be derived.

Since the degeneracy (1) and the potential energy (3) are now known, the partition function can be written. If the liquid is in open contact with a homogeneous bulk the grand canonical partition function has to be used.

$$\Xi(\{f_A\},L,T)=\sum_{\{n_A\}}Q(\{n_A\},L,T)\exp\left(\sum_A\frac{n_A f_A}{kT}\right) \tag{5}$$

Where L is the number of lattice sites, T he temperature, n_A the number of molecules of type A in the system and f_A is the partial Helmholtz energy. The set $\{n_A\}$ must satisfy the condition of a complete filling of the lattice, $\sum_A n_A = L$. For the canonical partition function, Q, we have

$$Q(\{n_A\},L,T)=\sum_{\{n_A^o\},\{n_{\alpha\beta}^d\}}\Omega(\{n_A^o\},\{n_{\alpha\beta}^d\})\exp\left(-\frac{U(\{n_A^o\},\{n_{\alpha\beta}^d\})}{kT}\right) \tag{6}$$

To find the distributions $\left\{n_A^o\right\}$ and $\left\{n_{\alpha\beta}^d\right\}$ for which (5) and (6) are at their maximum, the Lagrangian multiplier method has been used. To that end the following unconstrained function has been chosen.

$$\begin{aligned}L(\{n_A^o\},\{n_{\alpha\beta}^d\})=\ln\Omega(\{n_A^o\},\{n_{\alpha\beta}^d\})-\frac{U(\{n_A^o\},\{n_{\alpha\beta}^d\})}{kT}+\sum_A\frac{n_A f_A}{kT}\\+\sum_{\alpha,d}\lambda_\alpha^d\left(\sum_\beta n_{\alpha\beta}^d-n_\alpha^d\right)+\lambda\left(\sum_A n_A-L\right)\end{aligned} \tag{7}$$

With the last two terms on the right-hand side of (7) all auxiliary conditions are considered. The Lagrangian multipliers $\{\lambda_\alpha^d\}$ and λ can be obtained by solving the following set of equations

$$\frac{\partial L}{\partial n_{\alpha\beta}^d}=-\ln\phi_{\alpha\beta}^d-1+\lambda_\alpha^d+\lambda_\beta^{-d}-\frac{\upsilon_{\alpha\beta}}{kT}=0 \tag{8}$$

for all α, β , d and

$$\frac{\partial L}{\partial n_A^o} = -\ln\phi_A^o - 1 + q + \sum_{\alpha,d} q_{A\alpha}^{od}\left(\ln\phi_\alpha^d - \lambda_\alpha^d\right) + \lambda - \frac{\upsilon_A^o}{kT} + \frac{f_A}{kT} = 0 \qquad (9)$$

for all A and o. Here, q is the total number of nearest neighbors of a molecule, which equals the co-ordination number of the lattice. The parameter $q_{A\alpha}^{od}$ is the number of faces α in direction d of a molecule A with an orientation o. Now the following quantities are defined.

$$C \equiv \exp(\lambda - 1 + q/2) \qquad (10)$$

$$C_A^o \equiv \exp -\frac{\upsilon_A^o}{kT} \qquad (11)$$

$$G_\alpha^d \equiv \phi_\alpha^d \exp\left(1/2 - \lambda_\alpha^d\right) \qquad (12)$$

$$\Lambda_A \equiv \exp\frac{f_A}{kT} \qquad (13)$$

The distribution of the molecules over the different orientations can be calculated with help of

$$\phi_A^o = \Lambda_A G_A^o \qquad (14)$$

where G_A^o is the statistical weight of a molecule A in orientation o. This factor is given by

$$G_A^o = CC_A^o \prod_{\alpha,d}\left(G_\alpha^d\right)^{q_{A\alpha}^{od}} \qquad (15)$$

In (15) it is shown that the weight factor has three contributions. First there is a contribution which is independent of the molecule type, accounted for by the quantity C, where -kTlnC can be regarded as the extra work needed to create space for a molecule in an inhomogeneous system with reference to a homogeneous bulk[16]. The other two contributions are related to the different types of interactions.
Besides equation (13) another relation for Λ_A can be also derived.

$$\Lambda_A = \frac{\theta_A}{\sum_o G_A^o} \tag{16}$$

In this expression is $\theta_A = \sum_o \phi_A^o$.
Equation (16) it possible to normalize the amount of a component by fixing θ_A. The system is then closed for molecules of type A.
The volume fractions are found by solving the equations (8) and (9) for all α, β, d, A, o. This can be done with numerical methods. More details can be found in the appendix.

2.5 Interaction with the electric field

In the previous section no explicit expression of υ_A^o has been given. This parameter should contain the interaction of a molecule A with orientation o with the external electric field. This part of the interaction will now be described by a semi-macroscopic approach.
Each molecule A in the system has an ideal dipole with a permanent moment μ_A and isotropic polarizability α_A. These quantities are here considered as scalars. The ideal dipole is assigned to a sphere with a radius a and a permittivity of 1. The sphere is surrounded by a continuum with a dielectric constant ε. This radius of the sphere is determined by the overall density of the liquid.

$$a^3 = \frac{3}{4\pi\rho} \tag{17}$$

In this expression is $\rho = \sum_{A\neq 0,o} \phi_A^o / v$, where v is the volume of a lattice site. This expression for a has been used by Onsager[4].
If a homogeneous electric field is present in a liquid then the molecules will tend to orient themselves in the direction of the field. The field interacting with the dipole of a molecule differs form the Maxwell-field because the dipole will polarize its surroundings. The part of the field which is responsible for orienting a molecule $(E_d)_A$ is given by

$$(E_d)_A = \frac{gE}{1 - 2f\frac{\alpha_A \rho}{3\varepsilon_0}} \tag{18}$$

where $g \equiv 3\varepsilon/(2\varepsilon+1)$ and $f \equiv (\varepsilon-1)/(2\varepsilon+1)$. Although the electric field is a vectorial quantity, for the present purpose it suffices to represent it as a scalar. Choices with respect to the orientation of the lattice in the field (in section 2.3) and the ensuing reduction of the number of dipole orientations make it possible to express all quantities as scalars, that will result in equations which are rather simple to understand.

The other part of the field is generated by the permanent moment of the dipole, which polarizes its surrounding. This part is called the reaction field[18] R_A.

$$R_A^o = \frac{2f\frac{\rho}{3\varepsilon_0}}{1-2f\frac{\alpha_A\rho}{3\varepsilon_0}}\mu_A^o \qquad (19)$$

Here $\mu_A^o = \mu_A \cos\theta_o$, with θ_O the angle between the directions of the dipole moment and the field. It is easy to see that μ_A^o equals μ_A, 0 or $-\mu_A$ in the parallel, perpendicular or anti-parallel situation, respectively. The induced part of the dipole moment is caused by polarization of the central molecule by the mean total internal field, $(E_i)_A$[18], which equals

$$(E_i)_A = (E_d)_A + \langle R_A \rangle = (E_d)_A + \frac{2f\frac{\rho}{3\varepsilon_0}}{1-2f\frac{\alpha_A\rho}{3\varepsilon_0}}\frac{\sum_o \phi_A^o \mu_A^o}{\sum_o \phi_A^o} \qquad (20)$$

With the help of the different components of the internal electric field an expression for υ_A^o can be derived. This parameter is the electrical energy of a molecule A in an external electric field and can be expressed as follows[18].

$$\upsilon_A^o = -\mu_A^o \cdot (E_d)_A - \mu_A^o \cdot R_A^o/2 - \alpha_A (E_i)_A^2/2 \qquad (21)$$

Only the first of the three terms on the right-hand side of (21) is really orientation dependent, as follows from (19) and (20). The other two terms contain a factor of 1/2 caused by certain entropic contributions due to changes in the surroundings and in the charge distribution of a molecule[18].

2.6 The dielectric constant

If a dielectric medium is placed in an electric field the following expression can be given

$$D = \varepsilon_0 E + P \tag{22}$$

where D is the dielectric displacement, E is the Maxwell field and P the polarization[26]. By using the relation $D=\varepsilon_0\varepsilon E$ the polarization can be related to the relative dielectric constant.

$$P = \varepsilon_0(\varepsilon - 1)E \tag{23}$$

In order to give a microscopic picture of ε, the relation between P and the various volume fractions of the liquid constituents are needed. P is given by[18]

$$P = \sum_A \rho_A \langle \mu_A \rangle + \sum_A \alpha_A \rho_A (E_i)_A \tag{24}$$

where ρ_A is the density of a molecule A and $\langle \mu_A \rangle$ the mean value of the permanent moment in the direction of the electric field. Within the formalism of the FOSCF model the dielectric constant can be expressed as:

$$\varepsilon = 1 + \sum_{A,o} \frac{\phi_A^o \mu_A^o}{v\varepsilon_0 E} + \sum_{A,o} \frac{\alpha_A \phi_A^o (E_i)_A}{v\varepsilon_0 E} \tag{25}$$

The right-hand side of (25) consists of three terms. The first term is the relative dielectric constant of vacuum. The second term is the permanent part and the third is the induced part of ε. It is easy to see that for $E \to \infty$ the permanent part goes to zero. If the density increases the dielectric constant has to increase.

2.7 Temperature dependence of the dielectric constant

The permittivity has been calculated as a function of the temperature, at a fixed pressure (~10^5 Nm^{-2}) and in a small electric field (10^5 Vm^{-1}). By applying such a small field strength we can "measure" the dielectric constant without perturbing the liquid structure to much.

In figure 2 the predicted permittivity has been plotted and compared with experimental data[27] and results of MD simulations for a variety of water models[28-31].

The absolute value of the predicted permittivity is of the right order and at low temperatures (~273 K) also close to the experimental one. Most of the water models, used in MD calculations, are unable to predict the permittivity satisfactorily. Only the flexible SPC model[28] and the SPC/E model[30,31] come close to the experimental data. The advantage of the FOSCF calculations is that they have been made without tuning the interaction parameters on the dielectric behavior, see section 2.2. Therefore, the present results confirm the earlier experiences[17] that the theory treats bulk liquid water in a correct manner.

At high temperatures the dielectric constant is somewhat overestimated by the theory (~10% at 353 K). This is not very amazing. The calculations have been performed at a fixed pressure. Besseling and Lyklema[17] have already shown that at elevated temperatures the FOSCF theory overestimates the density. The permittivity increases with an increasing density, which follows from equation (25).

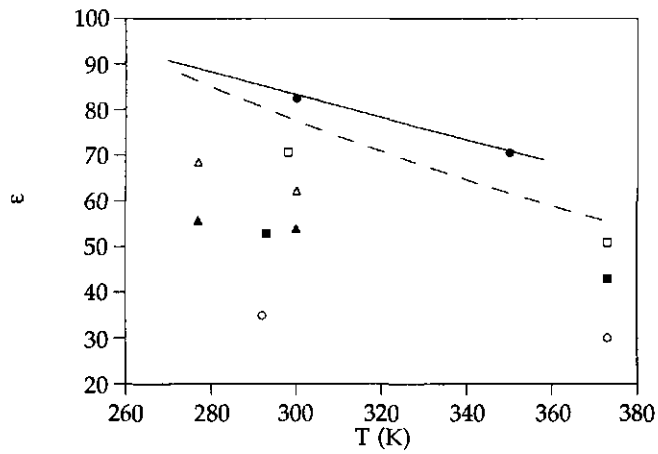

Figure 2 The temperature dependence of the permittivity at fixed pressure (~1 Atm.) and a low field strength (10^5 Vm^{-1}). Experimental results[27] (- - -), FOSCF calculations (——) and MD simulations with flexible SPC[28] (●), MCY[29] (○), TIP4P[42] (■), SPC/E[30] (□), SPC[31] (▲) and SPC/E[31](△).

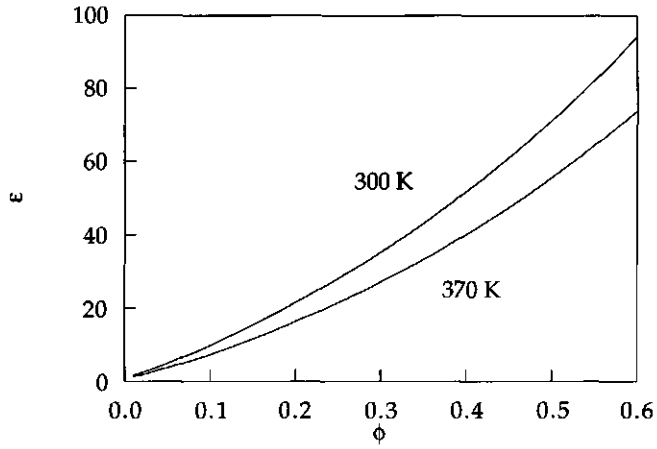

Figure 3 The density (volume fraction) dependence of the permittivity at two fixed temperatures (300 K and 370 K).

In figure 3 the dependence of the theoretical permittivity on the density has been plotted. It is clear from this figure that the permittivity is very sensitive to the density and the overestimation of the permittivity can be attributed to overestimation of the density.

From the dielectric constant we can extract some structural information by calculating the dipolar correlation parameter, g_K, with the help of the Kirkwood-Fröhlich equation[6].

$$\frac{\left(\varepsilon - n^2\right)\left(2\varepsilon + n^2\right)}{\varepsilon\left(n^2 + 2\right)^2} = \frac{\rho\mu^2}{9\varepsilon_0 kT} g_K \tag{26}$$

Here n is the refractive index, which can be calculated with the Clausius-Mossoti equation[18].

$$\frac{n^2 - 1}{n^2 + 2} = \frac{\rho\alpha}{3\varepsilon_0} \tag{27}$$

The correlation factor, g_K, gives information about the co-ordination of a central dipole by neighboring dipoles and the relative orientations of these

dipoles with respect the central dipole. An approximate geometrical formula is given by the following equation[32].

$$g_K = 1 + Z\langle \cos\theta_{ij} \rangle \qquad (28)$$

In this expression Z is the average co-ordination number of a dipole i and $\langle \cos\theta_{ij} \rangle$ the average of all orientations of the neighboring dipoles j.
In figure 4 the predicted correlation factor has been plotted and again compared with the experimental results[33] and MD predictions[28-31] The predictions of the FOSCF theory come close to the experimental values. The temperature dependence is not as strong as found experimentally but the sign and the order of magnitude are right. The slight underestimation of the slope can again be attributed to the overestimation of the density at higher temperatures. Of all the water models used in MD simulations only the SPC/E[30,31] model is able to predict the right temperature dependence.
The predictions of the permittivity and the Kirkwood correlation factor make clear that in small electric fields electrical interactions and hydrogen bonds can be treated independent of each other. The results also indicate that the

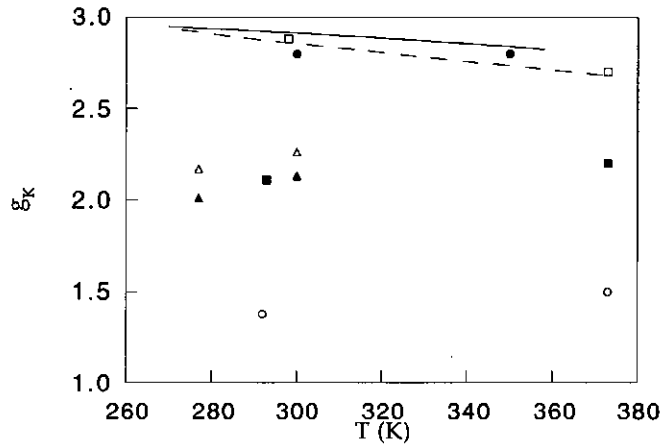

Figure 4 The temperature dependence of the Kirkwood correlation factor at fixed pressure (~1 Atm.) and a low field strength (10^5 Vm^{-1}). Experimental results[27] (- - -), FOSCF calculations (——) and MD simulations with flexible SPC[28] (●), MCY[29] (○), TIP4P[42] (■), SPC/E[30] (□), SPC[31] (▲) and SPC/E[31](△).

associative behavior of water, which is a consequence of the hydrogen bond network, strongly enhances the permittivity[19].

2.8 Dielectric saturation

Increasing the field strength in a liquid will have two effects. All dipoles will orient in the field, but after all dipoles have oriented, the polarization no longer follows the field and the dielectric constant decreases (dielectric saturation). Dielectric saturation and electrostriction are not additive phenomena. Nevertheless, treating them separately has some value in understanding the underlying physical principles. In this study, we only pay attention to the saturation phenomenon.

In this section the influence of the local structure of water on the saturation behavior is studied. This is done by fixing the density of water in the system. Calculations have been done at 300 K and a volume fraction of 0.555. In figure 5 the permittivity is computed as a function of the field strength. The predicted saturation curve has an unexpected feature. Before the permittivity decreases it passes through a maximum.

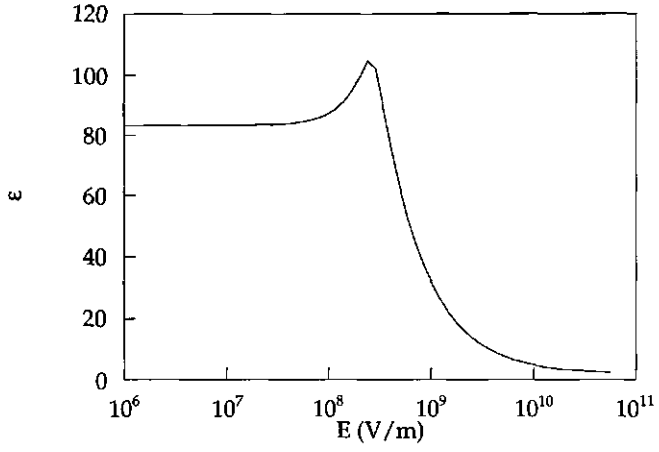

Figure 5 The field strength dependence of the dielectric constant at a fixed temperature (300 K) and density (ϕ=0.555).

For different liquids and liquid mixtures it is known that such a behavior is caused by strong co-operative orientation of the dipoles[18]. Although water is a strongly associated liquid a behavior as shown in figure 5 has so far not been reported. Scarce measurements, up to a field strength of 10^7 Vm^{-1}, indicate that the permittivity decreases monotoneously[33]. MD simulations, which go to 10^{10} Vm^{-1}, point in the same direction[34,35]. Other older semi-macroscopic theories[8,9,11] have also predicted the more accepted dielectric saturation behavior without a maximum. However this is not caused by a better description of water. In these simple theories the local tetrahedral structure around a water dipole is supposed not to change if a field is applied[8]. This results in an increase of the dipole moment. However the orientation of the dipoles is assumed not to be affected by its local surrounding.

On the other hand recent MD simulations of water in an applied field indicate that in some situations water does exhibit idiosyncracies. For instance, super cooled liquid water seems to crystallize (cubic ice, Ic) due to the presence of a strong electric field[36]. Normal liquid water, confined between two charged planes, also restructures in a high electric field[37,38].

As in our theory low-field permittivity is predicted well, the probably unphysical saturation behavior of the model may be a consequence of a poor description of the intermolecular interactions in a highly oriented system.

The structure of oriented water deviates from bulk water. Watts[39] has theoretically studied the influence of the electric field on the dipolar and O-H correlation functions of BNS (Ben Naim Stillinger) water. He calculated these functions in the absence and in the presence of a very high field ($\pm 10^{10}$ Vm^{-1}) and found that the O-H correlation disappeared and the dipole correlation appeared when the field was applied. This implies that the number of hydrogen bonds per unit volume decreases when the field strength increases. This phenomena could be caused by a weakening of this bond because the tendency to orient in the field could force the acceptor-donor pair out of favorable linear configuration. It could also be caused by the existence of additional local intermoleculair forces due to alignment of the dipoles.

There are two ways to tackle this problem. Either the model can be given more freedom in choosing its liquid structure or the interactions can be made field dependent. Within the framework of a lattice approach the former way is nearly impossible so we shall consider the latter. This means that we have to introduce a suitable field dependence of the hydrogen bond strength. We have one well known boundary condition, the zero field situation. To keep

the number of parameters as small as possible, only the hydrogen bond energy has been made field dependent. The following equation describes the chosen field strength dependence of the hydrogen (Acceptor-Donor) energy

$$u_{AD} = u^0_{AD} \exp -|E/\xi| \qquad (29)$$

where u^0_{AD} is the hydrogen bond energy in the absence of the electric field and ξ (Vm^{-1}) is a decay parameter.

In figure 6 again the field strength dependence of the dielectric constant has been plotted. The different curves corresponds to different values of ξ. The curve for ξ=0 represents the situation of no hydrogen bonding. In the linear region the permittivity drops to about 30, which is the Onsager value of the low-field permittivity[4]. The curve for ξ=∞ represents the situation of constant hydrogen bond energy. This curve is the same as that in figure 4.

The parameter ξ represents the field strength where the hydrogen bond network breaks down. If one would choose ξ=10^7 Vm^{-1}, much lower than the saturation point (where all dipoles have been oriented), a transition takes place from a linear region of high permittivity to one of low permittivity, representing a transition from a hydrogen bonded dipole system to a system of independent dipoles. Alternatively, for ξ=10^{10} Vm^{-1}, much higher than the saturation point, the calculated curve is nearly the same as in figure 5. This is logical. Up to the saturation point the hydrogen bond network plays a role in the field strength behavior. After this point all dipoles have oriented, the permanent moment has reached its maximum value, which is exactly the same for a hydrogen-bonded network of dipoles and an independent set of dipoles, equation (25).

Using ξ=$4 \cdot 10^8$ Vm^{-1} results in a curve of which the initial saturation, up to 10^7 Vm^{-1}, differs not much from the experimental results of Kolodziej[33], the permittivity is reduced by less than about 0.25%. At higher values of ξ, the maximum appears. So it is concluded that the maximum is a feature that is not at variance with physical reality. However, detecting its presence or absence experimentally is not an easy problem.

In figure 7 again saturation curves are shown, but now the influence of ξ on the maximum is shown in more detail. Although it is impossible to conclude from figure 5, 6 and 7 something about the real behavior of the hydrogen bond network, it is clear that the results are very sensitive to the way of modelling.

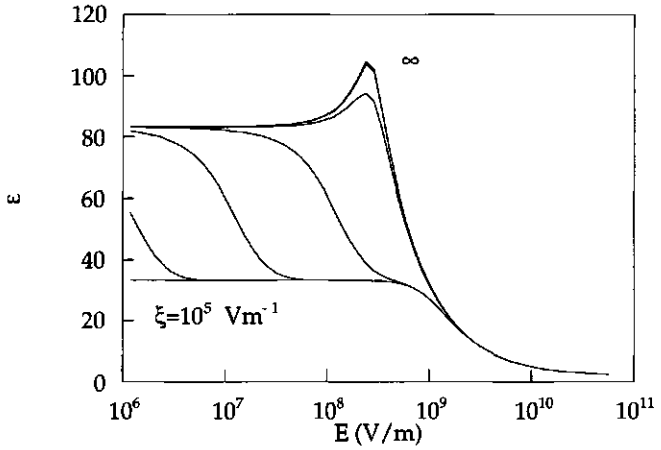

Figure 6 The field strength dependence of the dielectric constant at a fixed temperature (300 K) and density (ϕ=0.555). The different curves correspond with different values of the decay parameter ξ, which controls the field strength dependence of the hydrogen bond energy (ξ=10^5, 10^6, 10^7, 10^8, 10^9, 10^{10} and ∞ Vm^{-1}).

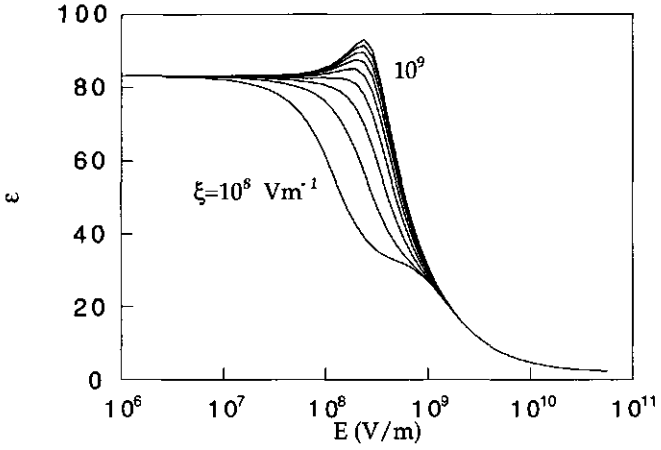

Figure 7 As figure 6, but for a narrow range of ξ ($1{\cdot}10^8$,$2{\cdot}10^8$,.....,$1{\cdot}10^9$ Vm^{-1}).

The point at which the maximum has been predicted coincides with the point where the dipole-field interaction becomes of order kT and of the same order as the local interactions (hydrogen bonds). This means that in this point the model is particulary sensitive to the way of modelling the interactions. Decoupling of the local interactions and the dipole-field interactions, the consequence of equation (3), fails around this point. It also means that the structure of water in a strong electric field is not simply the same as in the absence of a field.

2.9 Conclusions

With the help of the FOSCF theory the low field permittivity of water and its temperature dependence have been calculated. The results agree with experimental data of the temperature dependence of the dielectric constant and the Kirkwood-correlation factor. The hydrogen bonds substantially contribute to the high dielectric constant of water and a decoupling of hydogen bonds and dipole-field interactions appears to be justified.
The slight overestimation of the permittivity and the correlation factor at higher temperatures can be explained with the overestimation of the density at these temperatures.
The predicted field strength dependence does not in all respects agree with experiments and MD simulations. Under certain conditions a maximum in the permittivity is predicted, which may or may not be real. This maximum could be a consequence of the use of field-independent parameters for the local interactions (H bonds) and the lattice, which fixes the liquid structure.
By making the hydrogen bond energy field dependent it was possible to modify the saturation curve. The maximum is very sensitive to the value selected for this energy, which is rather logical because near this maximum the energy of a field-dipole interaction is close to the energy of a hydrogen bond. It is not yet possible to make definitive statements about the coupling of local and non-local interactions, although it is certain that, to agree with experiments the hydrogen bond structure has to break down. For this reason the properties of water at extremely high field strength deserve further theoretical and experimental study.

Appendix Numerical method

The set of equations (8) and (9) can be solved with a Newton-type iteration method, developed by Powell[40] and made more powerful by Scheutjens[41]. The iteration method needed for the FOSCF theory has already been described by Besseling and Scheutjens[16]. In this appendix only new features will be regarded.

The calculations are performed with a two-step iteration method. The inner loop is the same as used by Besseling. If the equations (18)-(20) are considered, it is easy to see that for start values for the permittivity ε, the density ρ and the mean orientation of the permanent dipole moment $\langle \mu_A \rangle$ are also needed. In the outer loop of the iteration these quantities will be iterated to their real values.The iteration variables are now defined as follows

$$x_\varepsilon \equiv \sqrt{\varepsilon} \tag{A.1}$$

$$x_{\mu_A} = \frac{\sum \phi_A^o \mu_A^o}{\mu_A \sum \phi_A^o} \tag{A.2}$$

With (A.1) and (A.2) values can be calculated for ε and $\langle \mu_A \rangle$, with these values the equations (18)-(20) become useful. After an iteration step these quantities are compared with the values calculated for these quantities from (14) and (24). This means that the following functions are iterated to zero.

$$f_\varepsilon \equiv 1 - \frac{x_\varepsilon^2}{\varepsilon} \tag{A.3}$$

$$f_{\mu_A} \equiv x_{\mu_A} - \frac{\sum \phi_A^o \mu_A^o}{\mu_A \sum \phi_A^o} \tag{A.4}$$

References

1. Hill, N.E., Vaughan, W.E., Price, A.H. & Davies, M. *Dielectric Properties and Molecular Behaviour* (Van Nostrand Reinhold Compagny, London, 1969).
2. Torrie, G.M., Kusalik, P.G. & Patey, G.N. *J. Chem. Phys.* **88**, 7827 (1988).
3. Leikin, S., Parsegian, V.A. & Rau, D.C. *Ann. Rev. Phys. Chem.* **44**, 369 (1993).

4. Onsager, L. *J. Am. Chem. Soc.* **58**, 1487 (1936).
5. Kirkwood, J.G. *J. Chem. Phys.* **7**, 911 (1939).
6. Frölich, H. *Theory of Dielectrics* (Clarendon Press, Oxford, 1958).
7. Kielich, S. in *Dielectric and Related Molecular Processes - Volume 1* (eds. Davies, M.) (Burlington House, London, 1972).
8. Booth, F. *J. Chem. Phys.* **19**, 391 (1951).
9. Booth, F. *J. Chem. Phys.* **23**, 453 (1955).
10. Buckingham, A.D. *J. Chem. Phys.* **25**, 428 (1956).
11. Schellman, J.A. *J. Chem. Phys.* **26**, 1225 (1957).
12. Stell, G., Patey, G.N. & Høye, J.S. *Adv. Chem. Phys.* **48**, 183 (1981).
13. Martina, E. & Stell, G. *Phys. Rev. A* **24**, 2765 (1981).
14. Rasaiah, J.C., Isbister, D.J. & Stell, G. *Chem. Phys. Lett.* **79**, 189 (1981).
15. Ramshaw, J.D. *J. Chem. Phys.* **73**, 5294 (1980).
16. Besseling, N.A.M. & Scheutjens, J.M.H.M. *J. Phys. Chem.* **98**, 11597 (1994).
17. Besseling, N.A.M. & Lyklema, J. *J. Phys. Chem.* **98**, 11610 (1994).
18. Böttcher, C.J.F. *Theory of Electric Polarization* (Elsevier, Amsterdam, 1973).
19. Goldman, S. & Joslin, C. *J. Phys. Chem.* **97**, 12349 (1993).
20. Scheutjens, J.M.H.M. & Fleer, G.J. *J. Phys. Chem.* **83**, 1619 (1979).
21. Scheutjens, J.M.H.M. & Fleer, G.J. *J. Phys. Chem.* **84**, 178 (1980).
22. Leermakers, F.A.M. & Scheutjens, J.M.H.M. *J. Chem. Phys.* **89**, 3264 (1989).
23. Smyth, C.P. *Dielectric Behavior and Structure* 1-441 (McGraw-Hill, New York, 1955).
24. Israelachvilli, J.N. *Intermolecular and Surface Forces* (Academic Press, London, 1985).
25. Franks, F. in *Water a comprehensive treatise* (eds. Franks, F.) (Plenum, New York, 1972).
26. Jackson, J.D. *Classical Electrodynamics* (John Wiley&Sons, New York, 1975).
27. in *CRC Handbook of Chemistry and Physics* (eds. Lide, D.R.) (CRC Press, Boca Raton, 1993).
28. Anderson, J., Ullo, J.J. & Yip, S. *J. Chem. Phys.* **87**, 1726 (1987).
29. Neumann, M. *J. Chem. Phys.* **82**, 5663 (1985).
30. Reddy, M.R. & Berkowitz, M. *Chem. Phys. Lett.* **155**, 173 (1989).
31. Smith, P.E. & Vangunsteren, W.F. *J. Chem. Phys.* **100**, 3169 (1994).
32. Oster, G. & Kirkwood, J.G. *J. Chem. Phys.* **11**, 175 (1943).
33. Kolodziej, H.A., Jones, G.P. & Davies, M. *J. Chem. Soc. Faraday Trans. II* **71**, 269 (1975).

34. Alper, H.E. & Levy, R.M. *J. Chem. Phys.* **91**, 1242 (1989).
35. Alper, H.E. & Levy, R.M. *J. Chem. Phys.* **94**, 8401 (1990).
36. Svishchev, I.M. & Kusalik, P.G. *Phys. Rev. Lett.* **73**, 975 (1994).
37. Wanatabe, M., Brodsky, A.M. & Reinhardt, W.P. *J. .Phys. Chem.* **95**, 4953 (1991).
38. Xia, X. & Berkowitz, M.L. *Phys. Rev. Lett.***74**, 3193 (1995).
39. Watts, R.O. *Chem. Phys.* **57**, 185 (1981).
40. Powell, M.J.D. in *Numerical methods for nonlinear algebraic equations* (eds. Rabinowitz, P.) (Gordon and Breach, London, 1970).
41. Scheutjens, J.M.H.M. *Newton.sim. A Simula class for unconstrained optimation.* (Wageningen, 1980).
42. Neumann, M. *J. Chem. Phys.* **85**, 1567 (1986).

Chapter 3

The adsorption of nonionic surfactants in hydrophilic cylindrical pores I: a thermodynamic analysis

Abstract The adsorption of a nonionic surfactant on a hydrophilic surface has been treated as a phase transition between a dilute, gas-like, (I) and a bilayer (II) phase. A Kelvin-like expression for the influence of the pore curvature on the adsorption behavior could be derived. According to this expression the shift in the chemical potential due to the curvature is proportional to the curvature energy of the bilayer.
Using a molecular model, which contains a mean-field approximation, the curvature energy has been related to the affinity for the surface of the bilayer. The curvature energy at the point of phase transition increases with the affinity of the surfactants for the surface. As a consequence, the effect of curvature on the phase transition increases with affinity. The higher the affinity the more formation of a bilayer in the pore is promoted over the same at a flat surface.
The chosen phase transition model will hold as long as the adsorption changes rapidly at a given concentration, which is at least the case for surfactants with short headgroups.

3.1 Introduction

The behavior of fluids in pores of mesoscopic size has been studied extensively from experimental[1-6] and theoretical points[7-10] of view. The partitioning of macromolecules between a bulk solution and a pore also has some history[11-14]. However the influence of pores on the adsorption of small molecules from solution, far away from a two-phase region, has never been studied systematically. This is not very surprising. Usually molecules, which are soluble, adsorb in layers with a thickness corresponding to their molecular size. The correlations of the molecules in such a layer extend over length scales of their own size. Therefore, the adsorption will only be influenced by a pore if its radius is of the same order as the thickness of the adsorbed layer or, for that matter, if the pore wall is curved on molecular length scales. In the case of relatively small molecules like surfactants it is very difficult to observe this phenomenon experimentally. In order to be able to couple changes in the adsorbed amount to the pore size, the standard deviation of the mean pore

size of a adsorbent has to be smaller than the difference in the mean pore size between different adsorbents, which is very difficult on that length scale.
Nevertheless, a few studies are known, which deal with the adsorption of nonionic[15,16] and cationic surfactants[17] on porous silica and glass. Although these experiments do not allow quantitative conclusions to be drawn, at least two qualitative trends have been established. First, the adsorption plateau value decreases if the pore size decreases. Second, the step in the adsorption isotherm shifts to lower concentration, particulary so if the pores become very narrow. Recently, we have published calculations with a Mean Field Lattice (MFL) theory, which reproduce these phenomena[18]. In the present study we intend to explain these phenomena from a more rigorously theoretical point of view. The behavior of liquid-liquid, liquid-gas[19-22] and membrane-like[23-25] surfaces have been studied extensively by theoreticians. They relate the curving behavior to properties of the flat surface. In the present study we will extend the ideas developed in that area and apply them to the case of adsorption of nonionic surfactants from solution on a porous hydrophilic solid surface.
To simplify the problem we will treat the pore as an infinitely long cylinder with a curvature J=-1/R. In the MFL theory the adsorption is regarded as a phase transition from a dilute to a bilayer-like surface phase. The appropriateness of this approach depends on the type of surfactant used.

3.2 The adsorption isotherm

As we want to study the influence of the pore on the adsorption of nonionic surfactant, we will spend a few words on the adsorption behavior of this type of surfactant.
Figure 1 is a schematic picture of an adsorption isotherm of a nonionic surfactant on a hydrophilic adsorbent. In this picture three regimes have been drawn. The first regime (I) corresponds to the situation of low surface coverage. Here, the driving force of adsorption is the interaction between the surface and the headgroup of the surfactant. Lateral interactions play a minor role. It seems reasonable to assume a flat conformation of the surfactant at the surface because this conformation reduces the number of unfavorable contacts between water and the hydrophobic tail segments. This mode of adsorption has been drawn in figure 2[a]. The last regime (II) is related to the situation of high surface coverage.

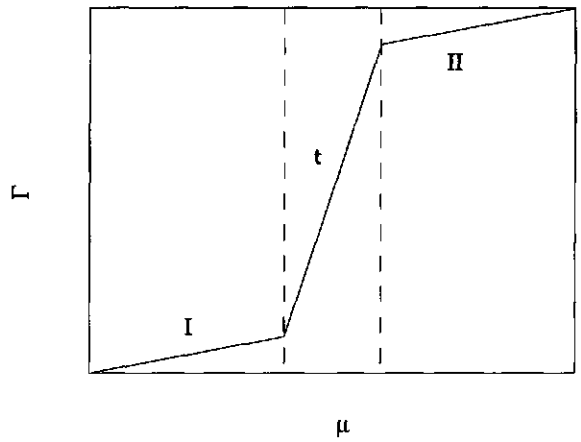

Figure 1 A schematical plot of the amount of a nonionic surfactant adsorbed at a hydrophilic surface against its chemical potential. The isotherm can be divided in three stages: (I) isolated molecules on the surface, (t) small aggregates on the surface, which grow with the chemical potential and (II) bilayer or micellar like structures, which cover the whole surface.

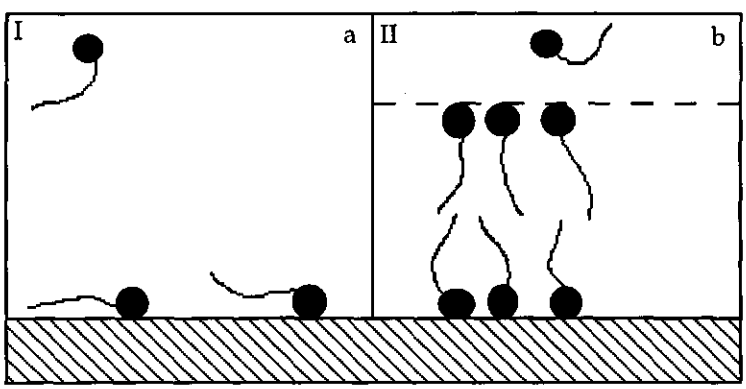

Figure 2 Possible structure of the adsorbed layer in phase I (a) and II (b). In phase I, the molecules adsorb isolated on the surface and have a flat conformation. In phase II, the molecules adsorb in bilayer or micellar-like structures on the surface.

Micellar or bilayer-like structures have been formed on the surface, for instance as in figure 2[b]. Regime t is the transition region between I and II. For surfactants usually a steep increase in adsorption is observed over a short concentration interval. The shape of the aggregates is not well defined because large form fluctuations play an important role. If the concentration range of t becomes very narrow, the adsorption step can be regarded as a pseudo first order phase transition from a dilute phase I to a condensed phase II, as shown in figure 3.

Until now, the exact structure of phase II was a subject of discussion, because methods used to elucidate this structure require much interpretation. However, it is clear that the aggregates on the surface are micelle- or bilayer-like structures. Experiments have shown that the step in the adsorption isotherm becomes steeper if the length of the headgroup decreases[26,27]. Neutron reflection[28,29] and AFM studies[30] appear to indicate that the bilayer-like associates in the adsorbed layer become larger if the headgroup is smaller. For example the adsorption isotherm of a $C_{12}E_5$ surfactant shows a very steep step[31]. From all these observations we conclude that the adsorption step approaches to a first order phase transition if the headgroup becomes smaller. This is the case that will be considered in this paper.

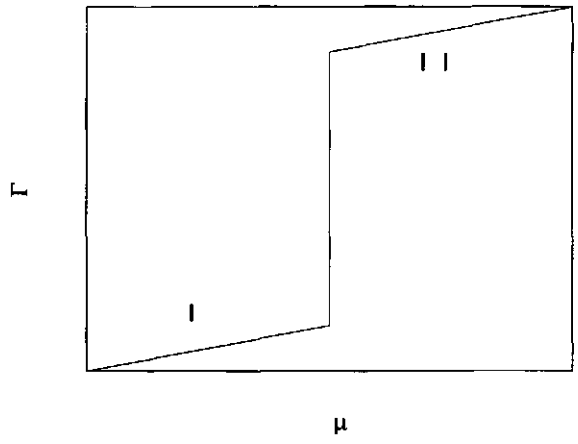

Figure 3 As in figure 1, but now stage t has disappeared.

3.3 Thermodynamics

3.3.1 Gibbs' law

If one studies adsorption from solution on a flat surface, the interfacial tension γ and the surface pressure π are the important properties. They contain information about the state of the surface and π can be determined by experiments.

$$\pi \equiv \gamma^* - \gamma \tag{1}$$

Here, γ and γ^* are the surface tensions of the surface with and without an adsorbed layer. The quantities γ and π can be related to the excess amounts of the different components with Gibbs' law,

$$A d\gamma = -A d\pi = -S^{\sigma} dT - \sum_{i=1}^{\nu} N_i^{\sigma} d\mu_i \tag{2}$$

where μ_i is the chemical potential of component i, A is the surface area, T the temperature and S^{σ} the excess entropy.
Equation (2) is not sufficient to describe the state of a cylindrical pore. The state of the pore is not only determined by the surface tension but also by the pressure difference Δp with the bulk,

$$\Delta p \equiv p^{\alpha} - p^{\beta} \tag{3}$$

where p^{α} and p^{β} are the pressure in the centre of the pore and in the bulk, respectively. If the bulk phase is in equilibrium with the pore phase, a pressure difference can have different origines. First, there may be an interface between the bulk and pore phase, which is curved, leading to a laplace pressure. Alternatively, a concentration difference between the bulk and the center of the pore may exist, because the decay length of the excess density profile is of the order of the pore radius, which gives rise to an osmotic pressure, which is commonly called the Donnan osmotic pressure. This is what happens in charged pores as the Debye screening length is of the same order of magnitude as the pore radius or less than that. In our case we have no interface and a pressure difference will be of the last type.

In a cylindrical pore, the object of this study, the influence of the curving on the adsorbed layer must also be made explicit. First, we have to define the system. It consists of a cylindrical pore in a solid, at equilibrium with a bulk solution with a constant composition. The length of the pore is so large, that end-effects can be neglected. The volume of the system, V, is the sum of the pore volume and the volume of the bulk solution. The solid is inert and not considered.

To come to an expression, equivalent to (2), we describe the state of our system at given V, T and μ's. The characteristic function of the system is therefore the grand potential Ω. A reversible change of the state of the system can be described as:

$$d\Omega = -SdT - p^{\beta}dV + \tau dA - \sum_{i=1}^{v} N_i d\mu_i + \kappa dJ \qquad (4)$$

where S is the total entropy, N_i the total number of molecules of component i and J the mean curvature of the surface, which is negative for a concave (pore) and positive for a convex surface. The intensive properties τ and κ are related to γ and Δp and phenomenologically defined through:

$$\tau = \left(\frac{\partial \Omega}{\partial A}\right)_{V,T,\mu's,J} \qquad (5)$$

$$\kappa = \left(\frac{\partial \Omega}{\partial J}\right)_{V,A,T,\mu's} \qquad (6)$$

The surface area A is an extensive variable and its variation at constant J, called for in (5), implies increasing the length of the pore at fixed radius. The curvature J is an intensive property. Integration of (4) results in:

$$\Omega = -p^{\beta}V + \tau A \qquad (7)$$

The system can be divided in a liquid phase β (the bulk), with p^{β} and V^{β}, a liquid phase a (the pore), with p^{α} and V^{α}, and a surface region, with γ and A, to which all interfacial excesses are assigned. Therefore, the grand potential of the total system can also be written as,

$$\Omega = -p^{\beta}V - \Delta p V^{\alpha} + \gamma A \qquad (8)$$

With equation (8) we are able to identify τ and κ in terms of γ and Δp. In equation (4),(7) and (8) V^{α}, A and J are related through,

$$V^{\alpha} = \frac{\pi L}{J^2} = -\frac{A}{2J} \tag{9}$$

$$A = -\frac{2\pi L}{J} \tag{10}$$

we obtain, using (7)-(9),

$$\tau = \gamma + \frac{\Delta p}{2J} \tag{11}$$

and, using (6) and (8)-(10),

$$\frac{\kappa}{A} = \left(\frac{\partial \gamma}{\partial J}\right)_{V,A,T,\mu's} + \frac{1}{2J}\left(\frac{\partial \Delta p}{\partial J}\right)_{V,A,T,\mu's} - \frac{\Delta p}{2J^2} = C - \frac{\Delta p}{2J^2} \tag{12}$$

Where C is the curvature Helmholtz energy of the surface layer. Henceforth we shall call C the curvature constant. With the help of (11) and (12) we can rewrite (4) to obtain,

$$d\Omega = -SdT - p^{\beta}dV + \left(\gamma + \frac{\Delta p}{2J}\right)dA - \sum_{i=1}^{v} N_i d\mu_i + A\left(C - \frac{\Delta p}{2J^2}\right)dJ \tag{13}$$

It is noted that (4) and (13) describe the state of the liquid part of the system, including the interfacial excesses but excluding the solid phase. Due to the inert character of this solid phase, the curvature is externally imposed; it is not an equilibrium property. As the pore forces the liquid into a certain geometry, Ω is not a minimum as a function of A, J and V^{α}, $\delta\Omega \neq 0$. Therefore there is no unique relation between the Δp, γ and C, like

$$\Delta p = -\gamma J + CJ^2 \tag{14}$$

which would have been obtained from (13) by differentiating with respect to J, keeping the length of the cylinder constant and using the equilibrium criterion that $\delta\Omega=0$. As a consequence, there is not necessarily a pressure difference between the pore and the bulk, even as the surface tension is non-

zero. This means that the Laplace equation, (14), may not be applied to this case.

In (7) and (8) the $-p^{\beta}V$ suffices to describe the state of the system if the pore is absent. Therefore the excess grand potential is defined as follows,

$$\Omega^{\sigma} \equiv \Omega + p^{\beta}V = -\Delta p V^{\alpha} + \gamma A \tag{15}$$

and its differential is given by,

$$d\Omega^{\sigma} = -SdT + Vdp^{\beta} + \left(\gamma + \frac{\Delta p}{2J}\right)dA - \sum_{i=1}^{v} N_i d\mu_i + A\left(C - \frac{\Delta p}{2J^2}\right)dJ \tag{16}$$

If we define the following excess quantities,

$$N^{\sigma} \equiv N - N^{\beta}\left(\frac{V}{V^{\beta}}\right) \tag{17}$$

$$S^{\sigma} \equiv S - S^{\beta}\left(\frac{V}{V^{\beta}}\right) \tag{18}$$

and recognize that we can write down the following Gibbs-Duhem equation for the solution with which the pore is at equilibrium,

$$Vdp^{\beta} - \left(\frac{V}{V^{\beta}}\right)\left(S^{\beta}dT + \sum_{i=1}^{v} N_i^{\beta} d\mu_i\right) = 0 \tag{19}$$

equation (16) can be rewritten in terms of excess quantities:

$$d\Omega^{\sigma} = -S^{\sigma}dT + \left(\gamma + \frac{\Delta p}{2J}\right)dA - \sum_{i=1}^{v} N_i^{\sigma} d\mu_j + A\left(C - \frac{\Delta p}{2J^2}\right)dJ \tag{20}$$

With (19), equation (20) can be rewritten as

$$d\Omega^{\sigma} = -S^{\sigma(1)}dT + \left(\gamma + \frac{\Delta p}{2J}\right)dA - \sum_{i=2}^{v} N_i^{\sigma(1)} d\mu_i + A\left(C - \frac{\Delta p}{2J^2}\right)dJ \tag{21}$$

where $S^{\sigma(1)}$ and $N_i^{\sigma(1)}$ are the relative excess entropy and amount of component i, respectively. These quantities are defined as:

$$S^{\sigma(1)} = S^{\sigma} - \frac{S^{\beta}}{N_1^{\beta}} \tag{22}$$

$$N_i^{\sigma(1)} = N_i^{\sigma} - \frac{\rho_i^{\beta}}{\rho_1^{\beta}} N_1^{\sigma} \tag{23}$$

Here, ρ_i^{β} and ρ_1^{β} are the bulk densities of component i and 1, the solvent, respectively. Note that we have eliminated the chemical potential of the solvent. For dilute solutions this is the usual procedure to obtain surface excesses in the Gibbs convention.

We can obtain a relation for the curvature constant C by cross-differentiating between the dA and dJ terms of equation (21):

$$C = \left(\frac{\partial \gamma}{\partial J}\right)_{A,T,\mu_i's} + \frac{1}{2J}\left(\frac{\partial \Delta p}{\partial J}\right)_{A,T,\mu_i's} \tag{24}$$

The curvature dependence of the excess amount adsorbed in the pore is another important quantity. It also follows from (21) by cross-differentiation:

$$\frac{1}{A}\left(\frac{\partial N_i^{\sigma(1)}}{\partial J}\right)_{\mu_i's,A,T} = \frac{1}{2J}\left(\frac{\partial \Delta p}{\partial \mu_i}\right)_{\mu_j's(j\neq i),A,J,T} - \left(\frac{\partial C}{\partial \mu_i}\right)_{\mu_j's(j\neq i),A,J,T} \tag{25}$$

Differentiation of (15) and equating the result with (21) results in Gibbs'law for a cylindrical pore.

$$A\left(d\gamma + \frac{1}{2J}d\Delta p\right) = -S^{\sigma(1)}dT - \sum_{i=2}^{\nu} N_i^{\sigma(1)} d\mu_i + ACdJ \tag{26}$$

If (26) is compared with its equivalent for a flat surface (2), the two differences are the addition of the ACdJ term, which accounts for the curvature Helmholtz energy of the adsorbed layer, and the $d\Delta p$ term, caused by the pressure difference between the interior of the cylinder and the bulk of the solution. For flat surfaces these two terms are absent. As the solution of our interest contains only two components, water (w) and a nonionic surfactant (s), and is rather dilute ($x_s << x_w$), we will henceforth drop the subscript i and make use of absolute excess amounts in the next section, $N_i^{\sigma(1)} \approx N_i^{\sigma}$ and $S^{\sigma(1)} \approx S^{\sigma}$. Water takes the role of component 1.

3.3.2 Phase transitions and curvature

In adsorbates on a pore[8,32] and also at a flat surface[33] phase transitions can occur. The curvature influences the bulk condition (μ's) where these phase transitions take place. Two stable phases will coexist if the excess grand potentials equal each other.

$$\Omega^{\sigma,I} = \Omega^{\sigma,II} \qquad \text{and} \qquad \gamma^{I} + \frac{\Delta p^{I}}{2J} = \gamma^{II} + \frac{\Delta p^{II}}{2J} \tag{27}$$

In our case, the phases I and II correspond with a surface of low coverage (isolated surfactant molecules) and high coverage (bilayer-like structure), respectively, see section 3.2.

To establish the coexistence conditions we consider the coupling between infinitesimal changes in (μ, T, J) have to be brought about in such a way that I and II remain at its equilibrium. From (26) it follows,

$$\begin{aligned}\left(S^{\sigma,I} - S^{\sigma,II}\right)dT + \left(N^{\sigma,I} - N^{\sigma,II}\right)d\mu \\ - A(C^{I} - C^{II})dJ + \frac{A}{2J}\left(\Delta p^{I} - \Delta p^{II}\right)dJ = 0\end{aligned} \tag{28}$$

Where μ is the chemical potential of the surfactant. This equation shows how changes in T, μ and J have to be related to maintain equilibrium. In the centre of the pore the two coexisting phases are not separated by an interface. Therefore, in equilibrium $\Delta p^{I} - \Delta p^{II}$ vanishes.

Then from (28), a Clapeyron-like expression for the curvature influence on the chemical potential, where the phase transition occurs, can be obtained,

$$\left(\frac{\partial \mu}{\partial J}\right)_{T} = \left(\frac{C^{I} - C^{II}}{\Gamma^{I} - \Gamma^{II}}\right)_{\mu,J} \tag{29}$$

where $\Gamma^{I}=N^{\sigma,I}/A$ and $\Gamma^{II}=N^{\sigma,II}/A$. In principle it is possible to calculate the chemical potential of the phase transition, $\mu^{\#}$, at given J as the dependencies on μ and J of C and Γ are known. To obtain an idea about what could happen, we expand γ in Taylor series with respect to $\Delta\mu^{ref} \equiv \mu - \mu^{ref}$ and J,

$$\gamma = \sum_{n,m\geq 0} \frac{1}{n!m!}\left(\frac{\partial^{n+m}\gamma}{\partial\mu^n\partial J^m}\right)_0^{ref} J^m\left(\Delta\mu^{ref}\right)^n = \sum_{n,m\geq 0} \frac{1}{n!m!}\alpha_{nm}J^m\left(\Delta\mu^{ref}\right)^n \quad (30)$$

where μ^{ref} is a reference chemical potential. With (30) the following expressions for C and Γ can be obtained.

$$\Gamma = -\frac{\partial\gamma}{\partial\mu} = -\sum_{n\geq 1,m\geq 0} \frac{1}{(n-1)!m!}\alpha_{nm}J^m\left(\Delta\mu^{ref}\right)^{n-1} \quad (31)$$

$$C = \frac{\partial\gamma}{\partial J} = \sum_{n\geq 0,m\geq 1} \frac{1}{n!(m-1)!}\alpha_{nm}J^{m-1}\left(\Delta\mu^{ref}\right)^n \quad (32)$$

With these equations (29) can in principle be solved. To obtain some feeling about the physics we now consider the leading (linear) terms,

$$\Gamma = -\alpha_{10} - \alpha_{11}J \quad (33)$$

$$C = \alpha_{01} + \alpha_{11}\Delta\mu^{ref} \quad (34)$$

where α_{10}=-Γ_0, the surface concentration at a flat surface, and α_{01}=C^{ref}, the curvature constant at μ^{ref}. Using (33) and (34), equation (29) can be rewritten to

$$\frac{\partial\mu}{\partial J} = \frac{\Delta C^{ref} + \Delta\alpha_{11}\Delta\mu^{ref}}{\Delta\Gamma_0 - \Delta\alpha_{11}J} \quad (35)$$

where $\Delta X = X^{II} - X^{I}$. If we solve (35) and take $\mu^{ref} = \mu_0^{\#}$, the chemical potential at the phase transition of the flat surface, the shift in the chemical potential at the phase transition, caused by the curvature, is calculated as,

$$\Delta\mu^{\#} = \left(\frac{\Delta CJ}{\Delta\Gamma_0 - \Delta\alpha_{11}J}\right)_{\mu_0^{\#}} \quad (36)$$

where $\Delta\mu^{\#} \equiv \mu_J^{\#} - \mu_0^{\#}$. Equation (36) is a Kelvin type of equation. Knowledge about the relation between ΔC and all molecular properties will be very interesting. The next step is therefore to provide such a molecular interpretation.

Generally the integration should cover the entire adsorbate. If we assume cylindrical geometry and homogeneity parallel to the surface, we can rewrite (42),

$$N_i^\sigma = 2\pi L \int_0^R \rho_i^\sigma(r) r dr \tag{43}$$

where the integral is independent of the choice of the lower boundary because the excess density vanishes in the center of the pore; we assume $\Delta p \approx 0$. By introducing a new coordinate, x=R-r, the distance from the surface, and using (10), the adsorbed amount, Γ_i, can be expressed in terms of the density profile:

$$\Gamma_i = \int_0^R \rho_i^\sigma(x)(1+xJ)dx \tag{44}$$

An explicit expression for the curvature dependence of the adsorbed amount is obtained by writing the following curvature expansion,

$$\Gamma_i = B_{i,0} + B_{i,1}J + B_{i,2}J^2 + O\left(J^3\right) \tag{45}$$

where $B_{i,0}$ equals $\Gamma_{i,0}$, the amount adsorbed on the flat surface. In section 3.3.2 already an expansion of Γ has been given. Here, we only look at the curvature dependence. Combination of (40), (44) and (45) gives the following expressions for $\Gamma_{i,0}$ and $B_{i,1}$ in terms of the density profile of the flat surface.

$$\Gamma_{i,0} = \int \rho_{i,0}^\sigma(x)dx \tag{46}$$

$$B_{i,1} = \left(\frac{\partial \Gamma_i}{\partial J}\right)_0 = \int \rho_{i,0}^\sigma(x)x dx + \int \left(\frac{\partial \rho_i^\sigma(x)}{\partial J}\right)_0 dx \tag{47}$$

In the case that the density profile of a surface layer is not very sensitive to its curvature, it follows from (46) and (47) that the adsorbed amount varies linearly with J:

$$\Gamma_i = \Gamma_{i,0}\left(1 + \delta_i^{(\rho)}J\right) \tag{48}$$

The quantity $\delta_i^{(\rho}$ gives useful information. First, if an adsorbed layer of thickness H is more or less symmetrical then $\delta_i^{(\rho)}$ equals H/2. In fact, $\delta_i^{(\rho)}$ is the centre of mass of the layer of i. Deviation of $\delta_i^{(\rho}$ from H/2 indicates asymmetry of the profile. In the case of a bilayer of surfactants on the surface, which is more or less symmetrical, $\delta_i^{(\rho)}$ is of the order of H/2. As the surface distorts the symmetry of the layer and this distortion will increase with increasing affinity of the molecules for the surface, $\delta_i^{(\rho)}$ will decrease with increasing affinity. In figure 4 four possible density profiles are shown, with their corresponding $\delta^{(\rho)}$ values.
Second, in the case of a binary mixture of solvent (w) and a nonionic surfactant (s), our interest, it is important to note that $\delta_s^{(\rho)} \approx \delta_w^{(\rho)}$, which follows from the simple notion that a water molecule cannot occupy the same site as a segment of a surfactant molecule.

3.4.4 The excess grand potential

The excess grand potential, another important quantity of interest, is found by integrating the excess grand potential density profile, $\omega^{\sigma}(\vec{r})$.

$$\Omega^{\sigma} = \int \omega^{\sigma}(\vec{r})d\vec{r} \qquad (49)$$

For a cylindrical geometry, assuming a constant grand potential density parallel to the pore surface, equation (49) can be rewritten as,

$$\Omega^{\sigma} = 2\pi L \int_0^R \omega^{\sigma}(r)rdr \qquad (50)$$

In the transformation of (48) into (49) the mean field approximation becomes again manifest. Using, as before, x=R-r and (6), $\gamma = \Omega^{\sigma}/A$ can be obtained from (50)

$$\gamma = \int_0^R \omega^{\sigma}(x)(1+xJ)dx \qquad (51)$$

The integration in (51) has R as the upper boundary. However, the outcome does not depend on the choice of the boundary for pores that are sufficiently wide.

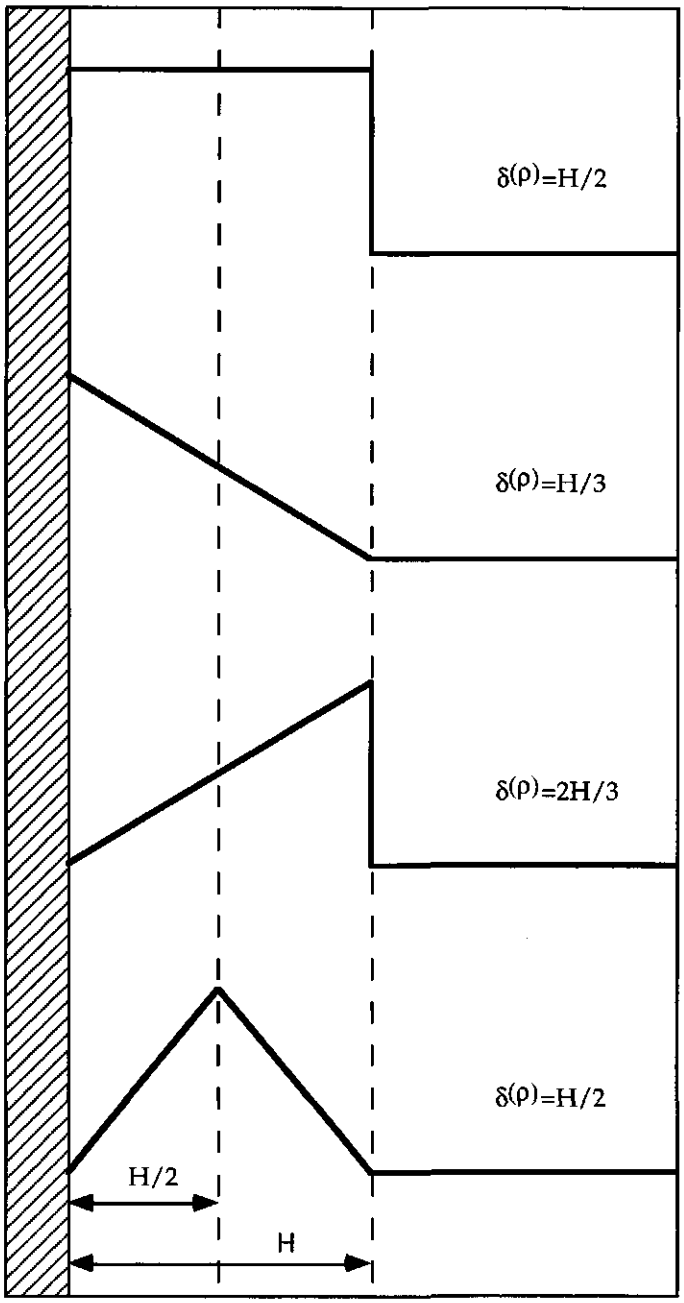

Figure 4 Different types of excess density profiles with their corresponding length scales $\delta(\rho)$'s . At a distance larger than H the excess density becomes zero.

Till now the curvature dependence of the interfacial tension γ has not been made explicit. We will follow a procedure which is equivalent to Helfrich's treatment of a curved membrane[23] and Tolman's approach of a liquid-gas interface[20]. The surface tension can be expanded in powers of J,

$$\gamma = A_0 + A_1 J + A_2 J^2 + O\left(J^3\right) \tag{52}$$

It is obvious that A_0 equals the interfacial tension of the flat surface, γ_0. Tolman expanded the surface tension γ and neglected all terms of order 2 and higher. Helfrich has neglected all terms of order 3 and higher by treating the bending of a membrane as being harmonic. He identified A_2 as half the rigidity constant k_c and A_1 as $-k_c J_0$, where J_0 is the spontaneous curvature of the surface.
To interpret γ_0 and A_1 we have to combine (39), (51) and (52).

$$\gamma_0 = \int \omega_0^{\sigma}(x)dx \tag{53}$$

$$A_1 = \left(\frac{\partial \gamma}{\partial J}\right)_0 = \int \omega_0^{\sigma}(x)x dx + \int \left(\frac{\partial \omega^{\sigma}(x)}{\partial J}\right)_0 dx \tag{54}$$

If the grand potential density profile $\omega^{\sigma}(x)$ is independent of J, the last term on the right hand side of equation (54) and all terms of order 2 and higher in equation (52) can be neglected. Under that condition the surface tension of a curved adsorbed layer is fully determined by the profile of the corresponding flat layer and becomes linearly dependent on the curvature,

$$\gamma = \gamma_0 + CJ = \gamma_0\left(1 + \delta^{(\omega)} J\right) \tag{55}$$

In our discussion of $\delta_1^{(\rho)}$ we have remarked that this parameter is a measure of the symmetry of the adsorbed layer. The physical meaning of $\delta^{(\omega)}$ is not as clear as that of $\delta_1^{(\rho)}$. However, we will see that with a suitable model of the adsorbed layer it is sometimes possible to make certain statements about $\delta^{(\omega)}$.

3.4.5 Curvature influence on the phase transition

The main goal of this section is to offer a microscopic interpretation of equation (36), in order to describe the influence of the curvature on the phase transition of an adsorbed layer. As in section 3.3.2 we will restrict ourselves to

the case of a binary mixture of surfactant (s) and water (w). To interpret (36) additional assumptions have to be made. In section 3.2 it has already been discussed that in phase I, a low coverage phase, the surfactants adsorb flat at the surface. As a consequence, not much curvature influence is expected on the surface tension, $C^{I} \approx 0$, and the adsorbed amount, $\Gamma_0^I \delta^{(\rho)} \approx 0$. Therefore (36) becomes:

$$\Delta\mu^{\#} = \left(\frac{C^{II}{}_J}{\Gamma_0^{II}\left(1+\delta^{(\rho),II}{}_J\right) - \Gamma_0^I} \right)_{\mu_0^{\#}} \tag{56}$$

At $\mu_0^{\#}$ the two surface phases coexist at the flat surface. In order to obtain insight into C^{II} at $\mu_0^{\#}$, we use (32) and consider only the leading linear terms,

$$C^{II} = \alpha_{01} + \alpha_{11}\Delta\mu^{ref} \tag{57}$$

where,

$$\alpha_{01} = C^{ref} = \gamma_0^{II}\delta^{(\omega)II}\Big|_{\mu^{ref}} \tag{58}$$

and

$$\alpha_{11} = -\Gamma_0^{II}\delta^{(\rho)II} \tag{59}$$

which implies that the adsorbed amount is assumed to be constant after the phase transition and the structure of the adsorbed layer is insensitive to the curvature. In the appendix we will investigate a quadratic $\Delta\mu$-dependency of C^{II}, which is more realistic but does not provide additional physical insight.
The only remaining parameter to be determined is C^{ref}. An easy point to choose as reference is the chemical potential where stable bilayers are formed in solution, μ^{bi}. Two important properties of such layers deserve attention. First, they are symmetrical. Therefore, the grand potential density profile has to be symmetric. Second, they have no surface tension[38]. Due to the symmetry of the grand potential density profile and the demand of a vanishing surface tension, $\int x\omega_0^{\sigma}(x)dx$ has to be zero. An adsorbed bilayer at μ^{bi} can be regarded as a perturbed free bilayer. The grand potential density profile can be written as follows,

$$\omega_0^{\sigma}(x) = \omega_0^{\sigma,f}(x) + \psi_0(x) \tag{60}$$

where $\omega_0^{\sigma,f}(x)$ is the profile of the free bilayer and $\psi_0(x)$ is the perturbation due to the surface. With the notions made above and (54) C^{bi} can be calculated:

$$C^{bi} = \int x\psi_0(x)dx = \gamma_0^{bi}\delta^{(\psi)} \tag{61}$$

In (60) $\delta^{(\psi)}$ is the distance to the solid surface weighted with ψ_0. This parameter is a measure for the range of the influence of the surface in the adsorbed layer. The adsorbed layer is a bilayer of surfactants and only the head-on adsorbed layer is in direct contact with the surface. Therefore, we expect that only within this layer does ψ_0 deviate significantly from zero. As ψ_0 changes from a non-zero value at x=0 to zero at x=H/2, $\delta^{(\psi)}$ has to be equal or smaller than H/4. In figure 5 three possible profiles are shown.
Using Gibbs'law the following expression for C^{II} at $\mu_0^{\#}$ can be obtained,

$$C^{II}\left(\mu_0^{\#}\right) = \Gamma_0^{II}\Delta\mu^{bi}\left(\delta^{(\psi)} - \delta^{(\rho)II}\right) + y \tag{62}$$

where $y \equiv \delta^{(\psi)}\gamma_0\big|_{\mu_0^{\#}}$ and $\Delta\mu^{bi} \equiv \mu_0^{\#} - \mu^{bi}$. Equation (62) contains two important features. First, if y is small, which will be assumed, the curvature constant of the adsorbed surfactant layer will be positive. In the case that surfactants have an affinity for the surface, the case of our interest, aggregates are formed on the surface before they are formed in the bulk solution. Therefore, $\Delta\mu^{bi}$ will have a negative sign. The quantity $\delta^{(\psi)} - \delta^{(\rho)II}$ also has a negative sign. As reasoned before, $\delta^{(\rho)II}$ will be of the order H/2 and $\delta^{(\psi)}$ is expected to be smaller than H/4. Second, the value of the curvature constant increases with increasing adsorption energy. In (62) $\Delta\mu^{bi}$ is a measure of the adsorption Gibbs energy. If this energy increases, the phase transition, the step, shifts to lower chemical potential and therefore $\Delta\mu^{bi}$ becomes more negative.

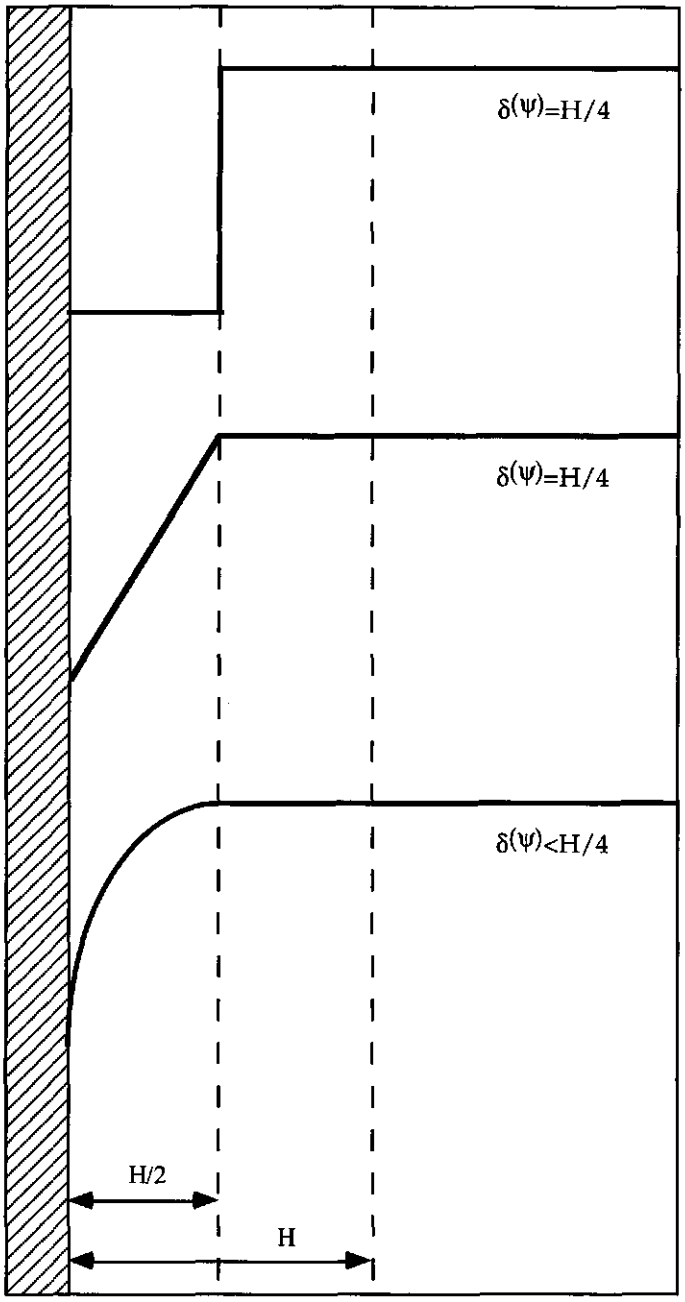

Figure 5 Different types of perturbation profiles, $\psi_0(x)$, with their corresponding length scales $\delta(\psi)$'s. The quantity ψ_0 varies from a finite value at x=0 to zero at the half of the bilayer, H/2.

The curvature influence on the phase transition is found by combining (56) and (62).

$$\Delta\mu^{\#} = \frac{\left(\Gamma_0^{II}\Delta\mu^{bi}\left(\delta^{(\psi)} - \delta^{(\rho)II}\right) + y\right)J}{\Gamma_0^{II}\left(1 + \delta^{(\rho)II}J\right) - \Gamma_0^{I}} \qquad (63)$$

The two important features in the behavior of the curvature constant, discussed above, reappear in (63). First, as long as y has a small value, $\Delta\mu^{\#}$ will be negative for pores (J<0) and positive for rod-like particles (J>0). In a pore the phase transition occurs at lower chemical potential than on a flat surface, which has been found experimentally[15]. Second, if the adsorption Gibbs energy increases, the position of the phase transition, $\mu^{\#}$, becomes more sensitive to the curvature.

The quantities $\delta^{(\psi)}$ and $\delta^{(\rho)II}$ nicely reflect the two competing effects, which determine the stability of the curved layer. The concave curved layer (pore) has lost stability due to the loss of regions which profit from the interaction of the layer with the surface (accounted for by the ψ_0 profile and reflected in $\delta^{(\psi)}$). On the other hand, the layer has gained stability due to the loss of regions which destabilize the layer (reflected in $\delta^{(\rho)II}$). Figure 6 shows what is happening with the volumes of the different parts of the layer if this layer is curved from flat to concave (pore). It is obvious that the volume of the destabilizing region at the solution side (A) decreases more than that of the stabilizing region at the surface side (B). As a consequence the layer has an increased stability

The impact of the presented analysis depends on application range of the linear approach, reflected in the equations (39), (40), (48) and (55). Significant influence of the curvature is only expected when the pore radius becomes of the order of the length scales $\delta^{(\rho)II}$ and $\delta^{(\psi)}$, i.e. a few times the thickness of an adsorbed layer. In a second paper, the curvature dependency of the surface tension has been studied with MFL calculations[39], which are not published at the moment. Anticipating the results of that study, we can state that the curvature constant at the point of phase transition can be predicted with an error of about 25%, which is high but enough to capture the qualitative physical features. The linear approximation becomes better with decreasing chemical potential of the surfactant.

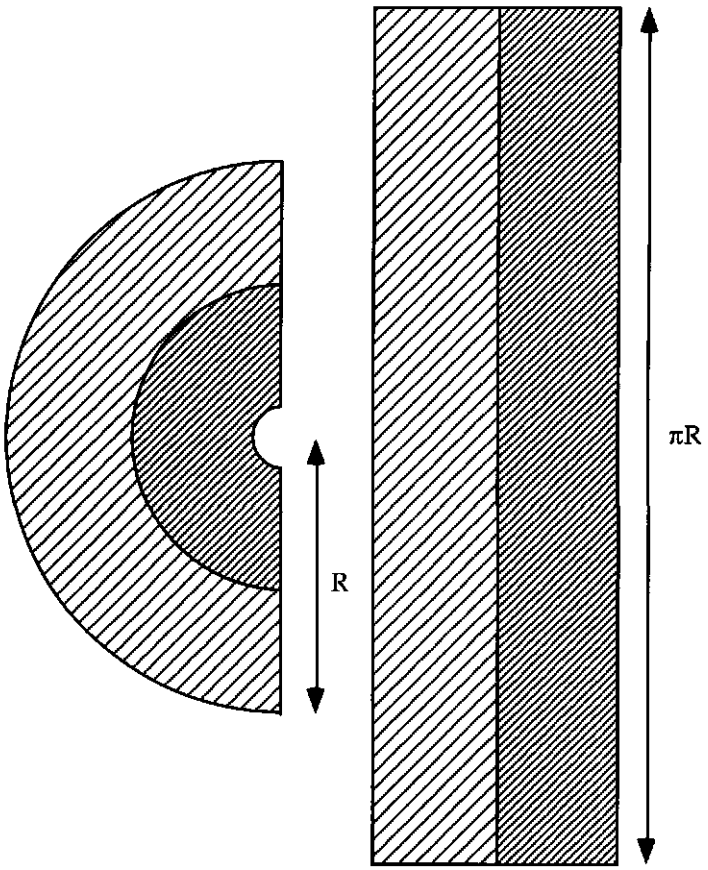

Figure 6 A schematical representation of the effect of a pore on the stability of a layer. The region adjacent to the surface, light gray, loose less volume as the one at the solution side, dark gray. If the surface and outer region stabilize and destabilize the layer, respectively, the overall stability increases due to the concave curvature.

3.5 Conclusions

The adsorption isotherm of a nonionic surfactant on a hydrophilic surface shows a step at a certain chemical potential. At this step the adsorbed amount changes from a small to a large value. This step can be regarded as a phase transition from a thin monolayer to a thick bilayer.

With classical thermodynamics it has been shown that the influence of the curvature on the phase transition in the adsorbed layer is related to the curvature constants of both phases at the chemical potential where the flat layer undergoes the phase transition, $C\left(\mu_0^{\#}\right)$. We have derived a Kelvin-type

of equation which shows that the shift of the chemical potential of phase transition is proportional to $C\left(\mu_0^{\#}\right)$.

By making a few assumptions we were able to relate $C\left(\mu_0^{\#}\right)$ with the affinity of the surface for the bilayer phase. In the absence of any affinity this constant goes to zero and curvature does not influence the position of the phase transition. The curvature constant increases with the affinity and therefore the curvature influence on the phase transition also increases. An adsorbed bilayer is stable at lower chemical potential in a pore as on flat surface. Given a certain surface area, the destabilizing influence of the unstable regions (at the solution side) decreases more than the stabilizing influence of the stable regions (at the surface side). This could be the explanation for Gu's observations[15]. He indeed observed that the step in the isotherm shifts to lower surfactant concentration with decreasing pore radius.

The most important assumption, which has been made, deals with the curvature dependency of the surface tension and the grand potential density profile. We have assumed a purely linear curvature dependency of the surface tension, which means that the grand potential density profile is assumed to be curvature insensitive. A first test of this assumption can be done with the help of MFL calculations, which will be published in part II[39].

Appendix

In section 3.4.5 we assumed a constant adsorbed amount of the bilayer phase (II). In this approximation, C was found to be linearly dependent on the chemical potential. In this appendix we show that a higher-order treatment does not affect the conclusion. To that end, we now also take into account the quadratic term in (32).

$$C = C^{bi} + \alpha_{11}\Delta\mu^{bi} + \frac{1}{2}\alpha_{21}\left(\Delta\mu^{bi}\right)^2 \qquad (A.1)$$

where,

$$\alpha_{11} = -\Gamma_0^{II}\delta(\rho)^{II}\Big|_{\mu^{bi}} \qquad (A.2)$$

and

$$\alpha_{21} = -\frac{\partial}{\partial\mu}\Gamma_0^{II}\delta^{(\rho)II}\Big|_{\mu^{bi}} \tag{A.3}$$

The curvature constant at μ^{bi} is given by the following equation,

$$C^{bi} = \delta^{(\psi)}\gamma_0^{bi} = \delta^{(\psi)}\gamma_0|_{\mu_0^{\#}} - \left(\alpha_{10}\Delta\mu^{bi} + \frac{1}{2}\alpha_{20}\left(\Delta\mu^{bi}\right)^2\right)\delta^{(\psi)} \tag{A.4}$$

where

$$\alpha_{10} = -\Gamma_0^{II,bi} \tag{A.5}$$

and

$$\alpha_{20} = -\frac{\partial\Gamma_0^{II}}{\partial\mu}\Big|_{\mu^{bi}} \tag{A.6}$$

Combination of (A.1) and (A.4) results in the following expression for the curvature constant at $\mu_0^{\#}$,

$$\begin{aligned} C^{II}\left(\mu_0^{\#}\right) = {} & \Gamma_0^{II,bi}\left(\delta^{(\psi)} - \delta^{(\rho)}\right)\Delta\mu^{bi} \\ & -\frac{1}{2}\frac{\partial\Gamma_0^{II}}{\partial\mu}\left(\delta^{(\psi)} + \delta^{(\rho)}\right)\Big|_{\mu^{bi}}\left(\Delta\mu^{bi}\right)^2 + y \end{aligned} \tag{A.7}$$

The difference between (62) and (A.7) is the quadratic term. In (A.7) $y \equiv \delta^{(\psi)}\gamma_0^{bi}$. The first term on the right-hand side is the same as in the linear approach. The linear term dominates the behavior of (A.7) as long as the change in the adsorbed amount at the interval $\Delta\mu^{bi}$ is much smaller than the adsorbed amount at μ^{bi}. This will generally be the case for surfactant systems and therefore the linear approximation is generally valid. The curvature constant will have a positive value and its value increases with increasing affinity of the headgroup for the surface.

List of symbols

A		area of the pore surface
C		curvature constant (curvature Helmholtz energy)
	C^I	curvature constant of phase I
	C^{ref}	curvature constant at μ^{ref}
	C^{bi}	curvature constant at μ^{bi}
	ΔC	difference in curvature constant between phase II and I
f^σ		excess Helmholtz energy density
H		thickness of a bilayer
J		mean curvature of the pore surface
L		length of the pore
N_i		amount of component i
	N_i^β	amount in the bulk
	N_i^σ	excess amount
	$N_i^{\sigma(1)}$	excess amount, relative to the solvent
p		pressure
	p^α	pressure in the pore
	p^β	pressure in the bulk
	Δp	pressure difference between the bulk and the pore
R		radius of the pore
S		entropy
	S^β	entropy of the bulk
	S^σ	excess entropy
	$S^{\sigma,I}$	excess entropy of phase I
	$S^{\sigma(1)}$	excess entropy, relative to the solvent
T		temperature
V		volume
	V^α	volume of the pore
	V^β	volume of the bulk solution
γ		surface tension
	γ^*	surface tension of a surface in contact with pure solvent
	γ_0	surface tension of a flat surface
	γ^I	surface tension of phase I
ψ		surface contribution to the stress profile
Γ_i		adsorbed amount of component i
	Γ_0	adsorbed amount at the flat surface
	$\Delta\Gamma$	difference in adsorbed amount between phase II and I
$\delta^{(q)}$		q-weighted averaged distance to the surface

	$\delta^{(\omega)}$	ω-weighted averaged distance to the surface
	$\delta_i^{(\rho)}$	ρ_i^{σ}-weighted averaged distance to the surface
μ_i		chemical potential of component i
	$\mu^{\#}$	chemical potential at phase transition
	$\mu_0^{\#}$	chemical potential at phase transition on a flat surface
	$\mu_J^{\#}$	chemical potential at phase transition on surface with curvature J
	μ^{ref}	chemical potential at a certain reference
	μ^{bi}	chemical potential at the point where stable bilayers are formed in solution
ν		total number of components
π		surface pressure
ρ		density
	ρ^{σ}	excess density
	ρ_0^{σ}	excess density in a flat layer
	ρ_i^{β}	bulk density of component i
ω		grand potential density
	ω^{σ}	excess grand potential density
	ω_0^{σ}	excess grand potential density in a flat adsorbed layer
	$\omega_0^{\sigma,f}$	excess grand potential density in a non-adsorbed flat layer
Ω		grand potential
	Ω^{σ}	excess grand potential
	$\Omega^{\sigma,I}$	excess grand potential of phase I

References

1 Keizer, A. de, Michalski, T. and Findenegg, G. H., *Pure Appl. Chem.* **63,** 1495 (1991).

2 Aukett, P. N., Quirke, N., Riddiford, S. and Tennison, S. R. *Carbon* **30,** 913 (1992).

3 Kaneko, K., Cracknell, R. F. and Nicholson, D. *Langmuir* **10,** 4606 (1994).

4 Thommes, M., Findenegg, G. H. *Langmuir* **10,** 4270 (1994).

5 Thommes, M., Findenegg, G. H. and Schoen, M. *Langmuir* **11,** 2137 (1995).

6 Page, J. H., Liu, J., Abeles, B., Herbolzheimer, E., Deckman, H. W. and Weitz, D. A. *Phys. Rev. E* **52,** 2763 (1995).

7 Balbuena, P. B., Gubbins, K. E. *Fluid Phase Equilibria* **76,** 21 (1992).

8 Binder, K., Landau, D. P. *J. Chem. Phys.* **96,** 1444 (1992).

9 Cracknell, R. F., Gubbins, K. E., Maddox, M. and Nicholson, D. *Acc. Chem. Res.* **28,** 281 (1995).
10 Gozdz, W. T., Gubbins, K. E. and Panagiotopoulos, A. Z. *Mol. Phys.* **84,** 825 (1995).
11 Gennes, P. G. de *Scaling Concepts in Polymer Physics* (Cornell University Press, Ithaca, 1979).
12 Jaeckel, A., Dayantis, J. *J. Phys. A - Math. Gen.* **27,** 7719 (1994).
13 Narasimhan, S. L. *J. Phys. A - Math. Gen.* **28,** 833 (1995).
14 Gorbunov, A. A., Skvortsov, A. M. *Adv. Coll. Interface Sci.* **62,** 31 (1995).
15 Gu, T., Zhu, B. *Colloids Surf.* **44,** 81 (1990).
16 Giordano, F., Denoyel, R. and Rouquerol, J. *Colloids Surf. A* **71,** 293 (1995).
17 Rietra, R. *M.Sc. Thesis* (Wageningen Agricultural University, Wageningen, 1993).
18 Huinink, H. P. Keizer, A. de, Leermakers, F. A. M. and Lyklema, J. *Progr. Colloid Polym. Sci.* **105,** 91 (1997).
19 Buff, F. P. *J. Chem. Phys.* **19,** 1591 (1951).
20 Tolman, R. C. *J. Chem. Phys.* **17,** 118 (1949).
21 Markin, V. S., Kozlov, M. M. and Leikin, S. L. *J. Chem. Soc., Faraday Trans. 2* **84,** 1149 (1988).
22 Blokhuis, E. M., Bedeaux, D. *HCR Adv.-Educ. Rev.*, 55 (1994).
23 Helfrich, W. *Z. Naturforschung* **28c,** 693 (1973).
24 Szleifer, I., Kramer, D., Ben-Shaul, A., Gelbart, W. M. and Safran, S. A. *J. Chem. Phys.* **92,** 6800 (1990).
25 Barneveld, P. A., Scheutjens, J. M. H. M. and Lyklema, J. *Langmuir* **8,** 3122 (1992).
26 Levitz, P.,Vandamme, H. andKeravis, D. *J. Phys. Chem.* **88,** 2228 (1984).
27 Levitz, P., Vandamme, H. *J. Phys. Chem.* **90,** 1302 (1986).
28 Böhmer, M. R., Koopal, L. K., Janssen, R., Lee, E. M., Thomas, R. K. and Rennie, A. R. *Langmuir* **8,** 2228 (1992).
29 Lee, E. M., Thomas, R. K., Cummins, P. G., Staples, E. J., Penfold, J. and Rennie, A. R. *Chem. Phys. Letters* **162,** 196 (1989).
30 Rutland, M. W., Senden, T. J. *Langmuir* **9,** 412 (1993).
31 Gellan, A., Rochester, C. H. *J. Chem. Soc. - Faraday Trans. 1* **81,** 2235 (1985).
32 Evans, R., Marconi, U. M. B. *J. Chem. Phys.* **86,** 7138 (1987).
33 Binder, K., Landau, D. P. *Adv. Chem. Phys.*, 91 (1989).
34 Steele, W. *The Interaction of Gases with Solid Surfaces* (Pergamon Press,

Oxford, 1974).

35 Cracknell, R. F., Nicholson, D. *Adsorption* **1,** 7 (1995).

36 Pasandideh-Fard, M., Chen, P., Mostaghimi, J. and Neumann, A. W. *Adv. Colloid Interface Sci.* **63,** 151 (1996).

37 Helfrich, W. in *Liquids at Interfaces, Les Houches XLVIII (1988),* edited by Charvolin, J., Joanny, J. F. and Zinn-Justin, J. (North-Holland, Amsterdam, 1990), pp. 212.

38 Leermakers, F. A. M., Scheutjens, J. M. H. M. and Lyklema, J. *Biophys. Chem.* **18,** 353 (1983).

39 Huinink, H. P. Keizer, A. de, Leermakers, F. A. M. and Lyklema, J. *Langmuir* **13,** 6618 (1997).

Chapter 4

The adsorption of nonionic surfactants in hydrophilic cylindrical pores II; mean field lattice calculations

Abstract The adsorption behavior of nonionic surfactants in hydrophilic cylindrical pores has been studied with a Mean Field Lattice (MFL) theory. The pore radius has two important influences on the adsorption isotherm. With decreasing radius (i) the adsorbed amount decreases and (ii) the step in the isotherm shifts to lower concentration. This behavior is rather generic. Neither the molecular architecture nor the adsorption energy influences these qualitative features. However, the position of the step in the isotherm becomes more sensitive to the curvature as the adsorption energy increases, just as has been predicted with the Semi Thermodynamic (ST) theory.
We have been partly successful in predicting the curvature behavior from the excess grand potential density profile of the flat adsorbed layer. All trends found with the full MFL calculations could be reproduced with the help of the curvature constants, calculated from the profile of the flat layer. However, the curvature constant was underestimated. At the step in the isotherm the error was about 25%.

4.1 Introduction

Although several studies have been dedicated to the subject of surfactant adsorption[1-5] and a variety of influences has been investigated, little is known about the surfactant behavior in porous substances. This is not very surprising from an experimental point of view. Not the irrelevance for society and industry but practical experimental difficulties cause this lack of knowledge. Significant influences of pores on the adsorption behavior are expected if the pore radii become of the order of the layer thickness. The maximum layer thickness in the case of surfactant adsorption is of the order of the total length of one surfactant molecule, i.e. about 2-4 nm[3,6,7]. It is very difficult to find a material with a homodisperse pore size distribution in this range.
Nevertheless, a few articles deal with the adsorption of nonionics in hydrophilic pores[8,9]. Although, none of these contain a systematic analysis of the influence of the pore radius, for reasons mentioned above, they demonstrate

two important features. First, the amount adsorbed at the plateau decreases with decreasing pore radius, which can be explained in terms of simple geometrical considerations. Second, the step in the isotherm, which is the most important feature of this type of systems, shifts to lower surfactant concentration with decreasing pore radius.
We have reproduced both features with a Mean Field Lattice (MFL) theory for a cylindrical pore[10]. Because of technical difficulties, this type of theories is the only viable approach to obtain insight beyond the general knowledge already available: "pores do something". In a preceding article a detailed thermodynamic analysis, combined with a first interpretation in terms of density profiles, has been made in order to get an idea what could happen[11]. Below, we will refer to this approach as the Semi Thermodynamic (ST) theory. With the help of this analysis we were able to explain both the experimental knowledge and the numerical outcomes of MFL theory in a qualitative way.
However, our first MFL calculations[10] dealt with only one particular surfactant and only one set of interaction parameters and the ST part[11] involved several approximations. Therefore, we will now present an extensive MFL analysis to obtain more generic knowledge about the adsorption behavior. After a short overview of the ST and MFL theories, MFL results for different surfactant types and adsorption energies will be discussed. This study deals with nonionic surfactants and cylindrical hydrophilic pores.
With the help of our ST analysis we were able to formulate two important statements. First, the chemical potential where the adsorption increases rapidly, $\mu^{\#}$, is related to the curvature constant (a measure of the curvature dependency of the surface tension) of the flat layer at that chemical potential. Second, this curvature constant increases with increasing affinity of the surface for the surfactant layer. Therefore, the curvature dependency of $\mu^{\#}$ increases with increasing adsorption energy. Both statements will now be tested with the help of the MFL calculations.

4.2 Surfactant adsorption

4.2.1 Nonionic surfactant adsorption and phase transitions

Adsorption isotherms of nonionic surfactants on hydrophilic surfaces have a very characteristic shape. At low concentration few or no molecules adsorb (I), at a certain concentration the adsorbed amount increases very rapidly (t) and beyond a certain concentration the adsorbed amount levels off to a more

or less constant value (II). In regime I the molecules adsorb isolated at the surface, in regime t the adsorption increases dramatically due to aggregation phenomena and in regime II large bilayer- or micellar-like patches are formed at the surface. The thickness of region t depends strongly on the architecture of the surfactant molecule. The transition from I to II becomes sharper with decreasing headgroup size[1,2,5]. In addition, the sizes of the bilayer-like patches in region II increase with decreasing headgroup size[3,6]. From both observations we can conclude that a phase transition model, in which region t is neglected, makes sense as long as the headgroup is not too big. This consideration has been used in our MFL calculations[10], which anyhow cannot reproduce the transition region due to the mean-field approximation, and in the thermodynamic analysis[11]. As we do not now consider the width of the transition, we can also invoke the MF approximation in the present study.

4.2.2 Adsorption, thermodynamics and microscopic backgrounds

In our preceding study[11] we have shown that the surface tension, γ, and the curvature constant, C, both thermodynamic quantities, are important for the understanding of the curvature behavior of adsorbed layers. Both quantities are related to the excess grand potential, Ω^σ, which describes the thermodynamic state of the system.

$$\gamma \equiv \left(\frac{\partial \Omega^\sigma}{\partial A}\right)_{V,T,\mu's,J} \tag{1}$$

$$C \equiv \frac{1}{A}\left(\frac{\partial \Omega^\sigma}{\partial J}\right)_{V,T,\mu's,A} \tag{2}$$

Where A is the surface area and J is the curvature, defined as 1/R (R is negative for a concave surface, a pore, and positive for a convex surface, a rod). The quantity Ω^σ can be related to microscopic properties with the help of the following equation:

$$\Omega^\sigma = \int \omega^\sigma(\vec{r})d\vec{r} \tag{3}$$

where $\omega^\sigma(\vec{r})$ is the excess grand potential density at a certain point $\vec{r}$. With the help of (3) γ and C can be related to the excess grand potential density profile. If the mean field approximation, homogeneity parallel to the surface,

is used, and it is assumed that curvature behavior of γ is dominated by the linear term in J, then the following expressions can be obtained from (1)-(3):

$$\gamma = \gamma_0 + CJ \tag{4}$$

$$\gamma_0 = \int \omega_0^{\sigma}(x)dx \tag{5}$$

$$C = \int \omega_0^{\sigma}(x)xdx + \int \left(\frac{\partial \omega^{\sigma}(x)}{\partial J} \right)_0 dx \tag{6}$$

Where γ_0 is the surface tension of a flat layer at the same μ, $\omega_0^{\sigma}(x)$ the excess grand potential density profile in that flat layer and x the distance to the surface. If the profile does not depend on curvature, γ is a strictly linear function of J and C is fully determined by the profile of the flat layer, because the second term on the right hand side of (6) will vanish.

4.2.3 Curvature influence on the adsorption, the ST theory

In this section a brief overview is given of the ST theory. For a detailed derivation and discussion the original paper[11] has to be consulted. The chemical potential at which a monolayer coexist with a bilayer, $\mu^{\#}$, depends on the radius of the pore. With the help of the approximations, $\Gamma \propto J$ and $\gamma \propto \mu$, a Kelvin-type of equation can be derived:

$$\Delta\mu^{\#} = \left(\frac{C^{II} J}{\Gamma_0^{II}\left(1 + \delta^{(\rho)II} J\right) - \Gamma_0^{I}} \right)_{\mu_0^{\#}} \tag{7}$$

where $\Delta\mu^{\#} \equiv \mu_J^{\#} - \mu_0^{\#}$. The quantities $\mu_0^{\#}$ and $\mu_J^{\#}$ are the chemical potentials at phase transition for a flat and curved surface, respectively. The curvature constant of the bilayer-like phase (II), C^{II}, is given by the following equation:

$$C^{II}\left(\mu_0^{\#}\right) = y + \left[\Gamma_0^{II}\left(\delta^{(\psi)} - \delta^{(\rho)II}\right) \right]_{\mu^{bi}} \Delta\mu^{bi} \tag{8}$$

where $\Delta\mu^{bi} \equiv \mu_0^{\#} - \mu^{bi}$, μ^{bi} is the chemical potential beyond which a free bilayer of the surfactant is stable in solution and $y \equiv \delta^{(\psi)}\gamma_0|_{\mu_0^{\#}}$.
The length scales $\delta^{(\psi)}$ and $\delta^{(\rho)II}$ are the ψ- and ρ^{σ}-weighted average distances to the surface, calculated from a bilayer at a flat surface for $\mu=\mu^{bi}$. The profile $\psi(x)$ is the difference between the excess grand potential density

profile, $\omega^{\sigma}(x)$, of the adsorbed and free bilayer. It has been shown that for $\mu=\mu^{bi}$ the C^{II} is fully determined by $\psi(x)$[11].
Equations (7) and (8) have two important features. First, the absolute value of $C^{II}\left(\mu_0^{\#}\right)$ increases with increasing adsorption affinity, captured in $\Delta\mu^{bi}$. Therefore, the curvature influence on the phase transition becomes larger with increasing adsorption energy. Second, if y is small, two competing effects, reflected in the various length scales, determine the sign of $C^{II}\left(\mu_0^{\#}\right)$. The surface-bilayer interaction, represented by $\delta^{(\psi)}$, which stabilizes the layer makes the layer in a pore less stable than in the corresponding flat layer. The accumulation of surfactants at the surface, represented by $\delta^{(\rho)II}$, which destabilizes the layer, works the other way around. Due to the fact that the ρ^{σ}-profile is more extended than the ψ-profile and to the negative sign of $\Delta\mu^{bi}$, $C^{II}\left(\mu_0^{\#}\right)$ is expected to be positive. Therefore, at given μ's, a bilayer in a pore will be more stable than a bilayer on a flat surface and $\Delta\mu^{\#}$ will be negative.

4.3 The MFL theory

4.3.1 Introduction

In order to use the equations (5) and (6), the stress profile, $\omega^{\sigma}(r)$, has to be related to the density profile. This will be done within the framework of a Mean Field Lattice theory (MFL), which has originally been developed by Scheutjens en Fleer to study polymer adsorption[12] and has successfully been applied to association colloids by Leermakers and Scheutjens[13] and to surfactant adsorption by Böhmer and Koopal[2]. We shall briefly review some main elements of the MFL theory in section 4.3; in section 4.4 the application to our system will be discussed. For a detailed description of the theory we refer to the literature[12,14].

4.3.2 Lattice

In the MFL theory space is divided into M lattice layers, each lattice layer has a thickness l. The lattice has a co-ordination number Z. Every lattice layer is characterized by its total volume ΔV and its total contact area with the preceding layer, A_{-1}, and the following layer, A_{+1}. Every lattice site has a volume v and an area a. If the lattice planes are flat a lattice site has Z_0 neigbors within the layer and Z_1 in the neigboring layers. In the case of a flat lattice the following transition probabilities can be defined for a step within a

where $\alpha(z)$ is a Lagrange parameter to ensure complete filling of the lattice. When $u_A(z)$ is known, a free segment weighting factor $G_A(z)$ can be defined.

$$G_A(z) \equiv e^{-u_A(z)/kT} \tag{20}$$

The statistical weight of a part of a chain molecule i, ending at segment number s in layer z, is given by the end segment distribution function (edf), $G_i(z,s\,|\,1)$ or $G_i(z,s\,|\,r_i)$, depending on the choice of the start segment (the first or the last).
Equation (20) is related to the edf with the following recurrent relation.

$$G_i(z,s\,|\,1) = G_i(z,s)\overline{G_i(z,s-1\,|\,1)} \tag{21}$$

Here $G_i(z,s)$ is the free segment weight factor, given by equation (20). The volume fraction profile of a component i is obtained from the edf's.

$$\phi_i(z) = \phi_i^{\beta} r^{-1} \sum_{s=1}^{r} \overline{G_i(z,s-1\,|\,1)} G_i(z,s) \overline{G_i(z,s+1\,|\,r)} \tag{22}$$

The volume fraction profile of a monomer type A can also be calculated.

$$\phi_A(z) = r^{-1} \sum_i \phi_i^{\beta} \left(\sum_s \delta_i(s,A) \overline{G_i(z,s-1\,|\,1)} G_i(z,s) \overline{G_i(z,s+1\,|\,r)} \right) \tag{23}$$

Where $\delta_i(s,A)$ is a dirac-delta function which equals one if the monomer type of the s^{th} segment is A and zero in all other cases. The total amount and the excess total amount of a component i are defined as $\theta_i \equiv \sum_z \phi_i(z)$ and $\theta_i^{\sigma} \equiv \sum_z \left(\phi_i(z) - \phi_i^{\beta} \right)$ respectively. By using first order Markov statistics, introduced by (21), and equation (18) a mean-field approximation is adopted. Within each layer the monomer, energy and free energy density are assumed to be homogeneous.
The following expression for the excess grand potential can be derived for our specific surfactant-solvent mixture,

$$\Omega^{\sigma} = \sum_{z=1}^{M} \omega^{\sigma}(z) \Delta V(z) \tag{24}$$

where,

$$\omega^{\sigma}(z) = -\frac{kT}{v}\left[\begin{array}{l} -\ln\left(\frac{1-\phi(z)}{1-\phi^{\beta}}\right) - \left(1-\frac{1}{r}\right)\left(\phi(z)-\phi^{\beta}\right) \\ +\frac{1}{2}\chi\left(\overline{\phi_B(z)} - \phi_B(z)\right) \\ +\chi\left(\phi_B(z)\overline{\phi_B(z)} - \left(\phi_B^{\beta}\right)^2\right) \end{array}\right] \qquad (25)$$

Here $\phi(z)$, ϕ^{β}, $\phi_B(z)$ and ϕ_B^{β} are the volume fractions of all surfactant monomers in layer x and the bulk and of the tail monomer (B) in layer z and the bulk, respectively. It is assumed that $\chi=\chi_{BW}=\chi_{AB}$ and that $\chi_{AW}=0$. This profile is often called the stress profile. The surface tension can be found from,

$$\gamma = \ell\sum_{z=1}^{M}\left[1+\ell(z-1/2)J\right]\omega^{\sigma}(z) \qquad (26)$$

The surface tension of the flat layer is therefore:

$$\gamma_0 = \ell\sum_{z=1}^{M}\omega_0^{\sigma}(z) \qquad (27)$$

The curvature constant of the flat layer can be found by differentiation of (26) with respect to J and developing at J=0.

$$C = \ell^2\sum_{z=1}^{M}(z-1/2)\omega_0^{\sigma}(x) + \ell\sum_{z=1}^{M}\left(\frac{\partial\omega^{\sigma}(z)}{\partial J}\right)_{J=0} \qquad (28)$$

Note that the last term of (28) vanishes if $\omega^{\sigma}(z)$ does not depend on the curvature. Equation (28) is the discrete equivalent of (6).

Figure 2 shows the stress profiles (solid lines) and the volume fraction profiles of the headgroups (dashed lines) of phase II at two different surfactant concentrations, ϕ=4.2·10^{-3}, where the phase transition occurs, $\phi^{\#}$, and ϕ=9.5·10^{-3}, where bilayers become stable in solution, ϕ^{bi}.

The thickness of the adsorbed layer is at $\phi^{\#}$ 10 layers and at ϕ^{bi} 11 layers, which is the length of a completely stretched A_3B_8 chain. Because we use equation (21) for the chain statistics, we overestimate the flexibility of the molecules and therefore we underestimate the thickness of the adsorbed layer. The stabilizing contribution comes from the headgroup region next to the surface, z≤2. This contribution has an energetic orgine: the attractive interaction between the headgroups and the surface. The region z>2 destabilizes the layer. This contribution has an entropic origine, because the adsorbed layer is a much more ordered than the bulk solution. If the concentration of surfactants increases then everywhere in the bilayer the stress decreases. The unstable region becomes less unstable and as a result the layer gains stability.

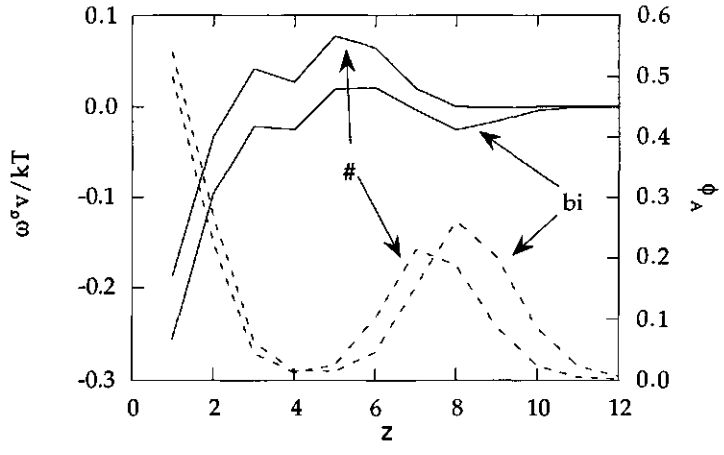

Figure 2 The excess grand potential density profile (solid lines) and the volume fraction profile of the headgroup segments (dashed lines) of an adsorbed bilayer of A_3B_8 surfactants. The curves marked with # and "bi" are the profiles of the bilayer which is just stable and one at incipient free bilayers stability respectively.

4.4.1.2 Influence of molecular architecture and adsorption energy

In the preceding section we have focused on one particular surfactant. Neither the influence of the molecular structure nor the adsorption energy has been discussed. Because these properties do not change the driving forces or the symmetry, the mechanism of adsorption and therefore the shape of the isotherm will not change very much. This does not mean that the adsorbed amounts are insensitive to changes in the interaction energy or molecular structure. In figure 3, the volume fraction, $\phi^{\#}$, at which the phase transition occurs, has been plotted as a function of the adsorption energy for different types of surfactants.

The phase transition shifts to a lower surfactant concentration upon increasing adsorption energy. The adsorbed layer as such will be less stable at low surfactant concentration, but the increased adsorption energy counteracts this. Additional calculations have shown that A_4B_8 surfactants seem to have a critical point at χ_{AS}=-8; below which phase transitions no longer occur. Also, all other surfactants show a tendency towards a critical point.

The chain length has a larger effect on the adsorption than the length of the headgroup. It is known from calculations for micelles in solution that the chain length has a large influence on the aggregation behavior[21], CMC values are very sensitive to the length of the surfactant tails, but not to the length of the hydrophobic headgroup.

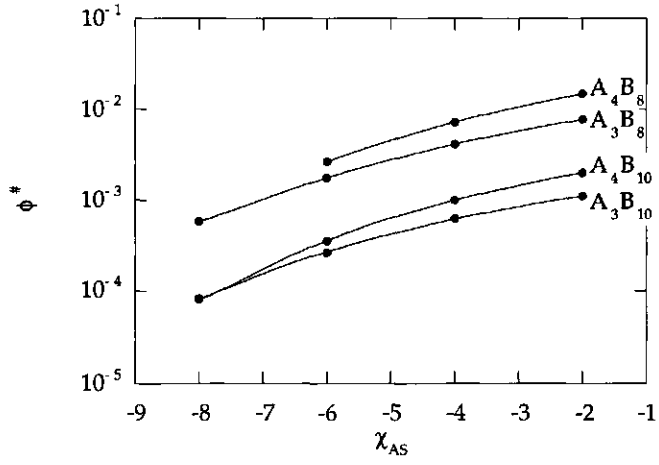

Figure 3 The surfactant bulk volume fraction of phase transition for a flat layer, $\phi^{\#}$, as a function of the adsorption energy, χ_{AS}.

4.4.2 Adsorption in pores

4.4.2.1 The adsorption isotherm

From earlier MFL calculations[10] it is known that the adsorption isotherm is influenced by the pore in two ways. First, the adsorbed amount decreases with decreasing pore radius. Second, the phase transition shifts to lower chemical potential of the surfactants. These effects have been explained by assuming that respectively the density (volume fraction) and grand potential density profile are insensitive to the curvature[11]. Both effects have been observed in experiments[8]. Figure 4 compares the adsorption isotherms of an A_3B_8 surfactant at a flat surface and in a pore (R=12). As before, the step in the adsorption isotherm, the phase transition, occurs at lower surfactant concentration in the case of the pore, and the adsorbed amount in the pore is smaller than that at the flat surface.

Let us now consider the curvature influence on the phase transition in more detail. The shift in the phase transition due to curvature is a rather general feature in MFL calculations. In figure 5 we have plotted the volume fraction of phase transition at a curved surface, $\phi^{\#}$, divided by the corresponding value

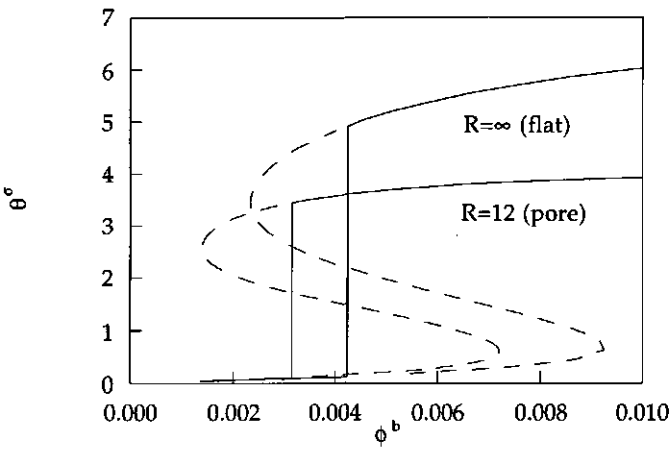

Figure 4 Adsorption isotherms of an A_3B_8 surfactant on: a flat surface (R=∞) and a cylindrical pore (R=12). The adsorbed amount, expressed as θ^{σ}, has been plotted against the volume fraction in the bulk, ϕ^{b}. The vertical solid lines represent the phase transitions.

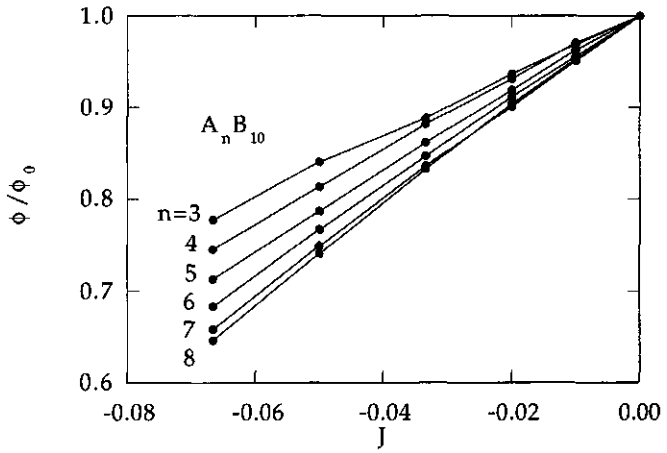

Figure 5 The bulk volume fraction of phase transition, normalized with respect to the flat layer, as a function of the curvature, for different different headgroup sizes.

for a flat surface, as a function of J (=-1/R) for surfactants with different headgroup lengths. If the pore radius decreases, J becomes more negative and the phase transitions of all surfactants shift toward lower concentrations. The shift becomes larger with increasing headgroup length. In figure 6, the same shift is plotted as a function of the tail length at fixed pore radius (R=15).
One of the most important conclusions of the ST theory was that the shift of the phase transition increases with increasing affinity. We have calculated the $\phi^{\#}$'s of the flat and curved layer (R=15) of an A_6B_{10} surfactant. In figure 7, the shift has been plotted as a function of the energy of interaction of a headgroup segment with the surface. The shift increases with a decreasing value of χ_{AS}, just as has been predicted from the ST theory.

4.4.2.2 The surface tension, its linear curvature dependency

As long as the surface tension and the adsorbed amount are strictly linear functions of J, we will be able to predict the behavior in pores from the behavior at the flat surface, equation (6). This observation has been used in the derivation of equation (8). We demonstrated that both the reduction of the adsorbed amount and the shift of the phase transition could be explained, under the condition that the structure of the adsorbed layer is independent of the curvature[10,11].

We have calculated C of an A_4B_8 surfactant from $\omega_0^\sigma(x)$ as a function of the bulk volume fraction, figure 11. The vertical solid line refers to the phase transition. Although the surfactants, in particular those with large headgroups adsorb in significant amounts on the surface before the phase transition, C^I is negligible over this range. Curvature dependency of Γ^I is also virtually absent. These two trends are consequences of the fact that the important contributions to C^I and Γ^I stem from the layer adjacent to the surface. In region I the corresponding length scales $\delta^{(\omega)}$ and $\delta^{(\rho)}$ are of the order of atomic radii and therefore already negligible on the scale of a few nanometers. It can be concluded that the stability of the bilayer-like phase (II) is indeed the important factor for the curvature behavior.

4.4.2.4 Free and adsorbed bilayers compared

In the ST model we have used the point where free-floating bilayers become stable as a reference. It was reasoned that $\omega^\sigma(x)$ at that point could be split in a contribution, which equals the profile of a free bilayer $\omega^{\sigma,f}(x)$ and a contribution due to the surface $\psi(x)$. The latter contribution would determine the behavior of C and γ_0 at $\mu=\mu^{bi}$.

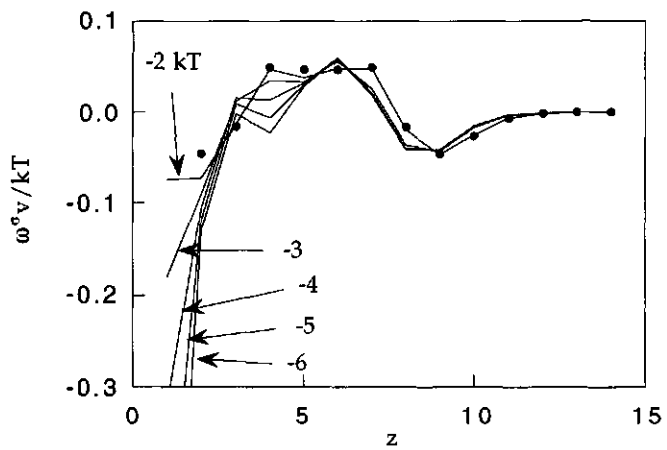

Figure 12 Excess grand potential density profiles of A_4B_8 bilayers at $\mu=\mu^{bi}$. The solid lines are curves of adsorbed layers with different adsorption energy and the dotted curve is the profile the free bilayer in solution.

In figure 12 the profiles of flat layers of A_4B_8 surfactants are shown. All profiles are calculated at μ^{bi}, and correspond to different adsorption energies, χ_{AS}. The black circles represent the profile of the free bilayer, $\omega^{\sigma,f}(z)$. In the surfactant layer adjacent to the surface $\omega^{\sigma}(z)$ and $\omega^{\sigma,f}(z)$ differ, but the structure near the solution side is the same as that in a free bilayer. The differences between $\omega^{\sigma}(z)$ and $\omega^{\sigma,f}(z)$ increase with increasing adsorption energy, which is expected because the perturbation due to the surface becomes stronger. Therefore, the idea that the influence of the surface can be regarded as a perturbation of the free bilayer profile has been justified.

4.4.3 The curvature constant as an indicator

If the curvature is small, the following expression for the shift in the chemical potential for the phase transition with curvature holds,

$$\Delta\mu^{\#} \propto \left(\frac{C^{II}}{\Gamma_0^{II} - \Gamma_0^{I}} \right)_{\mu_0^{\#}} \qquad (29)$$

where the ratio $C^{II}/\left(\Gamma_0^{II} - \Gamma_0^{I}\right)$ is a measure of the curvature sensitivity of the phase transition. From now on we will refer to this quantity as X: the curvature sensitivity. In the ST theory we calculated this quantity with the help of the profiles $\omega^{\sigma}(x)$ and $\rho^{\sigma}(x)$ of the flat layer. MFL calculations have shown that the curvature constant is not fully determined by the excess grand potential density profile of the flat layer, $\omega^{\sigma}(x)$. In section 4.4.2.1 the influences of the tail length, headgroup length and adsorption energy on the curvature dependency of the phase transition have been discussed with the help of MFL calculations. We now try to predict these trends on the basis of the $\omega_0^{\sigma}(x)$ and $\rho_0^{\sigma}(x)$ profiles, calculated with the MFL theory.

In figure 13 we have plotted X as a function of the headgroup length n for different A_nB_{10} surfactants (χ_{AS}=-4). The curvature sensitivity increases with increasing headgroup length. This is in agreement with the full MFL calculations, which predict an increase of the shift with increasing headgroup length, figure 5. Figure 14 shows the curvature sensitivity X as a function of the tail length n of different A_5B_n surfactants. The curvature sensitivity increases with increasing tail length. However, the tail length influence is not as strong as that of the length of the headgroup. Both observations agree with the results of the full MFL calculations, shown in figure 9.

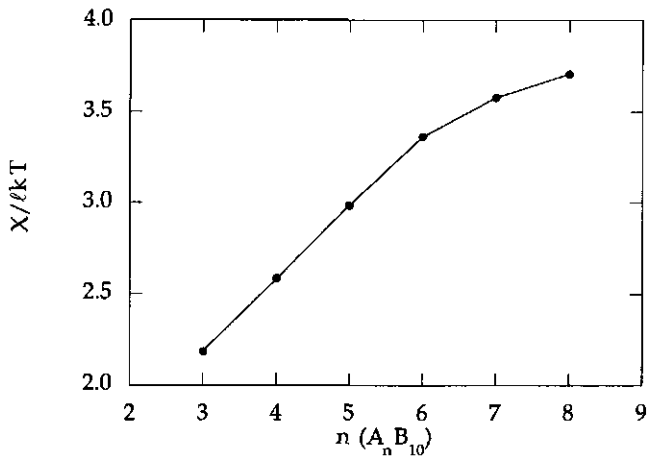

Figure 13 The curvature sensitivity, $X = C^{II}/\left(\Gamma_0^{II} - \Gamma_0^{I}\right)$, as a function of the number (n) of headgroup segments of an A_nB_{10} surfactant.

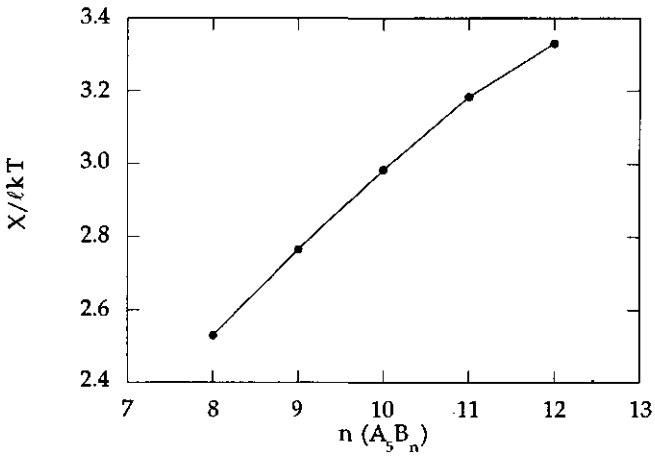

Figure 14 The curvature sensitivity as a function of the number (n) of tail segments of an A_5B_n surfactant.

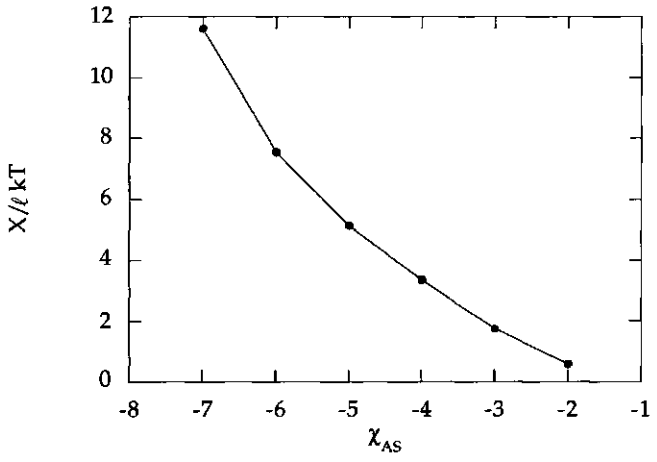

Figure 15 The curvature sensitivity as a function of the adsorption energy of an A_6B_{10} surfactant.

The influence of the adsorption affinity is shown in figure 15. In this figure X of an A_6B_{10} surfactant is plotted as a function of the adsorption energy χ_{AS}. The curvature sensitivity is strongly dependent on the adsorption energy, just as has been found in the full MFL calculations, figures 5 and 6.
We may conclude that the properties of layers in pores can be predicted from information about the flat layer, provided the curvature is not too strong. The influence of the molecular architecture and the adsorption energy can be semi-quantitatively predicted.

4.5 Conclusions

We have studied the adsorption of nonionic surfactants in hydrophilic pores with a Mean Field Lattice (MFL) theory. In the pore the adsorbed amount is smaller and the step in the isotherm occurs at a lower chemical potential than at the flat surface under otherwise identical conditions.
The influence of the radius of a cylindrical pore on the bulk volume fraction at which the phase transition occurs, $\phi^{\#}$, has been calculated for molecules with different molecular architectures and adsorption energies. The influence of the curvature on the phase transition increases with increasing headgroup length. If the tail length increases, the curvature sensitivity of the phase transition also increases. The adsorption energy has a rather strong influence.

The shift of the phase transition increases with increasing affinity of the surface for the headgroups. This confirms our previous statement of the Semi Thermodynamic (ST) analysis, that the curvature constant increases with increasing adsorption affinity.

The surface tension is almost linearly dependent on J. The deviations from linearity are caused by the fact that the excess grand potential density profile varies with the curvature. Therefore, the curvature constant calculated by using $\omega_0^\sigma(x)$, C_{flat}, deviate from the real curvature constant, found by fitting the γ-J curve, C_{fit}. Whether or not C_{flat} is a useful quantity depends strongly on μ. At the point where bilayers become stable in solution, μ^{bi}, C_{flat} seems to be wrong. However, at the point of phase transition, $\mu^{\#}$, the essential physics are not lost although the error in the predicted curvature constant is still high, ±25%. Therefore, we may conclude that the ST theory is semi-quantitatively correct.

We have tried to predict the influence of the molecular architecture and the adsorption energy on the curvature sensitivity of the phase transition from the excess grand potential density profile of the flat layer. All trends found in the full MFL calculations have been reproduced, which confirms the idea that the ST analysis captures the important physics.

References

1 Gellan, A. and Rochester, C. H., *J. Chem. Soc., Faraday Trans. 1* **81,** 2235 (1985).

2 Böhmer, M. R. and Koopal, L. K., *Langmuir* **6,** 1478 (1990).

3 Böhmer, M. R., Koopal, L. K., Janssen, R., Lee, E. M., Thomas, R. K. and Rennie, A. R., *Langmuir* **8,** 2228 (1992).

4 Tiberg, F., Jönsson, B., Tang, J. and Lindman, B., *Langmuir* **10,** 2294 (1994).

5 Seidel, J., Wittrock, C. and Kohler, H.-H., *Langmuir* **12,** 5557 (1996).

6 Lee, E. M., Thomas, R. K., Cummins, P. G., Staples, E. J., Penfold, J. and Rennie, A. R., *Chem. Phys. Letters* **162,** 196 (1989).

7 Rutland, M. W. and Senden, T. J., *Langmuir* **9,** 412 (1993).

8 Gu, T. and Zhu, B., *Colloids and Surfaces* **44,** 81 (1990).

9 Giordano, F., Denoyel, R. and Rouquerol, J., *Colloids Surf. A* **71,** 293 (1995).

10 Huinink, H. P., Keizer, A. de, Leermakers, F. A. M. and Lyklema, J., *Progr. Colloid Polym. Sci.* **105,** 91, (1997).

11 Huinink, H. P., Keizer, A. de, Leermakers, F. A. M. and Lyklema, J. *Langmuir* **13**, 6452 (1997).
12 Scheutjens, J. M. H. M. and Fleer, G. J., *J. Phys. Chem.* **83**, 1619 (1979).
13 Leermakers, F. A. M. and Scheutjens, J. M. H. M., *J. Chem. Phys.* **89**, 3264 (1989).
14 Evers, O. A., Scheutjens, J. M. H. M. and Fleer, G. J., *Macromolecules* **23**, 5221 (1990).
15 Kronberg, B. and Silveston, R., *Progr. Colloid Polym. Sci.* **83**, 75 (1990).
16 Blokzijl, W. and Engberts, J. B. F. N., *Angew. Chem. Int. Ed. Engl.* **32**, 1545 (1993).
17 Levitz, P., Vandamme, H. and Keravis, D., *J. Phys. Chem.* **88**, 2228 (1984).
18 Levitz, P. and Vandamme, H., *J. Phys. Chem.* **90**, 1302 (1986).
19 Wijmans, C. M. and Linse, P., *J. Phys. Chem.* **100**, 12583 (1996).
20 Lent, B. van, and Scheutjens, J. M. H. M., *Macromolecules* **22**, 1931 (1989).
21 Leermakers, F. A. M, Schoot, P. P. A. M. van der, Scheutjens, J.M.H.M. and Lyklema, J., in *Surfactants in solution*, Vol. 7, edited by K. L. Mittal (Plenum Publishing Corporation, 1989), pp. 43.
22 Huinink, H. P., *unpublished results* .

Chapter 5

Micellization at surfaces; theory of polydisperse rod-like micelles

Abstract A lattice model for polydisperse rectangles on a square lattice has been used to study the behavior of rod-like surfactant aggregates at the solid-liquid interface. In principle it is possible to obtain the three parameters of the model from 2D MFL (mean field lattice) calculations.
The aggregates grow with increasing chemical potential. If the caps become more unfavorable, the average length of the rod increases. If the average length exceeds a certain value, a second order transition from an isotropic to a nematic phase takes place. The growth of the aggregates is promoted by the nematic ordering.
A nearly exact relation between the number of aggregates at the surface at the isotropic-nematic transition line and the average aspect ratio has been found by a fit of the numerical data. If the number of aggregates decrease, the average aspect ratio to obtain nematic ordering has to increase.

5.1 Introduction

In the last years a variety of models, describing surfactant adsorption, have been developed[1-7]. However, most of these models have their limitations, due to the incorporated assumptions. Some models start with a detailed molecular picture, but neglect the finite sizes of the aggregates at the surface. Other models take into account the size of and the interaction between these surface micelles, but neglect molecular detail.

Böhmer et al.[5] have used a mean field lattice (MFL) theory to describe the surfactant adsorption of nonionic and ionic surfactants. The major advantage of their MFL model is its detailed description of the molecular properties of the surfactants. However, a price has to be paid. As a result of the mean field approximation density gradients are allowed in only one dimension, normal to the surface. Otherwise stated, homogeneous adsorption layers are predicted. We will refer to this theory as the 1D MFL model. However, recent experiments have shown that at sufficiently high chemical potential discrete aggregates, micelle-like, exist on the surface[8-11].

Recently Latjar et al.[6] have developed a model, based on the Scaled Particle Theory (SPT), to account for the inhomogeneity of the adsorbed layer.

Although their treatment of the inter-micellar interactions is rather sophisticated, they had to adopt a very simple model for the structure of, and the interactions within the micelle. Therefore, neither the 1D MFL model nor the SPT approach is able to combine a description on a molecular level with the possible discrete nature of aggregates at the interface.
Wijmans and Linse[12] have reported lattice Monte Carlo (MC) calculations dealing with the same problem. In principle all problems, mentioned above, could be solved by MC calculations. Despite their rigorous approach, the simulation time limits their box-size and number of molecules. The number of micelles, formed within the simulation box, was too low to sample the whole configurational space. Most of all, the involved simulation time restricts the number calculations which can be done, preventing a systematic study of the influences of all molecular parameters on the adsorption isotherm.
Böhmer et al.[5] have tried to overcome the limitations of their 1D MFL model by using a 2D model, which allows density gradients in two dimensions. With this model they were able to describe the equilibrium state of one single disk-like surface micelle pinned at a fixed position at the surface. However, they did not take care of the inter-micellar interactions and the configurational entropy of a collection of these micelles. It is questionable how general their results are, because inter-micellar interactions influence the size and the shape of aggregates.
In this study, we investigate a lattice model, developed by Herzfeld[13], which can describe a system of polydisperse rectangular particles. Herzfeld's theory belongs to the same category as the SPT approach: much attention is paid to the aggregate-aggregate interactions and little to the molecular structure of the aggregate. However, we will try to make clear how the parameters of the model can be extracted from a molecular model (f.e. the 2D MFL theory). With the Herzfeld-model the ordering behavior and the growth of polydipserse rods at a surface will be studied.

5.2 Polydisperse rod-like micelles on a surface

5.2.1 Equilibrium conditions

Consider a solid-liquid interface, with an area A, at temperature T, in equilibrium with a bulk solution of surfactants in water. The state of this system can be described with the grand potential, Ω^{σ}. In a density functional approach, the equilibrium state would be obtained by minimizing $\tilde{\Omega}^{\sigma}$ with

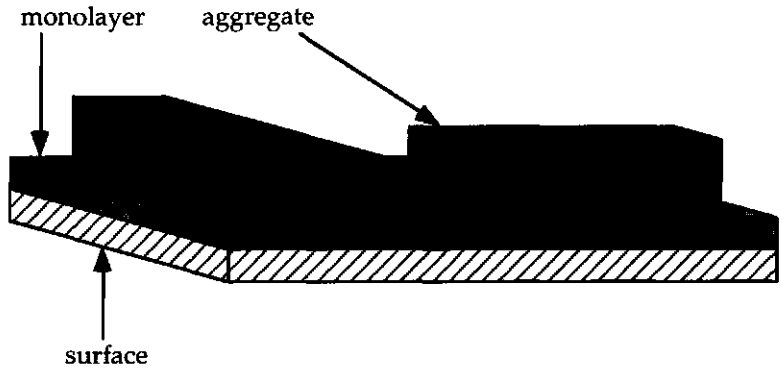

Figure 1 A schematical picture of two surfactant aggregates (dark grey) at a surface, embedded in a layer monolayer of surfactant molecules (light grey).

respect to the density profiles of the components at constant chemical potentials, μ's. We shall use $\tilde{\Omega}^{\sigma}$ to indicate non-equilibrium values of Ω^{σ}. Considering the complexity of the system, we shall describe the interfacial layer as a collection of polydisperse rods of uniform cross-section but variable length $\{N_i\}$, embedded in a homogeneous monolayer, as in figure 1. Let $\tilde{\Omega}^{\sigma}$ consist of two contributions

$$\tilde{\Omega}^{\sigma} = \tilde{\Omega}' + \tilde{\Omega}'' \tag{1}$$

where $\tilde{\Omega}'$ and $\tilde{\Omega}''$ represent the monolayer and the set of rods, respectively. In equation (1) it is assumed that the contributions of the monolayer and the micelles are additive. If a rod of type i occupies an area A_i, $\tilde{\Omega}'$ is given by

$$\tilde{\Omega}' = \Omega' = \left(A - \sum_i N_i A_i \right) \gamma' \tag{2}$$

where γ' is the surface tension of the monolayer. In equation (2), we have replaced $\tilde{\Omega}'$ by its equilibrium value Ω', assuming that the equilibrium structure of the monolayer is not affected by changing the distribution of the rods. The contribution of the rods is

$$\tilde{\Omega}'' = \sum_i N_i \left(F_i^{\sigma} - \sum_j n_{ij}^{\sigma} \mu_j \right) + \tilde{F}_{hr} \tag{3}$$

where F_i^σ is the excess Helmholtz energy of a fixed micelle of type i, n_{ij}^σ is the excess amount of molecules of type j in a micelle of type i, μ_j is the chemical potential of a molecule j and $\tilde{F}_{hr}$ is the Helmholtz energy of a collection of polydisperse hard rods in two dimensions. Equation (3) contains two important assumptions. First, the intra-micellar contributions, the sum term on the right hand side of (3), and the inter-micellar contributions, $\tilde{F}_{hr}$, are additive. Second, energetic interactions between the micelles are neglected, $\tilde{F}_{hr}$ only contains excluded area interactions. Therefore, if the model predicts an ordered structure of the adsorbed layer, this must be caused by hard rod interactions. In formula,

$$\tilde{F}_{hr} = -kT \ln Q_{hr}\left(\left\{N_i^k\right\}\right) \tag{4}$$

where the superscript k refers to the orientation of a rod and Q_{hr} the canonical partition function of a system of polydisperse hard rods, that we have to establish. To obtain the equilibrium state, we have to minimize the excess grand potential with respect to the distribution $\left\{N_i^k\right\}$.

$$\left(\frac{\partial \tilde{\Omega}^\sigma}{\partial N_i^k}\right)_{N_{i'}^{k'}s} = 0 \tag{5}$$

Combination of (1) and (5) results in

$$\frac{\partial}{\partial N_i^k}\left(\tilde{\Omega}' + \tilde{\Omega}''\right) = 0 \tag{6}$$

With (2) the first term on the left hand side becomes

$$\frac{\partial \tilde{\Omega}'}{\partial N_i^k} = -A_i \gamma' \tag{7}$$

The left hand side of equation (7) can be obtained by differentiation of equation (3) with respect to N_i^k

$$\frac{\partial \tilde{\Omega}''}{\partial N_i^k} = F_i^\sigma - \sum_j n_{ij}^\sigma \mu_j + \mu_{i,hr}^k \tag{8}$$

for any combination of i and k. The last term on the right hand side may be interpreted as the chemical potential of a hard rod of type i pointing in direction k, $\mu^k_{i,hr} \equiv \partial \tilde{F}_{hr}/\partial N^k_i$. The difference in excess grand potential between a rod i fixed at arbitrary position and orientation and a monolayer patch with the same area is defined as follows

$$\Omega^\sigma_i \equiv F^\sigma_i - \sum_j n^\sigma_{ij}\mu_j - A_i\gamma' \tag{9}$$

Combination of (7)-(9) results in the following equilibrium condition

$$\Omega^\sigma_i + \mu^k_{i,hr} = 0 \tag{10}$$

5.2.2 Configurational Helmholtz energy of polydisperse rectangles

In this section, we derive the configurational Helmholtz energy for a polydisperse set of rectangles on a lattice, according to the procedure developed and successfully applied to associating systems by Herzfeld and co-workers[13-17]. For a detailed explanation, these papers have to be consulted. The surface is treated as a square lattice with lattice constant λ. The number of directions k is two: x and y. The number of lattice sites is $L=A/\lambda^2$. A rectangle of type i pointing in direction k covers $x^k_i y^k_i$ lattice sites, where x^k_i and y^k_i are the lengths of the sides in the x and y direction, respectively, expressed in number of lattice sites. The canonical partition function of a collection of rectangles $\left\{N^k_i\right\}$ is given by

$$Q_{hr} = \frac{A^N}{\lambda^{2N}\prod_{i,k} N^k_i!} W \tag{11}$$

where $N = \sum_{i,k} N^k_i$ is the total number of particles. The permutational factor on the right hand side of (11) is the partition function of a collection of non-interacting ideal particles. The function W corrects for the excluded area interactions. To obtain W, the particles will be sequentially inserted in four stages, illustrated in figure 2. These stages have been chosen in such a way that the number of obstructions during the insertion of new, additional segments remains constant at each stage. Let us call the probability of stage τ P_τ, then

$$W = \prod_{\tau=1}^{4} P_\tau \tag{12}$$

The probability P_1 of the first stage is

$$P_1 = \frac{L!}{(L-N)!L^N} \tag{13}$$

where L!/(L-N)! is the number of ways to place N distinguishable segments on a lattice with L distinguisable sites and L^N is the number of ways to place N arealess segments.

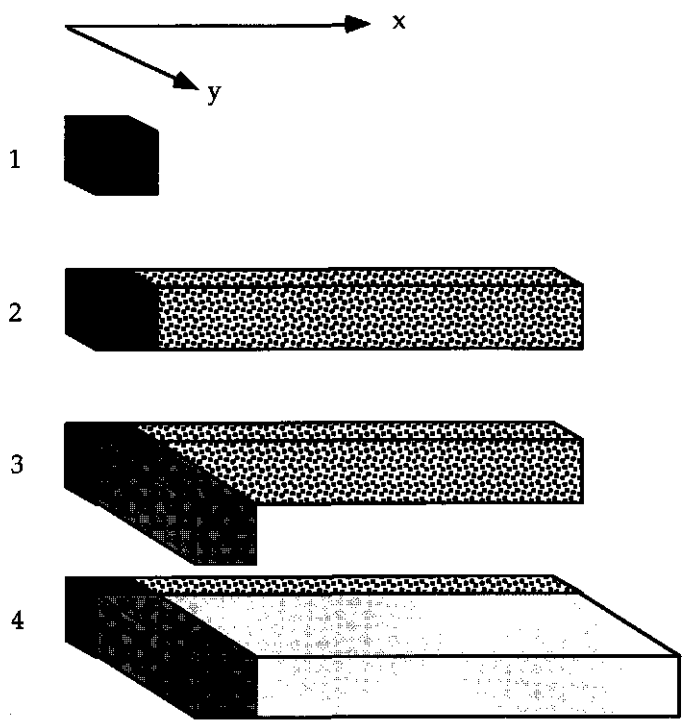

Figure 2 The four different stages of insertion: (1) one corner segment, (2) all other segments of the x-side, (3) all other segments of the y-side and (4) the segments within the L.

A general formula for the probabilities of the other stages is[13],

$$P_\tau = \frac{v_\tau!/(v_\tau - n_\tau)!}{(v_\tau + o_\tau)!/(v_\tau + o_\tau - n_\tau)!} \tag{14}$$

where v_τ is the number of vacancies before any segment of stage τ has been inserted, n_τ the number of segments belonging to stage τ and o_τ the number of obstructions during the insertion of segments of stage τ. Assuming random disposition of the segments,

$$v_2 = L - N, \;\; o_2 = N, \;\; n_2 = \sum_{i,k} N_i^k \left(x_i^k - 1\right) \tag{15}$$

and

$$v_3 = L - N - \sum_{i,k} N_i^k \left(x_i^k - 1\right), \;\; o_3 = \sum_{i,k} N_i^k x_i^k, \;\; n_3 = \sum_{i,k} N_i^k \left(y_i^k - 1\right) \tag{16}$$

The x- and y-sides of the rectangles are build in stage 2 and 3, respectively. After the insertion of the segments of the stages 2, we have rods of a thickness of one lattice site pointing in the positive x-direction. If all segments of stage 3 have been inserted, the surface is covered with L-shaped particles, with the sides pointing in the positive x- and y-direction.
An expression for P_4 is more difficult to obtain. Before the insertion is started, L-shaped particles are present. The segments are now added in such a way that only the corner segments of the other rectangles can obstruct the addition.

$$\begin{aligned} v_4 &= L - N - \sum_{i,k} N_i^k \left[\left(x_i^k - 1\right) + \left(y_i^k - 1\right)\right], \\ o_4 &= N, \\ n_4 &= \sum_{i,k} N_i^k \left(x_i^k - 1\right)\left(y_i^k - 1\right) \end{aligned} \tag{17}$$

One of our aims is to couple this rod-model with 2D MFL calculations. To match both lattice models, we have to take the same lattice spacing, compared to the sizes of the aggregates in both models. In the MFL calculations, an aggregate covers several lattice sites. Therefore, we can use the continuum

limit of the Herzfeld-model. The probabilities P_τ for the second, third and fourth stage follow from equation (14).

$$\lim_{\lambda\to 0} P_\tau = \left(\frac{v_\tau - n_\tau}{v_\tau}\right)^{o_\tau} \tag{18}$$

The probabilities of the first two stages approach unity.

$$\lim_{\lambda\to 0} P_1 = \lim_{\lambda\to 0} P_2 = 1 \tag{19}$$

If the mesh size of a lattice goes to zero, one single segment becomes a point (stage 1) and a rod, which has the thickness of segment, becomes a line (stage 2). Neither the point nor the line have an excluded area. The limit $\lambda \to 0$ of P_3 results in an expression, which is related with the ordering of the rods,

$$\lim_{\lambda\to 0} P_3 = e^{-K_x K_y/L} \tag{20}$$

where

$$K_x \equiv \sum_{i,k} N_i^k x_i^k \tag{21}$$

Finally, P_4 converts into an excluded area term

$$\lim_{\lambda\to 0} P_4 = (1-\phi)^N \tag{22}$$

where

$$\phi \equiv \sum_{i,k} N_i^k x_i^k y_i^k / L \tag{23}$$

In (22) $(1-\phi)^N$ is an isotropic excluded area term. Now we can formulate the canonical partition function of the collection of polydisperse rigid rectangles.

$$Q_{hr} = \frac{A^N}{\lambda^{2N}\prod_{i,k} N_i^k!}(1-\phi)^N e^{-K_x K_y/L} \tag{24}$$

In equation (24), $\exp(-K_xK_y/L)$ is the only factor which can induce anisotropy, for instance nematic ordering. Without this term, equation (24) goes over in a partition function, which would predict a Volmer-type isotherm . By inserting equation (24) in (4) and using the Stirling approximation $\ln Y! = Y\ln(Y/e)$, we obtain the Helmholtz energy.

$$\tilde{F}_{hr} = kT\sum_{i,k} N_i^k\left[\ln\left(\frac{N_i^k\lambda^2}{Ae}\right) - \ln(1-\phi)\right] + kT\frac{K_xK_y}{L} \qquad (25)$$

The chemical potential of a rectangle of type i with orientation k can be found by differentiation of (25) with respect to N_i^k.

$$\mu_{i,hr}^k = kT\ln\left(\frac{N_i^k\lambda^2}{A}\right) - kT\ln(1-\phi) + kT\left(\frac{N/L}{1-\phi}\right)x_i^k y_i^k + \frac{kT}{L}\left(K_x\frac{\partial K_y}{\partial N_i^k} + K_y\frac{\partial K_x}{\partial N_i^k}\right) \qquad (26)$$

From now on, we only allow polydispersity in the length of the rectangles, we restrict ourselves to polydisperse rods. The diameter and length corresponds with δ and r_i lattice sites, respectively, figure 3. The minimum length is δ. We introduce two additional parameters: the fraction of surface covered by caps, belonging to rods of type i with orientation k, which is proportional to the number of aggregates, $\psi_i^k \equiv N_i^k\delta^2/L$,and the fraction of surface covered by rods of type i with orientation k, $\phi_i^k \equiv N_i^k r_i\delta/L = N_i^k A_i/A$.

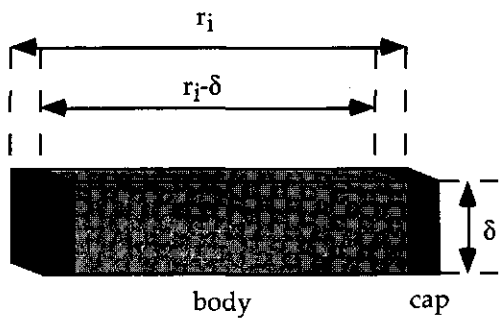

Figure 3 Our representation of a rod-like surface micelle of type i. The total length and the thickness are r_i and δ lattice sites respectively. The aggregate consists of two parts: the caps and the body. The smallest aggregate covers δ^2 lattice sites.

Figure 4 has been drawn to clarify the transfer from the more general formalism of equations (25) and (26) to expressions for polydisperse rods. The chemical potential of a rod of type i oriented in the x or y direction follows from (26) as illustrated by figure 4,

$$\mu^{x}_{i,hr} = kT\ln\left(\frac{\psi_i^x}{\delta^2}\right) - kT\ln(1-\phi) + kT\left(\frac{\psi}{1-\phi}\right)\frac{r_i}{\delta} + kT\left(\phi^x + \psi^y\right) + kT\left(\phi^y + \psi^x\right)\frac{r_i}{\delta} \tag{27}$$

$$\mu^{y}_{i,hr} = kT\ln\left(\frac{\psi_i^y}{\delta^2}\right) - kT\ln(1-\phi) + kT\left(\frac{\psi}{1-\phi}\right)\frac{r_i}{\delta} + kT\left(\phi^y + \psi^x\right) + kT\left(\phi^x + \psi^y\right)\frac{r_i}{\delta} \tag{28}$$

If we compare (27) and (28), it becomes clear that the last two terms of both equations, which have the product K_xK_y/L as their common origin, may differ between the x and y direction and hence can give rise to ordering phenomena.

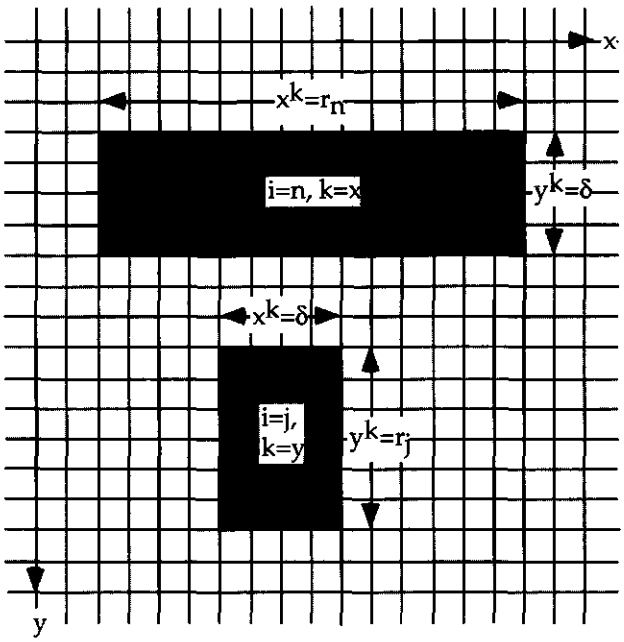

Figure 4 Schematical picture of two rod-like aggregates, placed on a lattice: one of type n, pointing in the x-direction, and one of type j, pointing in the y-direction.

Consider a system of monodisperse rods of length r and thickness δ. In equilibrium μ^x equals μ^y. It is obvious that the isotropic solution of the model always obeys this condition. For the anisotropic (nematic) solution, we derive with (27) and (28),

$$\ln\left(\frac{\psi^x}{\psi^y}\right) = \left(\psi^x - \psi^y\right)\left(r/\delta - 1\right)^2 \tag{29}$$

If the anisotropy is weak $\ln\left(\psi^x/\psi^y\right) \approx \psi^x/\psi^y - 1 = \left(\psi^x - \psi^y\right)/\psi^y$ and equation (29) reduces to:

$$\psi \approx 2\psi^y = \frac{2}{\left(r/\delta - 1\right)^2} \tag{30}$$

This equation provides us with a critical value of ψ above which the model has, besides an isotropic solution, also an anistropic one. Because the maximum surface coverage $\phi=1$ and $\phi=\psi r/\delta$, a system of rods with $r < r^* = \left(2+\sqrt{3}\right)\delta$ will not have an anisotropic solution.

5.2.3 Linear micelles

In the preceding paragraph we have focused on the inter-micellar interactions. If we want to calculate the equilibrium state of the aggregates at the surface, we have to combine (10) with (27) and (28). In this section we will calculate the coverage of the surface and the average rod length in both directions. To do this, we need an interpretation of Ω_i^σ in (10). We approximate the Helmholtz energy part of Ω_i^σ with

$$F_i^\sigma = f_{mid}\delta r_i + \Delta f_{cap}\delta^2 \tag{31}$$

where f_{mid} is the Helmholtz energy per lattice site in the body of the rod and Δf_{cap} is the excess in the caps. So, we have assumed that the rod has only two different chemical environments: the cap and the body. With the help of

$$\beta\delta r_i \equiv \sum_j n_{ij}^\sigma \mu_j \tag{32}$$

and

$$A_i\gamma' = \lambda^2\gamma'\delta r_i \tag{33}$$

we arrive at an expression for Ω_i^{σ}:

$$\Omega_i^{\sigma} = \left(f_{mid} - \beta - \lambda^2\gamma'\right)\delta r_i + \Delta f_{cap}\delta^2 = \Omega_{mid}\left(\frac{r_i}{\delta}\right) + \Delta\Omega_{cap} \tag{34}$$

where we have used $\Delta\Omega_{cap} \equiv \Delta f_{cap}\delta^2$ and $\Omega_{mid} \equiv \left(f_{mid} - \beta - \lambda^2\gamma'\right)\delta^2$. Below, we will try to interpret these two parameters within the framework of the MFL theory. First, for reasons of simplicity, we define the quantities C, B_x and B_y.

$$C \equiv (1-\phi)\exp\left[-\left(\frac{\psi}{1-\phi} + \phi + \psi + \frac{\Omega_{mid} + \Delta\Omega_{cap}}{kT}\right)\right] \tag{35}$$

$$B_x\delta^2 \equiv \frac{\psi}{1-\phi} + \phi^y + \psi^x + \frac{\Omega_{mid}}{kT} \tag{36}$$

$$B_y\delta^2 \equiv \frac{\psi}{1-\phi} + \phi^x + \psi^y + \frac{\Omega_{mid}}{kT} \tag{37}$$

Combination of (35)-(37) with (27), (28) and (10) results in expression for the amount of rods of type i in the directions x and y

$$\psi_i^x = \delta^2 C e^{-B_x i} \tag{38}$$

$$\psi_i^y = \delta^2 C e^{-B_y i} \tag{39}$$

The variable i is defined such that $r_i\delta = \delta^2 + i$, which means that i is the number of lattice sites covered by the body of the rod. The area fraction of rods of type i in direction x is

$$\phi_i^x = \left(1 + i\delta^{-2}\right)\psi_i^x \tag{40}$$

From now on, we will only give the results for the rods laying in the x direction. The treatment of the rods in the y direction is the same. The total number of rods pointing in the x direction can be obtained by summation over i from zero to infinity.

$$\psi^x = \delta^2 \sum_{i=0}^{\infty} C e^{-B_x i} \tag{41}$$

This summation can be approximated by an integral, which is definite for the chosen interval

$$\psi^x \approx \delta^2 \int_{i=0}^{\infty} C e^{-B_x i} di = \frac{C\delta^2}{B_x} \tag{42}$$

Another property of interest is the average rod length in both directions $\langle r_x \rangle$ and $\langle r_y \rangle$, which can be obtained as,

$$\langle r_x \rangle = \delta \frac{\sum \left(1 + i\delta^{-2}\right) C e^{-B_x i}}{\sum C e^{-B_x i}} \approx \delta + \frac{B_x}{\delta} \int_{i=0}^{\infty} i e^{-B_x i} di = \delta \left(1 + \frac{1}{B_x \delta^2}\right) \tag{43}$$

Here, $1+i\delta^{-2}$ is the length of a rod of type i normalized by minimum length δ, the aspect ratio. The average length diverges as B_x goes to zero. That B_x is coupled to $\langle r_x \rangle$, follows from equation (38), where $1/B_x$ plays a similar role as the Debye-screening length for electrolytes. If B_x decreases, the importance of the contribution of the longer rod lengths increases and $\langle r_x \rangle$ increases.
We obtain the area fraction of rods, aligned in direction x, by multiplying (42) with $\langle r_x/\delta \rangle$.

$$\phi^x = \langle r_x/\delta \rangle \psi^x \approx \frac{C\delta^2}{B_x} \left(1 + \frac{1}{B_x \delta^2}\right) \tag{44}$$

To have a measure of the fluctuations in the rod-length, we calculate the standard deviation of r_x,

$$\sigma_{r_x} = \sqrt{\langle r_x^2 \rangle - \langle r_x \rangle^2} = \frac{1}{B_x \delta} \tag{45}$$

which equals the second term on the right-hand side of (43). We can conclude that size fluctuations become more important with increasing average rod length. Therefore, polydispersity has to be taken into account in a model, meant to describe the behavior of rod-like aggregates.

To calculate (42)-(45) a numerical procedure has to be used, which is described in the appendix. To find the absolute minimum, we have to compare the Ω^{σ}'s of all minima. If we have two solutions, an isotropic and a nematic phase, the equilibrium phase is found by comparing the Ω^{σ}'s of both phases. If we combine (1) with the solutions (38) and (39), the following expression for Ω^{σ} can be obtained

$$\Omega^{\sigma} = A\gamma' - \frac{kTL}{\delta^2}\left[\psi + \frac{\phi\psi}{1-\phi} + \left(\phi^x + \psi^y\right)\left(\phi^y + \psi^x\right)\right] \qquad (46)$$

5.2.4 Molecular interpretation of the parameters

The model, described in the preceding section, has three input parameters: (i) Ω_{mid}, (ii) $\Delta\Omega_{cap}$ and (iii) δ. These parameters have a molecular origin. Knowledge of the relation between molecular properties, like adsorption energy, surfactant architecture and solubility of the surfactant headgroup, and these parameters is important to determine which outcomes of the model have physical significance.

Although there are several molecular models of surfactant aggregation[18-20], none of these have a direct link with molecular properties. Only the MFL theory, originally developed to study polymer adsorption[21] and later applied to surfactant aggregation[22], links aggregate structures and properties with single surfactant properties. In this section, we briefly discuss how Ω_{mid}, $\Delta\Omega_{cap}$ and δ can be extracted from MFL calculations.

With 2D MFL calculations the equilibrium structure of a single aggregate at a fixed position at the surface can be calculated[5]. This can be done in two different lattice geometries: cylindrical and flat. The cylindrical geometry results in disk-like aggregates. Infinite rods are calculated with the flat geometry. The parameters Ω_{mid}, $\Delta\Omega_{cap}$ and δ have to be obtained at the same surfactant chemical potential. Therefore, both the equilibrium structure of the disk and the infinite cylinder (rod) have to be calculated at the same surfactant chemical potential. A 1D calculation gives us the surface tension of the corresponding monolayer γ'.

The diameter of the disk provides us with a value for δ. The parameters Ω_{mid} and $\Delta\Omega_{cap}$ are obtained by,

$$\Omega_{mid} = \frac{\delta}{\ell}\left(\Omega^{\sigma}_{2D,flat} - A_{flat}\gamma'\right) \qquad (47)$$

$$\Delta\Omega_{cap} = \Omega^{\sigma}_{2D,cyl} - A_{cyl}\gamma' - \Omega_{mid} \qquad (48)$$

where A_{flat} and A_{cyl} are the surface areas of the calculation boxes for the two different geometries and ℓ is the length of the box with the flat geometry.

5.3 Results

5.3.1 Growth of randomly oriented aggregates

In the model, polydispersity is allowed and the average length of a surface micelle depends on the parameters Ω_{mid}, $\Delta\Omega_{cap}$ and δ. If the aggregates become sufficiently long, nematic ordering will take place. Therefore, knowledge of the growth behavior of the aggregates is important. This knowledge will be obtained by studying a system of randomly oriented aggregates: the isotropic phase (I).

In figure 5 the surface coverage ϕ is plotted as a function of Ω_{mid} for different values of $\Delta\Omega_{cap}$ (δ^2=50). Because Ω_{mid} linearly depends on the chemical potential of the surfactant μ_j (34), the curves in figure 5 can be regarded as adsorption isotherms. This figure has three main features: (i) there is significant adsorption for $\Omega_{mid}>0$, (ii) for $\Omega_{mid}>0$ the adsorption decreases with increasing $\Delta\Omega_{cap}$ and (iii) the co-operativity of the adsorption increases with increasing $\Delta\Omega_{cap}$.

(i) The adsorption in the region $\Omega_{mid}>0$ is not favored by the intra-micellar contribution (37) to Ω^{σ}, which is positive and therefore destabilizes a surface aggregate. Nevertheless, the surfactants adsorb in large amounts. This is caused by the fact that the aggregates have translational entropy, which compensates the unfavorable intra-micellar contribution.

(ii) In systems with unfavorable caps, surfactant adsorption is low in the region $\Omega_{mid}>0$ and increases rapidly when Ω_{mid} becomes negative. In the region $\Omega_{mid}>0$ aggregates are stabilized by their translational entropy (i). To be more precise, they are stabilized by their partial translational entropy (10). As the caps become more unfavorable, the partial entropy has to increase to stabilize the aggregates and therefore the number of aggregates per surface area have to decrease.

(iii) The shape of the isotherms make clear that the co-operativity of the adsorption increases when the caps become more unfavorable. If the caps become more unfavorable, then the surfactants adsorb in larger rods. Figure 6

shows that this indeed happens. The aggregate-size increases with increasing $\Delta\Omega_{cap}$.

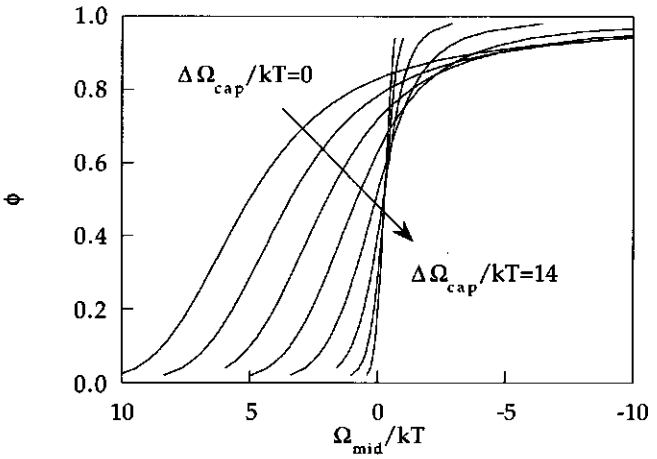

Figure 5 The fraction of the surface covered by aggregates, ϕ, as a function of the Ω_{mid}/kT for $\Delta\Omega_{cap}/kT$=0, 2, ..., 12, 14 (δ^2=50).

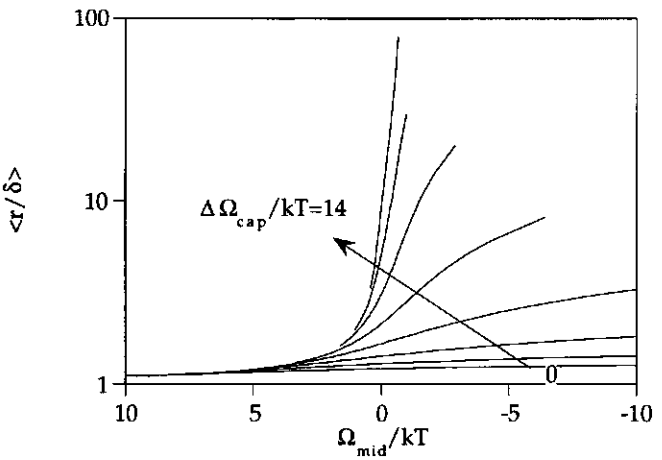

Figure 6 The average aspect ratio as a function of Ω_{mid} for for $\Delta\Omega_{cap}/kT$=0, 2, ..., 12, 14 ($\Delta\Omega_{cap}$ increases in the direction of the arrow).

5.3.2 The adsorption isotherm and the isotropic-nematic transition

In section 5.3.1 the system has been forced to be isotropic. Now we allow the aggregates to order at the surface. In figure 7 the total surface coverage ϕ (solid lines) and the excess grand potential, Ω^σ (dashed lines), have been plotted as a function of Ω_{mid}/kT with δ^2=50 and $\Delta\Omega_{cap}/kT$=12. Above $\Omega_{mid}/kT \approx -0.02$, the model has only one solution: the isotropic phase. Below this point a nematic phase (N) also is a solution of the model. The Ω^σ-curve makes clear that the nematic phase is the real equilibrium phase, $\Omega_N^\sigma \leq \Omega_I^\sigma$. The I-N transition is a second order phase transition, because Ω^σ splits up in the N and I branches, which never cross each other again.
In section 5.3.1 we have already seen that the adsorption becomes more co-operative with increasing $\Delta\Omega_{cap}$. Figure 7 shows that ordering increases the co-operativity too. Therefore, we can conclude nematic ordering promotes the growth of the surface aggregates[23].
In figure 8, $\langle r/\delta \rangle$ has been plotted as a function of Ω_{mid}/kT . In the isotropic region, the average length slowly increases with decreasing Ω_{mid}. After the I-N transition, the length rapidly increases in the direction of alignment and decreases in the other direction.

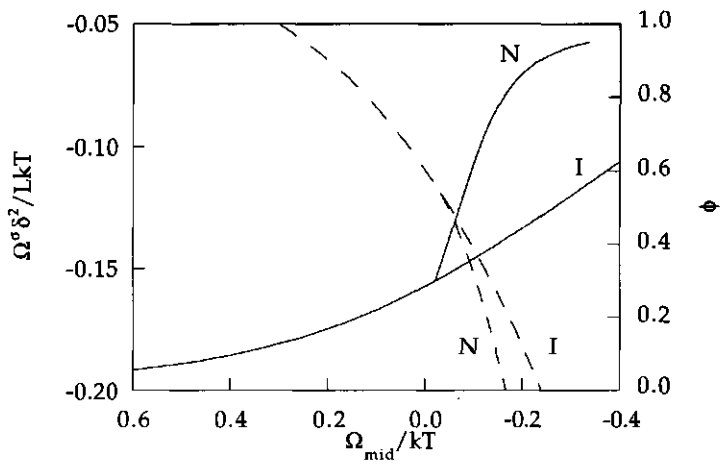

Figure 7 The excess grand potential (dashed lines) and the surface fraction covered by rods (solid lines) as a function of Ω_{mid} for $\Delta\Omega_{cap}/kT$=12. The branches labelled with N and I correspond with the nematic and the isotropic solution of the model, respectively.

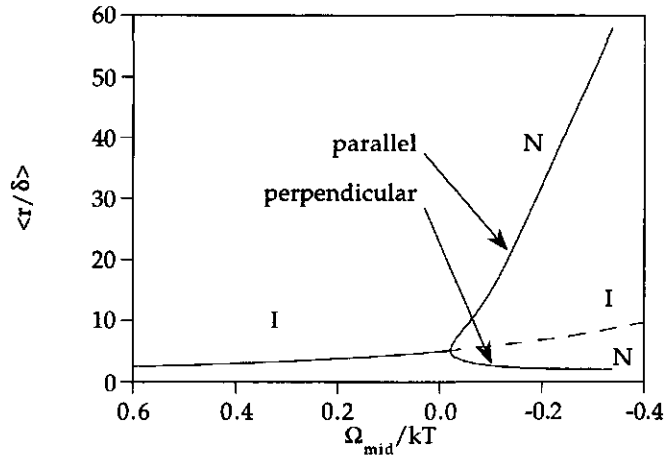

Figure 8 The average aspect ratios as a function of Ω_{mid} in the two lattice directions. After the I-N transition $\langle r/\delta \rangle$ becomes dependent on the mode of orientation: parallel or perpendicular

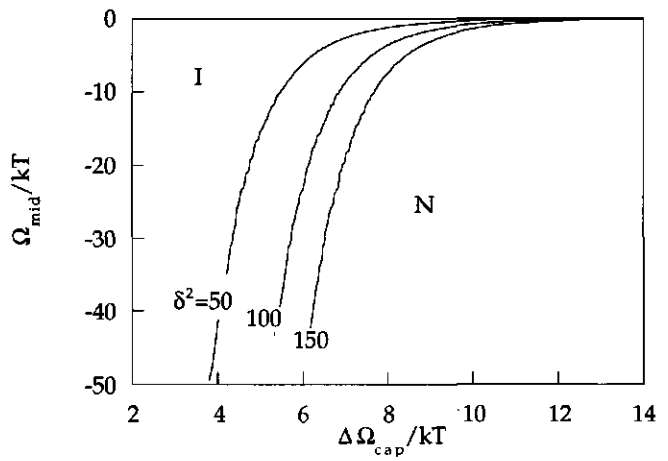

Figure 9 The isotropic-nematic transition lines for different cap sizes δ^2. The isotropic (I) and nematic (II) regions are on the left and right side of the curves, respectively.

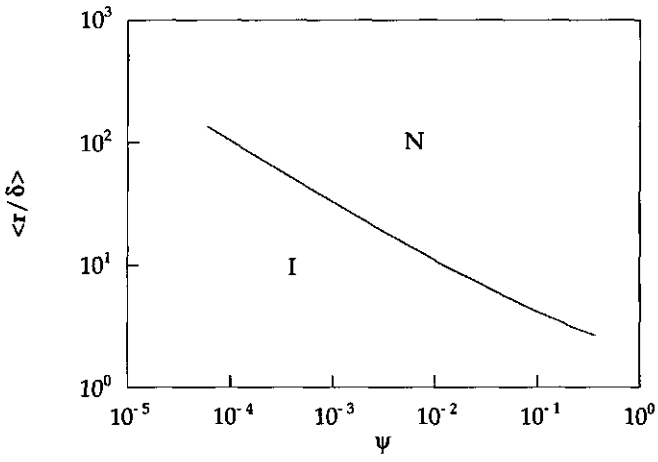

Figure 10 *The relation between ψ and $\langle r/\delta \rangle$ at the I-N transition line.*

5.3.3 The isotropic-nematic transition line

The I-N transition is the most interesting feature of the model. In this section we investigate this transition in more detail. For three different cap-areas δ^2, we have calculated Ω_{mid} at the phase transition as a function of $\Delta\Omega_{cap}$, figure 9. For every $\Delta\Omega_{cap}$, the I-N transition has a second order character. The absence of a region of first order transitions must be a consequence of the dimensionality of the model. Herzfeld and co-workers[15] predicted with the same model first order transitions in solutions of polydisperse rods. If the caps are more favorable than the body of the rod, $\Delta\Omega_{cap}<0$, then the contribution of the body, Ω_{mid}, has to become very negative to induce a I-N transition.

The two important quantities with respect to the I-N transition are the total cap fraction ψ and the average aspect ratio $\langle r/\delta \rangle$ at the transition. In figure 10 we have plotted $\langle r/\delta \rangle$ against the ψ for δ^2=50. The cap fraction is proportional to the total number of aggregates per unit area. Calculations for different cap sizes have shown that the relation between $\langle r/\delta \rangle$ and ψ is independent of the cap size. The following equation fits the curve very well:

$$\psi = \frac{1}{\left(\langle r/\delta \rangle - 1\right)^2} \tag{49}$$

At the end of section 5.2.2, we have derived an analogous expression for monodisperse rods (30). Although we cannot give a mathematical derivation of (49), we think that this formula is an exact outcome of the model. The only difference between (49) and (30) is a factor of 2. If the average rod length is small, nematic ordering can only occur at very high coverages. According to equation (49), no I-N transition will occur when $\langle r \rangle$ cannot reach a critical value, $\langle r^* \rangle = \frac{1}{2}\left(3+\sqrt{5}\right)\delta$, which corresponds to $\psi^* = 4\left(1+\sqrt{5}\right)^{-2}$. Combination of (36), (43) and (49) shows that ψ equals ψ^* for $\Omega_{mid} \rightarrow -\infty$ and $\Delta\Omega_{cap} \rightarrow -\infty$. Due to the presence of size fluctuations ordering can take place at $\langle r^* \rangle < r^*$, compare (30) with (49).

With the help of equation (49) it is possible to relate ψ at the transition with $\Delta\Omega_{cap}$. In figure 11 we have plotted $\ln\psi$ as a function of $\Delta\Omega_{cap}/kT$. For high values of $\Delta\Omega_{cap}$ the curves becomes linear and the slope seems to be independent of δ^2. This indicates that at low coverages ψ is an exponential function of $\Delta\Omega_{cap}$. If $\Delta\Omega_{cap}$ decreases, ψ becomes in the independent of the cap size and tends to a constant value of about 0.38, which is in agreement with ψ^*, obtained from (49).

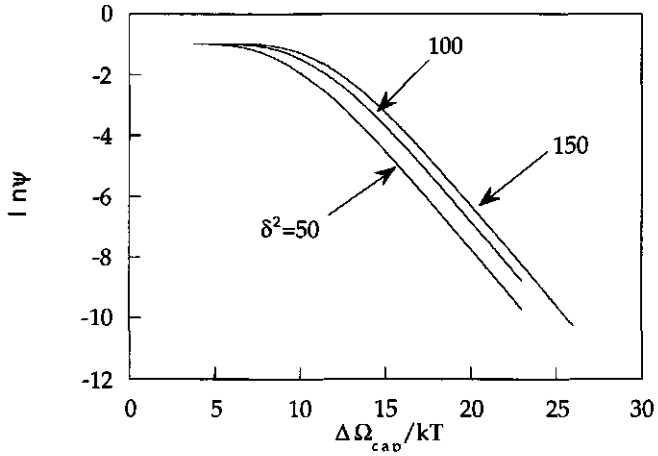

Figure 11 The logarithm of ψ as a function of $\Delta\Omega_{cap}$ for different cap sizes.

With equation (49) it is possible to obtain a relation between ψ and $\Delta\Omega_{cap}$ for every value of ψ, which will be done below. By combination of (43) and (49) we obtain

$$B\delta^2 = \psi^{1/2} \tag{50}$$

The subscribt of B has been dropped, because at the I-N transition an isotropic system is present. With the help of (49) and (50) equation (35) can be written as

$$C = \left(1 - \psi^{1/2} - \psi\right)\exp\left[-\left(\psi + \frac{1}{2}\psi^{1/2} + \frac{\Delta\Omega_{cap}}{kT}\right)\right] \tag{51}$$

The relation between ψ and $\Delta\Omega_{cap}$ is now found by insertion of (50) and (51) in (42).

$$\frac{\psi^{3/2}}{1 - \psi^{1/2} - \psi}\exp\left(\psi + \frac{1}{2}\psi^{1/2}\right) = 2\delta^4 \exp\left(-\frac{\Delta\Omega_{cap}}{kT}\right) \tag{52}$$

For diluted systems, ψ is small, ψ becomes and exponential function of $\Delta\Omega_{cap}$.

$$\psi = \left(2\delta^4\right)^{2/3}\exp\left(-\frac{2}{3}\frac{\Delta\Omega_{cap}}{kT}\right) \tag{53}$$

From (53) we learn that the slopes for high values of $\Delta\Omega_{cap}$ in the curves in figure 11 equal 2/3.

5.4 Conclusions

To study the aggregation behavior of surfactants at the solid-liquid interface, a lattice model[13] has been used. In the model a collection of rectangles, with a constant thickness δ and a variable length r, is placed on a square lattice. Due to the anisotropy of the aggregates, nematic ordering can occur. The model has an isotropic (I) and a nematic (N) solution. The real equilibrium situation can be found by comparison of the excess grand potential of both phases.
The input parameters Ω_{mid}, $\Delta\Omega_{cap}$ and δ can be obtained from a molecular model, which can calculate the equilibrium structure of disk-like aggregate

and an infinite rod at the same chemical potential. In principle the MFL theory is a good candidate for this procedure.

Growth of the aggregates in the isotropic phase ultimately leads to an isotropic-nematic transition. Although the positive intra-micellar contributions (Ω_{mid}, $\Delta\Omega_{cap}$) do not favor association, adsorption takes place because the aggregates are stabilized by their translational entropy. The co-operativity of the adsorption increases with increasing $\Delta\Omega_{cap}$ (the caps become increasingly unfavorable), which means that the surfactants adsorb in longer rods.

The growth of the rods with decreasing Ω_{mid} (increasing chemical potential) leads to a second-order I-N transition. Beyond this transition, the average length of the rod increases rapidly. The co-operativity of the adsorption is enhanced. At the I-N transition line, the cap fraction ψ scales nicely with $\langle r/\delta \rangle - 1$ to the power minus two. Although, this equation could not be derived analytically, it has to be an exact result of the model because an analogous expression could be derived for a monodisperse hard rod system. With the help of this equation, we were able to derive relations between $\Delta\Omega_{cap}$ and ψ at the transition for every value of ψ. In the limit of low surface densities ψ becomes a exponential function of $\Delta\Omega_{cap}$.

Appendix Numerical scheme

We have solved the equations (35)-(37), (42) and (44) with the help of a Newton-type iteration method, developed by Powell[24] and made more powerful by Scheutjens[25]. A given combination of Ω_{mid}/kT and $\Delta\Omega_{cap}/kT$ can have two solutions: an isotropic (I) and a nematic (II) phase, which can be characterized by ψ^x, ψ^y, ϕ^x and ϕ^y.

Four variables x_n have been defined. These will be iterated to values, which are consistent with (35)-(37), (42) and (44). The variables x_n's are related with ψ, ψ^x, ϕ and Ω_{mid}/kT by

$$\psi = \frac{e^{x_1}}{1+e^{x_1}}, \quad \psi^x = \frac{e^{x_2}}{1+e^{x_2}}, \quad \phi = \frac{e^{x_3}}{1+e^{x_3}} \quad \text{and} \quad \frac{\Omega_{mid}}{kT} = x_4 \qquad (A.1)$$

The quantities $\Delta\Omega_{cap}/kT$ and ϕ^x are used as input parameters and fixed during the iteration process. With (A.1) and(35)-(37), (42) and (44) we can calculate the set: $\tilde{\psi}$, $\tilde{\psi}^x$, $\tilde{\phi}$ and $\tilde{\phi}^x$. Every iteration variable x_n corresponds with a function g_n, which has to be iterated to zero.

$$g_1 = \frac{\psi - \breve{\psi}}{\psi + \breve{\psi}},\ g_2 = \frac{\psi^x - \breve{\psi}^x}{\psi + \breve{\psi}},\ g_3 = \frac{\phi - \breve{\phi}}{\phi + \breve{\phi}} \text{ and } g_4 = \frac{\phi^x - \breve{\phi}^x}{\phi^x + \breve{\phi}^x} \qquad (A.2)$$

Acknowledgements

We gratefully acknowledge Prof. J. Herzfeld. Her comments helped us to apply her lattice model to the problem of surfactant adsorption.

List of symbols

A		surface area
	A_i	area covered by a micelle of type i
	A_{cyl}	surface area in a 2D MFL calculation in a cylindrical geometry
	A_{flat}	surface area in a 2D MFL calculation in a flat geometry
F		Helmholtz energy
	F_i^{σ}	the excess Helmholtz energy of an aggregate of type i
	$\tilde{F}_{hr}$	Helmholtz energy of a collection of polydisperse hard rods
f_{mid}		excess Helmholtz energy per covered lattice site of the body of the micelle
	Δf_{cap}	difference between the Helmholtz energy of the cap and the body per covered lattice site.
N		total number of aggregates
	N_i	number of aggregates of type i
	N_i^k	number of aggregates of type i, pointing in direction k
n_{ij}^{σ}		excess number of molecules of type j in an aggregate of type i
n_τ		number of segments in stage τ
o_τ		number of obstructions of stage τ
P_τ		insertion probability of stage τ
Q		canonical partition function
r		rod length, expressed in lattice sites
	r_i	rod length of a micelle of type i
	r^*	minimum rod length needed for ordering
	$\langle r_x \rangle$	average rod length of the aggregates lying in the direction x
	$\langle r_y \rangle$	average rod length of the aggregates lying in the direction y
v_τ		number of vacancies of stage τ
W		function which corrects for excluded area interactions
x_i^k		length in x-direction of an aggregate of type i pointing in

		direction k, expressed in lattice sites.
y_i^k		length in y-direction of an aggregate of type i pointing in direction k, expressed in lattice sites.
γ'		surface tension of the monolayer
δ		thickness of a rod, expressed in lattice sites
ϕ		fraction of the surface, covered by rods
	ϕ^k	fraction of the surface, covered by rods, pointing in direction k
	ϕ_i^k	fraction of the surface, covered by rods of type i, pointing in direction k
λ		lattice constant
μ		chemical potential
	μ_j	chemical potential of a molecule of type j
	$\mu_{i,hr}^k$	chemical potential of a hard rod of type i, pointing in direction k
ψ		fraction of the surface, covered by caps (cap fraction)
	ψ^*	critical cap fraction
	ψ^k	cap fraction of rods, pointing in direction k
	ψ_i^k	cap fraction of rods of type i, pointing in direction k
Ω		grand potential
	Ω^σ	excess grand potential
	$\tilde{\Omega}^\sigma$	non-equilibrium excess grand potential
	Ω'	monolayer part of $\tilde{\Omega}^\sigma$
	$\tilde{\Omega}''$	micellar part of $\tilde{\Omega}^\sigma$
	Ω_i^σ	excess grand potential of a rod of type i at a fixed position

References

1 Böhmer, M. R. and Koopal, L. K., *Langmuir* **6,** 1478 (1990).

2 Levitz, P., *Langmuir* **7,** 1595 (1991).

3 Zhu, B. and Gu, T., *Adv. Coll. Interface Sci.* **37,** 1 (1991).

4 Cases, J. M. and Villieras, F., *Langmuir* **8,** 1251 (1992).

5 Böhmer, M. R., Koopal, L. K., Janssen, R., Lee, E. M., Thomas, R. K. and Rennie, A. R., *Langmuir* **8,** 2228 (1992).

6 Lajtar, L., Narkiewicz-Michalek, J., Rudzinski, W. and Partyka, S., *Langmuir* **9,** 3174 (1993).

7 Israelachvili, J., *Langmuir* **10,** 3774 (1994).

8 Rutland, M. W. and Senden, T. J., *Langmuir* **9,** 412 (1993).

9 Patrick, H. N., Warr, G. G., Manne, S. and Aksay, I. A., *Langmuir* **13,** 4349 (1997).
10 Grant, L. M. and Ducker, W. A., *J. Phys. Chem.* **101,** 5337 (1997).
11 Jaschke, M., Butt, H. J., Gaub, H. E. and Manne, S., *Langmuir* **13,** 1381 (1997).
12 Wijmans, C. M. and Linse, P., *J. Phys. Chem.*, **100,** 12583 (1996).
13 Herzfeld, J., *J. Chem. Phys.* **76,** 4185 (1982).
14 Herzfeld, J., *J. Chem. Phys.* **88,** 2776 (1987).
15 Herzfeld, J. and Taylor, M. P., *J. Chem. Phys.* **88,** 2780 (1987).
16 Taylor, M. P., Berger, A. E. and Herzfeld, J., *J. Chem. Phys.* **91,** 528 (1989).
17 Taylor, M. P. and Herzfeld, J., *J. Phys.: Condens. Matter* **5,** 2651 (1993).
18 Israelachvili, J. N., Mitchell, D. J. and Ninham, B. W., *J. Chem. Soc., Faraday Trans.* 2 **72,** 1525 (1976).
19 Nagarajan, R. and Ruckenstein, E., *Langmuir* **7,** 2934 (1991).
20 Puvvada, S. and Blankschtein, D., *J. Phys. Chem.* **96,** 5567 (1992).
21 Scheutjens, J. M. H. M. and Fleer, G. J., *J. Phys. Chem.* **83,** 1619 (1979).
22 Leermakers, F. A. M., Scheutjens, J. M. H. M. and Lyklema, J., *Biophys. Chem.*, **18,** 353 (1983).
23 Odijk, T., *Current Opinion Coll. Interface Sci.* **1,** 337 (1996).
24 Powell, M. J. D., in *Numerical Methods for Nonlinear Algebraic Equations,* edited by Rabinowitz, P., (Gordon and Breach, London, 1970).
25 Scheutjens, J. H. M. H., *Newton.sim. A Simula class for unconstrained optimation* (Wageningen, 1980).

Summary

The aim of this study was to investigate the behavior of surfactants in porous media by theoretical means. The influence of curvature of a surface on the adsorption has been studied with a mean field lattice (MFL) model, as developed by Scheutjens and Fleer. An analytical theory has been developed to interpret the MFL results. The chapters three and four, which form the core of this thesis, have been devoted to the background and the outcomes of both theories. These theories contain various approximations and therefore limitations. In the flanking chapters two and five attempts to overcome two of these approximations have been described. First, the MFL theory considers water as built up from isotropic monomers. As a consequence, the theory cannot predict the characteristic behavior of water. An alternative model could be the Besseling theory, which is based on the quasi-chemical approach. Some elaborations of this water model have been reported in chapter two. Second, the MFL theory, as used in the chapters three and four, always assumes homogeneous surfactant layers, which is inherent to its mean field approximation. However, it is well known that adsorption layers of surfactants often consist of discrete aggregates. The Herzfeld model has been chosen to study the discrete nature of the adsorbed layer. The theory and its outcomes, dealing with aggregation and ordering behavior of surfactant aggregates at interfaces, have been described in the last chapter.

In chapter two a lattice model for water, developed by Besseling, has been extended by incorporation of the electrostatic interactions of the water molecules with each other and with an external electrostatic field. This could have been the first step towards a better description of water near charged interfaces or in charged pores and electrosorption phenomena. The water-water and water-field interactions have been treated with the reaction field approach of Onsager. Expressions have been obtained for the dielectric constant of the water in an external field.
At low field strengths, the predicted permittivity is close to the experimental one. The temperature dependence has also been reproduced. The dipolar correlation factor has been obtained by using the Clausius-Mossoti equation for the refractive index and the Kirkwood-Fröhlich expression for the dielectric constant. The predicted correlation factor and its temperature

dependence agree well with experimental data. However, the field strength behavior of the model is unexpected. Before saturation the predicted permittivity passes through a maximum. By modifying the hydrogen-bond interaction the saturation could be manipulated. However, this latter procedure does not have a sound physical origin. Somehow, if water molecules orient in large amounts, their interactions change. Therefore, investigations with this theory were not continued and much more simple models for water had to be chosen to study surfactant adsorption.

An analytical theory for nonionic surfactants in hydrophilic cylindrical pores has been developed in chapter three. The adsorption has been approximated with a phase transition model. Above a certain surfactant concentration a monolayer of isolated molecules converts into a bilayer. With the help the thermodynamics of phase transitions, the surfactant chemical potential at phase transition could be related to the curvature of the pore. The shift in this chemical potential due to the curvature is in first approximation proportional to the curvature constant of the bilayer. A molecular model, mean field type, has been used to interpret this curvature energy. Both the curvature energy and the surface tension can be calculated from the excess grand potential density profile. The curvature constant has been calculated from the profile of a flat layer, which is allowed as long as this profile is not very sensitive to the curvature. An equation, which relates the chemical potential at phase transition, the curvature, the structure of the layer and the affinity, has been derived.
Our model predicts that the chemical potential of phase transition decreases with decreasing pore radius. The adsorbed bilayer becomes more stable when the pore radius decreases. Experiments confirmed these trends. If the affinity of the adsorbed layer for the surface increases, the curvature influence on the chemical potential of phase transition increases.

To test the analytical theory and to obtain generic knowledge about the influence of curvature on surfactant adsorption, MFL calculations have been performed, which have been described in chapter four. Contrary to the analytical model, the MFL theory allows changes in the structure of the adsorbed layer with curvature.
The position of the phase transition in a curved system has been calculated as a function of the adsorption energy and the size of the tails and the headgroups. No matter what parameters were used, the MFL calculations

always predicted that the surfactant chemical potential of phase transition decreases with decreasing pore radius, which confirmed the outcome of the analytical model. Especially the adsorption energy turned out to have a strong influence on the sensitivity of phase transition for the curvature. The shift in the chemical potential of the phase transition becomes stronger with increasing adsorption energy, as has also been predicted with the analytical theory.
The most important approximation of the analytical theory, which has been tested with MFL calculations, is the curvature independency of the structure of the adsorbed layer. The surface tension of an adsorbed bilayer has been calculated as a function of the curvature for different chemical potentials. The curvature constant has been obtained as a function of the chemical potential by fitting these curves and calculating it from the excess grand potential density profile of a flat layer. It turned out that the last procedure, which is also used in the analytical theory, underestimates the value of the curvature constant. As long as this constant has a considerable value, the error made by this procedure does not effect the essential physics. Therefore it may be concluded that the analytical theory still captures the important physics despite its severe assumptions.

Both the analytical theory and the MFL model neglect the existence of discrete surfactant aggregates at the surface. To remedy this shortcoming, in chapter 5 the Herzfeld model has been applied to the adsorption of rod-like aggregates at a solid-water interface. The adsorbed layer was represented as a collection of rod-like polydisperse particles embedded in a monolayer of surfactants. An equilibrium condition has been derived, stating that the intrinsic excess grand potential of a rod of a given length plus its hard rod chemical potential has to be zero. The intrinsic excess grand potential has been divided into cap and body contributions, which are in principle the only two input parameters of the model. To calculate the hard rod chemical potential, the Herzfeld lattice model has been used. Rods are represented as rectangles. These rectangles have been placed on a square lattice. As a consequence the number of possible orientations of a rod is two.
By combining the Herzfeld model and the equilibrium condition, expressions for the length distributions in both directions have been obtained. With these distributions expressions were derived for the total number of rods, the average aspect ratio and the standard deviation of this aspect ratio, all in both directions. The distributions have exponential forms, with decay parameters equal to the average aspect ratio minus one and the standard deviation of the

aspect ratio. The close relationship between the average aspect ratio and its standard deviation has made clear that size fluctuations are very important in systems with large rods.
Calculations have been performed on isotropic systems. Adsorption isotherms have been calculated for different cap Helmholtz energies. These isotherms show that the surfactants already adsorb in large amounts when the aggregates as such are not stable. However the collection of aggregates is stabilized by the translational entropy. If the caps become more unfavorable the co-operativity of the adsorption increases, because the length of the adsorbed aggregates increases. Adsorption isotherms have also been obtained for systems, which are allowed to order. It has been shown that at a certain surfactant chemical potential a second order isotropic-nematic phase transition occurs. After this transition the growth of the aggregates is promoted in the direction of alignment and inhibited in the direction perpendicular to that.
The isotropic-nematic transition line has been calculated. It turned out that ordering can take place at much lower surface densities of rods when the average aspect ratio increases. The cap fraction is inversely proportional to the average aspect ratio minus one to the power two at the transition line. Although this expression could not be derived, the close resemblance with an equation, derived for monodisperse rods, confirmed that it is an exact outcome of the model. With the formula found, a relation between surface density at the transition line and the Helmholtz energy of the end caps has been derived, which showed that the nematic ordering takes place at lower rod densities when the caps become more unfavorable.

In the end of my study it has become more and more evident that the phase behavior of surfactants at interfaces should be at least as rich as in solution. As experimental techniques to investigate the structure of micelles at a surface are becoming available (e.g. AFM), we expect that the possible morphologies will become known to us in increasing detail in the near future. This thesis may assist the explorations, directed to fill the gaps in our knowledge of the behavior of surfactants at the solid-water interface, and thus allows us to use surfactants more effective in its applications.

Samenvatting

Het kleinste onderdeel waaruit de natuur is opgebouwd wordt molecuul genoemd. Dat dit zeker geen onbeduidend deeltje is, blijkt wel uit het feit dat bijvoorbeeld één liter water ongeveer 33.000.000.000.000.000.000.000.000 watermoleculen bevat. Een uitermate gelukkige bijkomstigheid van bijna alle moleculen is dat ze niet ongevoelig zijn voor de nabijheid van andere moleculen. Hun wisselwerking is een subtiel spel van aantrekking en afstoting. Wanneer de aantrekking maar sterk genoeg is gaan ze klonteren. Zijn de klontjes vloeibaar, dan spreken we over druppels. Zijn ze vast, dan noemen we ze kristallen of glazen. In veel gevallen hebben moleculen een sterke voorkeur voor hun eigen soortgenoten. Vanwege deze sterke voorkeur kiezen ze er vaak voor om samen te klonteren met soortgenoten, ondanks het feit dat het echt niet onplezierig voor hun is om met andere aanwezige moleculen in contact te treden. Lekkere jus bewijst dit elke dag weer. Omdat watermoleculen vrij narcistisch van aard zijn, worden de oliedeeltjes wel gedwongen om de bovenkant van de braadpan op te zoeken. Geheel onterecht krijgen de oliemoleculen het stempel hydrofoob (=watervrezend). Nu zijn er wel soorten stoffen die door het water worden geaccepteerd. Deze moleculen worden hydrofiel (=waterminnend) genoemd. Zij hebben met de watermoleculen gemeen dat ze er weinig voor voelen om in de olie te gaan zitten.

De schepping bevat echter ook een type molecuul dat zich weinig aantrekt van deze conventies. Dit type gaat onder de namen detergent, surfactant en/of amfifiel door het leven. De naam detergent verwijst naar het feit dat met deze moleculen iets schoongemaakt kan worden. Met de namen surfactant en amfifiel dalen we af naar de microwereld. Deze categorie moleculen heeft de neiging om op te hopen bij allerlei grensvlakken, zoals het water-lucht-, water-olie- en water-bodemdeeltjesgrensvlak, en wordt daarom surfactant genoemd (surface is het engelse woord voor oppervlak). Een veel gebruikt woord voor ophoping aan een grensvlak is adsorptie. Amfifiel is onmiskenbaar de naam die het beste de aard van het molecuul beschrijft, omdat ze ons wijst op het dubbelzinnig gedrag van het molecuul; enerzijds is het molecuul hydrofiel en anderzijds hydrofoob. Het molecuul bestaat daadwerkelijk uit een hydrofiele kop en hydrofobe staart(en). Het is dit schizofrene karakter van het molecuul dat aanleiding geeft tot het adsorberen

aan grensvlakken. En dit ophopen is weer de oorzaak achter de schoonmaakkracht van het molecuul.
Wanneer water te veel van deze surfactantmoleculen bevat, dan worden deze gedwongen om te aggregeren, d.w.z. in groepjes bij elkaar te gaan zitten. In eerste instantie kiezen ze voor kleine bolvormige aggregaten, die micellen worden genoemd. Deze klontjes groeien wanneer de hoeveelheid surfactant in water toeneemt. Zo kunnen onder andere lange staafvormige micellen en grote platen (bilagen) ontstaan. Al deze aggregaten hebben gemeenschappelijk dat de staarten en de koppen respectievelijk aan de binnen- en buitenkant van de aggregaten zitten.
Een groot vast deeltje bevordert dit aggregeren. Nog voordat de moleculen in het water micellen vormen, gaan ze al groepsgewijs op het oppervlak van het vaste deeltje zitten. Dit gebeurt omdat het surfactantmolecuul zich aangetrokken voelt tot het vaste deeltje. Worden de koppen aangetrokken dan spreekt men van een hydrofiel deeltje. De staarten worden aangetrokken door zogenaamde hydrofobe deeltjes. Als er maar genoeg surfactantmoleculen in het water aanwezig zijn, dan kan het hele oppervlak van het vaste deeltje omgeven worden door een laag van surfactantmoleculen. Hydrofobe deeltjes worden dan omgeven door een enkele laag moleculen, die met de koppen naar het water zijn georiënteerd. Hydrofiele deeltjes worden omgeven door een dubbele laag moleculen. De eerste laag bestaat uit moleculen die met hun kop grenzen aan het vaste deeltje en in de tweede laag zitten de moleculen met hun kop naar het water. Met deze beschrijving suggereren we dat deze lagen perfect zijn. In veel gevallen bestaat de laag echter uit een verzameling dicht op elkaar gepakte micellen of halve micellen. Deze micellen kunnen net als in water bol- of staafvormig zijn.
Het hierboven geschetste adsorptiegedrag is nu het onderwerp van dit proefschrift. Uit het voorgaande is wel duidelijk dat al veel bekend is over surfactantadsorptie. Ons grote vaste deeltje kan voor het oog, lees sterke lichtmicroscoop of electronenmicroscoop, een egaal deeltje lijken, soms kan zo'n deeltje echter een heel stelsel van buizen, poriën, herbergen. Deze poriën kunnen allerlei diameters hebben. Het mengsel van water- en surfactantmoleculen kan soms doordringen in dit gangenstelsel. Wanneer de diameter van een porie hoogstens een paar maal groter is dan de totale lengte van het molecuul, dan is het waarschijnlijk dat de wijze van ophoping aan het porieoppervlak zal verschillen van die aan het buitenoppervlak van het vaste deeltje. Dit proefschrift beschrijft onderzoek dat tot doel had om iets meer te weten te komen over het adsorptiegedrag aan het porieoppervlak.

Wetenschappelijk werk bestaat uit kijken wat er gebeurt, meten, en bedenken wat er zou kunnen gebeuren, theorievormen. Beide activiteiten vragen dusdanig veel ervaring, dat je jezelf wel moet richten op één van beiden als je onderzoekstijd beperkt is. Het onderzoek, beschreven in dit proefschrift was gericht op theorievorming. Het hart van dit proefschrift wordt gevormd door de hoofdstukken drie en vier. In deze hoofdstukken zijn met behulp van een tweetal theorieën ideeën gevormd over de mogelijke invloed van de porie op het adsorptiegedrag van surfactantmoleculen. De gebruikte theorieën bevatten echter een aantal haken en ogen. Twee van deze haken en ogen zijn het primitieve beeld van een watermolecuul en het feit dat aangenomen wordt dat de surfactantmoleculen altijd in nette lagen op het oppervlak van een vast deeltje gaan zitten. De hoofdstukken twee en vijf zijn gewijd aan deze twee beperkingen.

Zoals al duidelijk is gemaakt, speelt water een belangrijke rol in het adsorptieproces van surfactantmoleculen. In hoofdstuk twee is een aspect van water besproken, dat in technische termen diëlectrisch gedrag wordt genoemd. Een watermolecuul bestaat uit twee waterstofatomen en één zuurstofatoom. Het molecuul heeft een V-vorm en het zuurstofatoom zit in de punt van de V. Door deze specifieke ruimtelijke combinatie van atomen heeft het molecuul twee belangerijke eigenschappen. Ten eerste is het molecuul aan de puntkant van de V een klein beetje negatief en aan de pootjeskant van de V een klein beetje positief geladen. We zeggen dan dat het molecuul een dipoolmoment heeft. Wanneer je echter alle ladingen bijelkaar optelt, blijft er niets van over. Ten tweede trekt het waterstofatoom erg sterk aan het zuurstofatoom van een naburig watermolecuul, wat waterstofbrugvorming wordt genoemd. In water is een heel netwerk van deze bruggen aanwezig.
Wanneer je een beker water tussen twee tegengesteld geladen platen zet, dan gaan de watermoleculen zich een beetje oriënteren. Ze gaan met de punt van de V in de richting van de positief geladen plaat staan. Dit noemen we polarisatie en het leidt tot het diëlectrisch effect. Omdat watermoleculen door hun waterstofbruggen erg sterk aan elkaar trekken, sleuren ze elkaar ook mee wanneer ze zich oriënteren. In verhouding tot andere vloeistoffen heeft water daarom een erg hoge diëlectrische constante. Deze constante is zo gedefinieerd dat hij veel lager is voor vloeistoffen die niet zo sterk op electrisch velden reageren.
Met behulp van de Besseling theorie hebben we voorspeld dat de diëlectrische constant van water verandert van ongeveer 90 naar 75 wanneer de

temperatuur stijgt van 0° naar 100°C. Dit bleek heel goed te kloppen met wat ooit al gemeten is. Wanneer je de lading op de al eerder geschetste platen vergroot, de sterkte van het electrische veld neemt dan toe, dan gaan steeds meer watermoleculen zich oriënteren. Boven een zekere veldsterkte zijn bijna alle moleculen georiënteerd en valt er dus weinig meer te oriënteren. Dit wordt diëlectrische verzadiging genoemd. Wij hebben berekend hoe de diëlectrische constante verandert met toenemende sterkte van het electrische veld. Boven een zekere veldsterkte treed de verzadiging inderdaad op, de diëlectrische constante daalt dan sterk. Volgens onze voorspelling vindt er voor deze daling eerst een stijging plaats. Dit is in tegenstelling met alles wat tot nu toe gedacht en gemeten is. Omdat we de oorzaak van deze afwijkende voorspelling niet kenden en ook andere onbevredigende resultaten hadden geboekt met de Besseling theorie, zijn we gestopt met dit model. Aan surfactantmoleculen, waar het om begonnen was, is door ons dus nooit gerekend met dit watermodel. Voor het eigenlijke doel van het onderzoek, surfactantadsorptie aan porie-oppervlakken, hebben we daarom gebruik gemaakt van een tweetal andere theorieën.

In hoofdstuk drie is beschreven hoe een eenvoudige model, die de afkorting ST heeft meegekregen, is ontwikkeld, dat ondanks zijn beperkingen toch voorspellingen deed die in overeenstemming waren met metingen. In hoofdstuk vier zijn berekeningen besproken, die uitgevoerd zijn met een bestaande theorie, die ooit ontwikkeld is door Scheutjens en Fleer, die wij aanduiden met de afkorting MFL.
In beide onderzoekingen hebben we ons gericht op de adsorptie van ongeladen surfactantmoleculen in buisvormige poriën met een hydrofiel oppervlak. De hoeveelheid moleculen die op een oppervlak zit hangt sterk samen met het aantal (concentratie) dat in water aanwezig is. Een grafiekje waarin we de geadsorbeerde hoeveelheid uitzetten tegen de concentratie wordt een adsorptieisotherm genoemd. Voor ongeladen surfactantmoleculen en hydrofiele oppervlakken heeft de isotherm een tamelijk karakteristieke vorm. Bij hele lage concentraties zitten er nauwelijks moleculen op het oppervlak. De geadsorbeerde hoeveelheid stijgt licht met de concentratie. De surfactantmoleculen adsorberen onafhankelijk van elkaar op het oppervlak. Vanaf een zekere concentratie vertoont de adsorptieisotherm een sterke stijging, om bij nog hogere concentraties weer af te vlakken. De sterke stijging valt samen met ontstaan van aggregaten op het oppervlak. Hoe groter deze

aggregaten zijn, des te sterker de stijging van de adsorptie. De afvlakking heeft te maken met het feit dat het oppervlak op een zeker moment vol is.
Zowel de ST- als de MFL-theorie maken zich niet druk om de tussenregio. Ze nemen aan dat de moleculen altijd in nette lagen of laagjes op het oppervlak zitten. Dit is nu net niet het geval in de regio waar de sterke stijging plaatsvindt, want daar zitten ze in klontjes bij elkaar. Door deze aanname laten de resultaten een sprong in de geadsorbeerde hoeveelheid zien. Een dergelijke sprong wordt in de natuurkunde een faseovergang genoemd. Hoewel een dergelijke sprong dus in de werkelijkheid nauwelijks voorkomt, kan de regio waarin de sterke stijging plaatsvindt beschouwd worden als een overblijfsel van de faseovergang. We hebben de invloed van de porie op deze faseovergang met behulp van onze theorieën voorspeld, want dat zegt ons iets over de invloed van de porie in de werkelijkheid. Het type surfactant-molecuul en de surfactant-oppervlak wisselwerking bleken de invloed van de porie niet belangrijk te veranderen. Voorspeld werd dat de faseovergang altijd naar lagere concentraties verschuift wanneer de straal van de porie kleiner wordt.
Hoewel de hoofdstukken drie en vier er ingewikkeld uitzien, bleek het met de gebruikte theorieën ontwikkelde idee betrekkelijk eenvoudig te zijn. Ruwweg zijn er twee tegenwerkende factoren: de wisselwerking tussen de surfactant-kop en het oppervlak en de ophoping van surfactantmoleculen. De wissel-werking tussen de kop en het oppervlak begunstigt de aanwezigheid van moleculen aan het oppervlak. De ophoping van materiaal is echter niet gunstig. Dat dit zo is blijkt uit het feit dat de surfactantmoleculen die los in het water zijn nog niet de neiging hebben om te aggregeren. Wanneer de straal van een porie nu verkleind wordt kunnen er per oppervlakte eenheid gewoon minder moleculen ophopen wegens ruimtegebrek. Door de straal van de porie te verkleinen kunnen de moleculen een laag vormen die minder ongunstig is. Technisch gesproken: de laag wordt stabieler doordat de straal verkleind wordt. En een adsorptielaag kan bij lagere concentratie ontstaan wanneer hij stabieler is.

Het meest onbevredigende aspect van de ST- en MFL theorie is het feit dat van te voren opgelegd wordt dat de surfactantmoleculen nette lagen vormen op het oppervlak, terwijl nu juist bekend is dat de geadsorbeerde lagen in veel gevallen bestaan uit een verzameling losse aggregaten. In hoofdstuk vijf is een theorie, ontwikkeld door Herzfeld, geschiktgemaakt voor surfactantadsorptie. In deze theorie worden de surfactantaggregaten beschouwd als rechthoeken,

die kunnen variëren in de lengte en in de breedte en in twee richtingen kunnen liggen. We hebben de theorie uitgewerkt voor staafvormige micellen met een constante dikte en een variabele lengte. Ook is er rekening gehouden met het feit dat een surfactantmolecuul zich niet even prettig in de kop voelt als in het midden van de staaf.
Uit berekeningen bleek dat het aantal surfactants op het oppervlak en de gemiddelde lengte van de staven toenemen wanneer de surfactant-concentratie toeneemt. Tevens bleek dat de staven gemiddeld groter waren als de surfactantmoleculen zich onprettiger voelden in de uiteinden van deze staven. De berekeningen lieten zien dat bij een bepaald gemiddelde staaflengte en een bepaalde hoeveelheid staven op het oppervlak de staven zich in één richting gaan oriënteren. Deze overgang wordt de isotroop-nematische overgang genoemd en vindt plaats omdat de willekeurig liggende staven elkaar te veel gaan hinderen en het daarom gunstiger is voor de staven om in één richting te gaan liggen. Het bleek dat na deze overgang de gemiddelde lengte van de staven die netjes opgelijnd lagen sterk groeide met toenemende concentratie. De gemiddelde lengte van de loodrecht georiënteerde staven blijkt echter af te nemen met de concentratie.

Aan het eind van mijn onderzoek is het me in toenemende mate duidelijk geworden dat er enorm veel kan gebeuren met surfactantmoleculen aan het oppervlak van een vast deeltje. Omdat er steeds meer technieken beschikbaar komen om te kijken naar de vorm van de surfactantaggregaten op oppervlakken, verwachten we dat onze kennis op dit gebied sterk zal toenemen. De inhoud van dit proefschrift draagt bij aan pogingen om iets meer te begrijpen van surfactantadsorptie en de aggregaten die daarbij een rol spelen.

Levensloop

Hendrik Pieter Huinink, die de auteur van dit boekje heet te zijn, zag het levenslicht op 30 december 1969 op een zolderverdieping in Rotterdam. Zijn lotgevallen tussen 1969 en 1988 hebben hem als persoon gevormd, maar mogen vanwege de conventies niet beschreven worden. Zijn VWO-diploma behaalde hij in 1988 aan de Driestar te Gouda. In de maand september van dat jaar reisde hij af naar Wageningen om de studie Moleculaire Wetenschappen te gaan volgen. In 1993 studeerde hij af op de vakken Fysische Chemie, Moleculaire Fysica en Reformatorische Wijsbegeerte. Van 1993 tot 1997 was hij in dienst van het NWO werkzaam bij de vakgroep Fysische en Kolloïdchemie van de Landbouwuniversiteit, wat heeft geleid tot dit proefschrift. Vanaf oktober 1997 werkt hij bij de afdeling Product Physics van Shell International Chemicals in Amsterdam.